AN OUTSIDER LOOKS AT FRICTION STIR WELDING

REPORT #: ANM-112N-05-06 **JULY 2005**

By

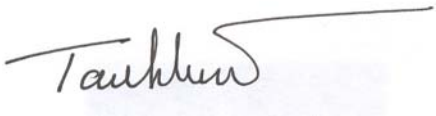

Terry Khaled, Ph.D.
Chief Scientific / Technical Advisor, Metallurgy
Federal Aviation Administration
3960 Paramount Boulevard.
Lakewood, CA 90712
(562) 627-5267
terry.khaled@faa.gov

ABSTRACT

Friction stir welding (FSW) is a fairly recent technique that utilizes a nonconsumable rotating welding tool to generate frictional heat and plastic deformation at the welding location, thereby affecting the formation of a joint while the material is in the solid state. The principal advantages of FSW, being a solid-state process, are low distortion, absence of melt-related defects and high joint strength, even in those alloys that are considered nonweldable by conventional techniques. Furthermore, friction stir (FS) welded joints are characterized by the absence of filler-induced problems / defects, since the technique requires no filler, and by the low hydrogen contents in the joints, an important consideration in welding steels and other alloys susceptible to hydrogen damage. FSW can be used to produce butt, corner, lap, T, spot, fillet and hem joints, as well as to weld hollow objects, such as tanks and tubes / pipes, stock with different thicknesses, tapered sections and parts with 3-dimensional contours. The technique can produce joints utilizing equipment based on traditional machine tool technologies, and it has been used to weld a variety of similar and dissimilar alloys as well as for welding metal matrix composites and the for the repair of existing joints. Replacement of fastened joints with FS welded joints can lead to significant weight and cost savings, attractive propositions for many industries. This document reviews some of the FSW work performed to date, presents a brief account of mechanical testing of welded joints, tackles the issue of generating joint allowables, and offers some remarks and observations. The author of this document has never been involved in any FSW research or development programs and, as such, is an outsider to the field. It is the view of this author, however, that FSW is a leap forward in manufacturing technology, a leap that will benefit a wide range of industries, including the transportation industry in general and the airframe industry in particular. This document will eventually be posted at the following public web site: http://www.faa.gov/aircraft/air_cert/design_approvals/csta/publications

TABLE OF CONTENTS

1.0 INTRODUCTION

Friction stir welding (FSW) is a fairly recent welding technique, invented by The Welding Institute (TWI), Cambridge, UK. [1] This technique utilizes a nonconsumable rotating welding tool to generate frictional heat and deformation at the welding location, thereby affecting the formation of a joint, while the material is in the solid state. The principal advantages of FSW, being a solid-state process, are low distortion, absence of melt-related defects and high joint strength, even in those alloys that are considered nonweldable by conventional techniques (e.g., 2xxx and 7xxx series aluminum alloys). Furthermore, friction stir (FS) welded joints are characterized by the absence of filler-induced problems / defects, since the technique requires no filler. Finally, the hydrogen contents of FSW joints tend to be low, which is important in welding steels and other alloys susceptible to hydrogen damage.

FSW has been successfully used to weld similar and dissimilar cast and wrought aluminum alloys, steels, as well as titanium, copper and magnesium alloys, dissimilar metal group alloys and metal matrix composites. The technique can be used to produce butt, corner, lap, T, spot, fillet and hem joints as well as to weld hollow objects, such as tanks and tube / pipe, and parts with 3-dimensional contours. Apart from producing joints, FSW is also suitable for repair of existing joint. The primary industrial and research interest, however, has been focused on butt welding aluminum alloy sheet and plate up to 3.00 in. thick. FSW was also used to produce butt joints between metals of different thicknesses and between tapered sections. FSW can be performed in all positions (horizontal, vertical, overhead and orbital), and it can produce or repair joints utilizing equipment based on traditional machine tool technologies.

Replacement of fastened joints with FS welded joints can lead to significant weight and cost savings, attractive propositions for many industries, including the transportation industry in general and the airframe industry in particular. The weight savings would come about as a result of the elimination of the fasteners and, where butt joints are involved, the overlap required to install the fasteners. The cost savings would be realized by a decrease in design, manufacturing, assembly and maintenance times, brought about by the potential decrease in part count. Using FS welded joints instead of fastened joints would also eliminate the stress concentration effects associated with fastener holes, improve corrosion performance by eliminating the fasteners as a source of dissimilar metal contact and, in the case of butt joints, by eliminating joint interfaces and the attendant crevice, fretting and other types of corrosion. Finally, the use of FS welded joints can eliminate or at least minimize the need for sealants, locking compounds and the like.

It is generally believed that FSW of the relatively low melting materials, such as aluminum alloys, has matured to the point where it can be used in applications such as commercial and military aircraft. The ever growing list of FSW users includes Boeing, Airbus, Eclipse, BEA, Lockheed Martin, NASA, US Navy, Mitsubishi, Kawasaki, Fokker as well as other industrial concerns in the US, Europe and Japan.

2.0 PURPOSE & LIMITATIONS

The purpose of this document is to review some of the FSW work performed to date. This review should not be considered an all-inclusive or an in-depth one, since it is limited to those publications available to the author. The document is offered on a best-effort basis, due to the proprietary nature of the FSW process and the fact that the author had no involvement in the research or development aspects of this fairly new technology. Accordingly, the reader is urged to seek technical advice from appropriate sources. Furthermore, the document should not be construed as reflecting a Federal Aviation Administration (FAA) position on FSW. FAA applicants are hereby advised that setting requirements and granting approvals are the responsibility of the cognizant FAA certification organizations. Every effort is made here to avoid presenting FS welded joint property data. However, there are cases where presenting such data becomes a logical choice. In such cases, the property values quoted are intended only for information and must not be considered as design allowables. Furthermore, the graphs and depictions offered represent apparent trends or shapes, intended for visualization purposes only. They are approximate, not to scale, and not intended as accurate duplicates of the data reported by the authors cited. All units in the SI system, presented in the publications reviewed, are converted to their approximate equivalent units in the Imperial (in.-lb) system for presentation herein.

3.0 DOCUMENT LAYOUT

Section 4 presents background information regarding solid state welding (4.1), FS technology (4.2), and heat treatment of some aluminum alloys (4.3). Some abbreviations of a general nature are also introduced (4.4). Section 5 is an introduction to FSW. The contents of that section are based on the publications reviewed in this effort. In addition, section 5 includes a brief account of the mechanical testing of welded joints; a more detailed account is presented in the Appendix. Sections 6-8 present somewhat detailed accounts of the publications

reviewed in this effort. Section 6 pertains to work on butt joints of aluminum (6.1) and magnesium (6.2) alloys, steels (6.3), titanium (6.4) and copper (6.5) alloys and dissimilar metal group alloys (6.6). Sections 7 and 8, respectively, pertain to work on lap and spot joints. Section 9 deals with the issue of generating joint allowables. Section 10 offers some observations and remarks.

References are cited in the ordinary manner; viz., superscript numerals. Because of the general nature of sections 4 and 5, the references may be grouped and cited at the headings, cited individually after particular quotations or both. In sections 6-8, the references will be cited where the particular publication is being reviewed. Footnotes are indicated in the text as superscript letters in square brackets, and the footnote content appears at the bottom of the same page in *Italics*. Illustrations will be presented as close as possible to where they are first referenced in the text, not at the end of the text.

4.0 BACKGROUND

4.1 Solid State Welding, Overview [2-4]

FSW, the subject matter of this document, is the newest addition to friction welding (FRW), a solid state welding process. Solid state welding, as the term implies, is the formation of joints in the solid state, without fusion. Solid state welding includes processes such as cold welding, explosion welding, ultrasonic welding, roll welding, forge welding, coextrusion welding and FRW. Conventional FRW in its simplest form involves two axially aligned parts, one rotating and the other stationary. The stationary part is advanced to make contact with the other, at which point an axial force is applied and maintained to generate the frictional heat required to affect welding at the abutting surfaces and form a solid-state joint. The joint is achieved by upset forging at the elevated temperatures generated by friction. There are two FRW techniques. The first is direct / continuos drive FRW, where constant energy is provided by a source for the desired duration. The second is inertia drive FRW, where a rotating flywheel provides the required energy. A variant of the conventional techniques, radial friction welding, is used for hollow sections, such as tube and pipe. Here, a solid ring is rotated and compressed around the abutting beveled ends of the stationary pipes / tubes to be welded. A support mandrel is located at the bore, at the welding position, to prevent the collapse of the pipe / tube ends. Another variant is friction surfacing, where metal layers are deposited on a substrate. Here, a rotary consumable is brought into contact with a moving substrate to affect metal transfer from the consumable to the substrate.

4.2 Friction Stir (FS) Technology [5, 6]

FSW is a member of the FS technology family. The other members of that family are FS processing for superplasticity, FS casting modification (also referred to as FTMP or friction thermomechanical processing), FS microforming, FS powder processing, FS channeling and FS processing for low temperature formability.

4.3 A Note on Aluminum Alloys

Since the majority of work reviewed in this document pertains to aluminum alloys, it is important to discuss some of the heat treatment aspects of these alloys. A three-step sequence is used to heat treat 2xxx, 6xxx and 7xxx series and other heat treatable aluminum alloys, to higher strength levels. The first step is solution heat treatment and it consists of heating to some prescribed elevated temperature (around 900 F) and soaking there for a prescribed period of time. The second step is to cool the alloy fast enough (e.g., by quenching), so as to retain the elevated temperature microstructure. As will become clear shortly, cold working, forming or straightening of quenched wrought alloys should be performed as soon as possible after quenching. The third step is aging (AKA precipitation heat treatment). Aging involves soaking the alloy for a period of time at some temperature that is lower than that used for solution treatment. For the aluminum alloys of concern here, aging is performed in the room temperature to 375 F temperature range. Aging at room temperature is referred to as natural aging. Aging at temperatures above room temperature is referred to as artificial aging. Aging causes precipitation within the grains, with the attendant increase in strength and hardness, at the expense ductility. Other properties also change as a result of aging.

4.3.1 Natural Aging

After quenching, the alloy is in the unstable -AQ temper. At room temperature, the alloy remains in that temper for a period that ranges from a few minuets to an hour or so, depending on the particular alloy. During that period, the solution treated microstructure remains as it was at the solution treatment temperature; i.e., remains unchanged. At the end of that period, the temper changes to the -W temper, also an unstable temper. This is

accompanied by changes in properties; e.g., the strength and hardness will increase and the ductility will decrease. As more precipitation occurs with time, the properties will progressively evolve; e.g., strength will progressively increase and ductility will progressively decrease with time. After a few days (or about 96 hr), 2xxx and 6xxx alloys reach a stable condition, referred to as the -T4 temper where no further property changes would take place. An additional increment of strength can be obtained in 2xxx alloys if the alloy is cold worked in the -AQ temper or during the early stages of the -W temper, and then naturally aged, for about 96 hr, to a stable condition referred to as the -T3 temper. While it is generally accepted that natural aging for 96 hr is sufficient to develop a stable temper (-T3 or -T4), it is reported, in FSW literature, that natural aging continues for over one month in AA 6013 [7] and over 2.5 years in AA 2195. [8] The 7xxx alloys do not reach the stable -T3 and -T4 tempers. Rather, strength and other properties continue to evolve with time for years at room temperature; in fact, it is reported [9] that AA 7050 aluminum alloy age hardens indefinitely at room temperature. In other words, it should be assumed that 7xxx alloys remain in an unstable and evolving -W temper indefinitely, unless the alloy is artificially aged. Therefore, test results obtained in various 7xxx-W alloy investigations cannot be directly compared unless the periods of natural aging indicated (e.g., -W 0.5 hr) are the same. Unfortunately, however, researchers tend not to indicate these periods.

4.3.2 Artificial Aging

Aging at temperatures above room temperature is artificial aging. The properties constantly evolve with aging time at the aging temperature. For example, strength and hardness increase with time to some peak values, beyond which both strength and hardness decrease, with further increases in aging time; strength and hardness peaks may or may not occur at the same aging time. The decrease in strength and hardness is referred to as overaging. For a given alloy, the peak strength (hardness) values that can be achieved by artificial aging are higher than that achieved by natural aging. As the artificial aging temperature is increased, peak strength / hardness shifts to shorter times, and the loss of strength, due to overaging, occurs more rapidly. Peak strength may increase or decrease as the aging temperature increases, depending on the alloy and temperature range. Due to peak shift to shorter times and the more rapid overaging, precise time and temperature control is essential at the higher aging temperatures, to avoid undesirable overaging or underaging. [a] In general, the -T4 or -W tempers maybe aged to the -T6 temper (2xxx and 6xxx alloys). The -T3 temper (2xxx alloys) maybe aged to -T8 temper. In 7xxx alloys, the -W temper may be directly aged to the -T6 or -T7 temper. Alternately, the -T6 temper may be artificially overaged to the -T7 temper. The -T7 type tempers are for enhanced corrosion performance, with some sacrifice in strength.

4.4 Abbreviations

Some abbreviations of a general nature are used throughout this document. These are presented alphabetically below, together with what they mean.

EDS: energy dispersive spectrometry. %e: percent tensile elongation. F_{tu}: ultimate tensile strength. F_{ty}: tensile yield strength. GMAW: gas metal arc welding. GTAW: gas tungsten arc welding. NDI: nondestructive inspection. OM: optical microscope / microscopy. SEM: scanning electron microscope / microscopy. TEM: transmission electron microscope / microscopy.

5.0 INTRODUCTION TO FSW

A brief description of the FSW process for various types of joints is presented in 5.1. Some of the terms and conventions used in FSW are introduced in 5.2. FS welded joint profiles and the various weld zones encountered are detailed in 5.3. The issue of processing variables is tackled in 5.4. An attempt to outline the factors that control weld microstructures is presented in 5.5. Some advanced FSW concepts are discussed in 5.6. The topic of mechanical testing of welded joints is treated in 5.7.

5.1 Process Description

Brief process descriptions are given below for butt joints (5.1.1), lap joints (5.1.2) and other joint types (5.1.3). The contents of this section are based on the publications reviewed in this document.

---

[a] *Underaging means aging for shorter than specified times or at lower than specified temperatures. The result is lower-than-target strength.*

5.1.1 Butt Joints: [4, 10-13]

The two workpieces to be welded, with square mating (faying) edges, are fixtured (clamped) on a rigid backplate, Figure 1a. The fixturing prevents the workpieces from spreading apart or lifting during welding. The welding tool, consisting of a shank, shoulder and pin (Figure 1b), is then rotated to a prescribed speed and tilted with respect to the workpiece normal. The tool is slowly plunged into the workpiece material at the butt line, until the shoulder of the tool forcibly contacts the upper surface of the material and the pin is a short distance from the backplate (Figure 1c). A downward force is applied to maintain the contact and a short dwell time is observed to allow for the development of the thermal fields for preheating and softening the material along the joint line. At this point, a lateral force is applied in the direction of welding (travel direction) and the tool is forcibly traversed along the butt line (Figure 1 d), until it reaches the end of the weld; alternately, the workpieces could be moved, while the rotating tool remains stationary. Upon reaching the end of the weld, the tool is withdrawn, while it is still being rotated. As the pin is withdrawn, it leaves a keyhole at the end of the weld. Shoulder contact leaves in its wake an almost semi circular ripple in the weld track, as depicted schematically in Figure 1d.

As the tool is moved in the direction of welding, the leading edge of the pin, aided by certain other tool features, if present, forces the plasticized material, on either side of the butt line, to the back of the pin. In effect, the material

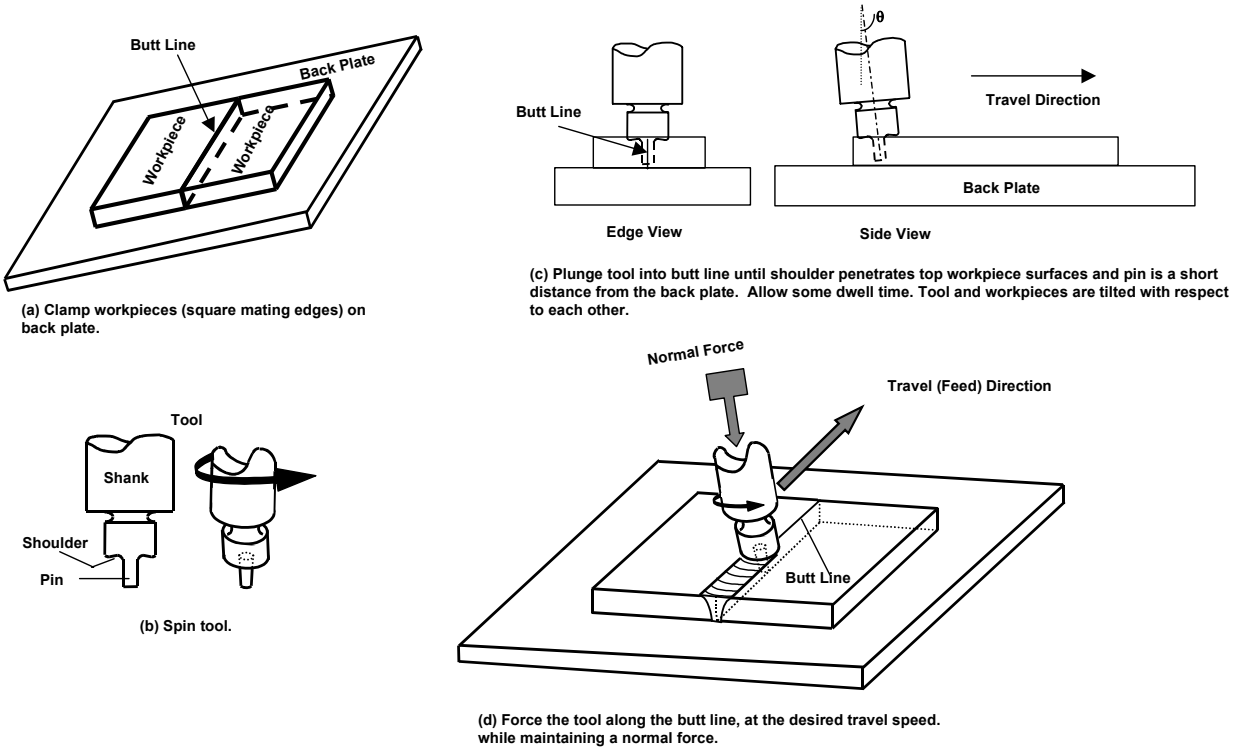

Figure 1: Process description, butt joints.

is transferred from the leading edge of the tool to the trailing edge of the pin (i.e., the material is being stirred) and is forged by the intimate contact of the shoulder and the pin profile. Some believe that the stirring motion tends to break up oxides on the faying surfaces, allowing bonding between clean surfaces. It should be noted that, in order to achieve full closure of the root, it is necessary for the pin to pass very close to the backplate, since only limited amount of deformation occurs below the pin, and then only close to the pin surface. An open root (lack of penetration) is a potential failure site. This aside, Figure 1c depicts that the tool axis and the workpiece normal are tilted with respect to each other by a small angle, θ, typically in the 2-4^{O} range; this angle can be achieved by tilting either the tool or the workpieces. It is said that this tilting aids in the compaction of the material behind the tool, but it has the drawback of limiting the ability to execute nonlinear welds and can also limit the welding speed. [12]

As a consequence of the FSW method, the start and end of the joint will not be fully welded, particularly at the end of the weld, where the keyhole is left. Furthermore, in FSW steel and other high melting alloys, a small-diameter

hole is predrilled in the butt line, to lessen the forces acting on the welding tool during the plunge. It has been recommended, therefore, that the weld start and end regions be machined off. Even with the use of run-on run-off tabs, Ekman *et al*. [13] report that low joint strengths resulted at the workpiece / tab interfaces (Figure 2), necessitating the removal of material, approximately corresponding to the thickness of the workpiece, from either end.

5.1.2 Lap Joints [14-16]

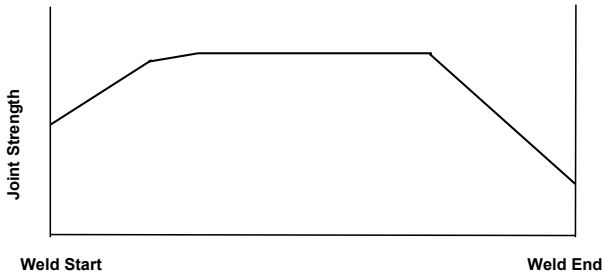

Figure 2: Strength variation along a butt joint.

The same operational principles discussed above for butt joints apply to lap welds, except as follows. In a lap joint there is no butt line, where the tool can be plunged between the workpieces and, as such, the pin must penetrate through the top member. Furthermore, it is essential for the stirring motion to break up the scale, oxides and the other contaminants at the interface. This makes lap welds fundamentally different from butt welds. For butt welds, the primary stirring is in plane of the abutting surfaces being welded. By contrast, lap welds need out of plane stirring, across the interface of the two members being welded. This being so, Brooker *et al*. [14] indicate that the principal difference between a tool for lap welds and one for butt welds is the introduction of a second shoulder, located at the interface between the two details being welded (Figure 3). The lap joint publications reviewed in this document do not specifically indicate that predrilling of a start hole was required.

In lap joints, one must distinguish between the top and bottom members, since the former is in contact with the shoulder. The end of the pin must penetrate completely through the top member, and extend some distance into the bottom member. It is not required, however, that the pin end pass very close to the bottom of the bottom member, since, in contrast to butt joints, there is no root closure to be concerned about. Nevertheless, one must not underestimate the effect of the penetration distance into the lapped (bottom) member on the mechanical properties of the joint. The notches on either side of the joint (Figure 4) are potential sites for crack initiation and, as such, they have a profound effect on mechanical properties. In general, while lap joints are not as strong as butt joints, they have adequate static [14] and fatigue [16] properties to replace fastened joints.

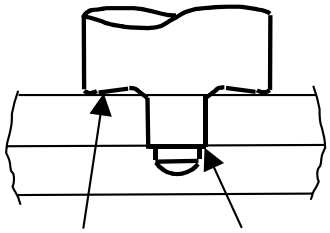

Figure 3: A tool for lap Joints.

5.1.3 Other Joint Types

FSW has been used to prepare spot joints with and without the end keyhole. Spot welds can be either of the butt or lap type. The specifics are presented in section 8. FSW has been also used to prepare T-joints [16] and corner joints, [17] Figure 5. Based on this figure, a T-joint could be viewed as a special lap joint and, as such, the notches on either side of the weld are potential crack initiation sites. Designing with T-joints is challenging, since care must be taken to avoid compression failure of the web (vertical member). Figure 5 suggests that a corner joint is in essence either a special butt joint (butt configuration) or a special lap joint (rabbet configuration). Apart from the above types of joint, FSW has been used to prepare, among others, fillet welds [18] and hem joints. [19] Not much technical information is published on the T, corner, fillet or hem joints and, as such, they will not be considered any further in this document.

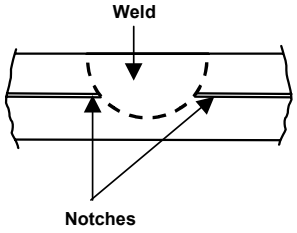

Figure 4: Notches in a lap joint.

5.2 Conventions & Terminology

Following the convention used by Colligan, [11] we define the advancing and retreating sides of a FS weld as follows. The side of the welding tool where surface motion (due to spinning) is in the same direction as the travel direction is referred to as the advancing side. The opposite side, where surface motion opposes the travel direction, is referred to as the retreating side. Some authors refer to the advancing and retreating sides as the shear and flow sides, respectively; this terminology, however, will not be used here. Figure 6 depicts the advancing and retreating sides in a butt weld, together with some other commonly used FSW terminology. As

indicated in section 5.1.1, the tool and workpiece are tilted, by an angle θ, with respect to each other. Colligan [11] and Hirano *et al*. [18] indicate that the tilt is away from the travel direction, as shown in Figure 7. This tilt gives rise to a shoulder plunge, P, defined by Cederqvist *et al*., [15] as shown in Figure 7; P = 0.5 D sin θ, where D is the shoulder diameter. It is to be noted that the shoulder plunge defined above is for the case where the middle of tool contacts the workpiece; other researchers may use different approaches. The terms and definitions

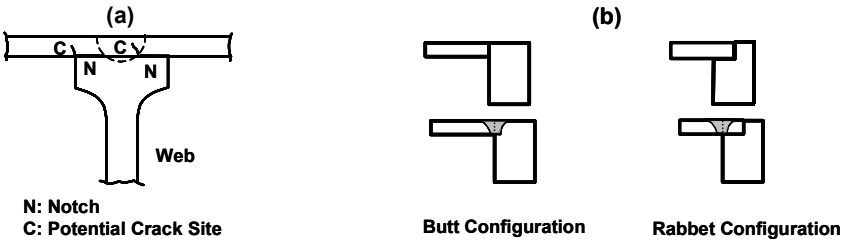

Figure 5: T (a) and corner (b) joints.

discussed above and depicted in Figures 6 and 7 apply to all types of FS welded joints. However, the terms advancing and retreating sides, leading and trailing edges, and travel direction are not applicable to spot welds, since no travel is involved. The term joint profile is used throughout this document, for all types of joints. Joint profile is the shape of the outermost boundary of the weld that borders the base metal and it includes the face and root of the weld. Joint profile can be discerned by preparing a weld cross section, perpendicular to the length of the weld, and viewing it as shown in Figure 8 for butt and lap joints.

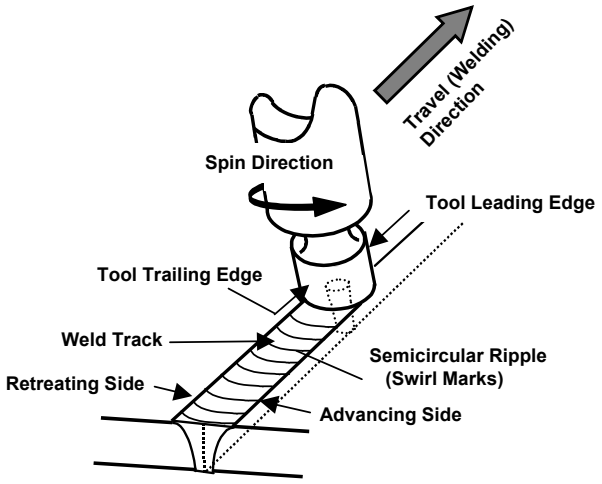

Figure 6: Terminology

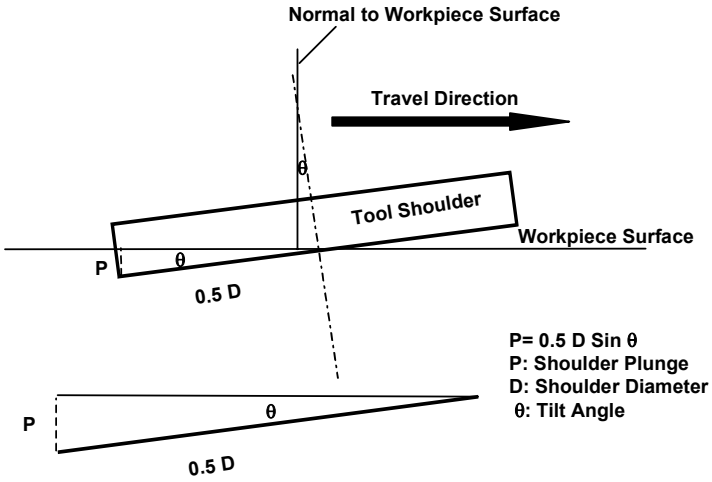

Figure 7: Shoulder plunge.

The terms face, root and toe of the weld, Figure 9, are used with butt joints and occasionally with other types of joints. The terms overmatching and undermatching, respectively, indicate a weld that is stronger than the base metal and a base metal that is stronger than the weld. The term penetration ligament is occasionally used in conjunction with FS welded butt joints. The penetration ligament, as defined by Ding and Oelgoetz, [20] is the distance from the tip (end) of the pin to the backside of the workpiece. Another term that appears in FS welded butt joints is the kissing bond. According to Oosterkamp *et al*., [21] a kissing bond is a descriptive term for two surfaces lying extremely close together, but not close enough for the majority of the original surface asperities to have deformed sufficiently to affect the formation of atomic bonds. Kissing bonds are extremely difficult to detect by most of the NDI methods that are commonly used for weld inspection. Depending on their location and extent, kissing bonds can have a detrimental effect on fatigue life, impact properties and through thickness load carrying capacity. A third term frequently used with butt joints is joint efficiency. Joint efficiency is defined as the ratio $(F_{tu})_{joint}$ / $(F_{tu})_{base\ metal}$, expressed as a percentage. The ultimate strength of the base metal must be obtained in the same direction in which the joint is tested, using specimens from the same heat; base metal minimum (design)

strength should not be used here. Therefore, if the joint is tested in the longitudinal direction of the product, then the ultimate base metal strength in the longitudinal direction must be used. Similarly, the ultimate base metal transverse strength must be used if the joint is tested in the transverse direction of the product. Note that, so far, we have been referring to the longitudinal and transverse directions of the base metal product. There is also the issue of weld orientation with respect to test direction; i.e., the longitudinal-weld and transverse-weld testing

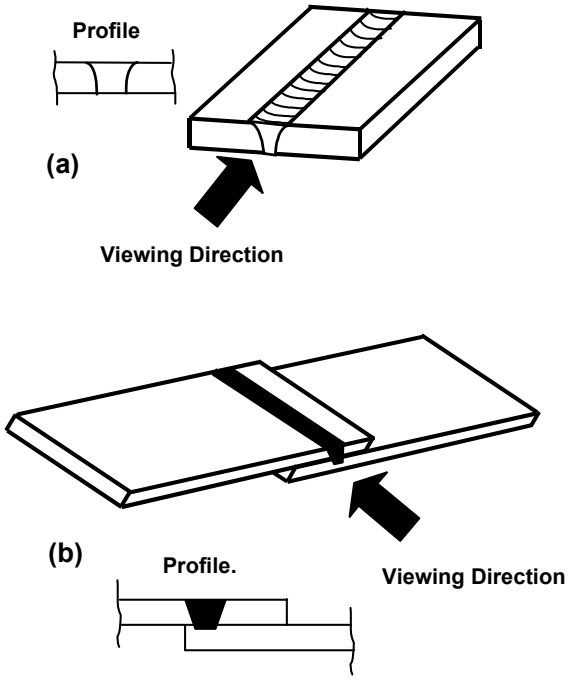

Figure 8: Joint Profile.
(a) Butt Joint.
(b) Single Lap Joint.

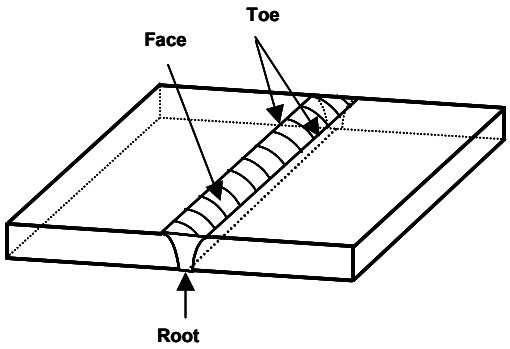

Figure 9: Face, root and toe of the weld.

configurations, to be discussed in section 5.7 and the Appendix. Figure 10 depicts the various weld orientation-working direction combinations in butt welded sheet and plate products. For dissimilar metal butt welding, joint efficiency is computed on the basis of the strength of the weakest member of the dissimilar couple.

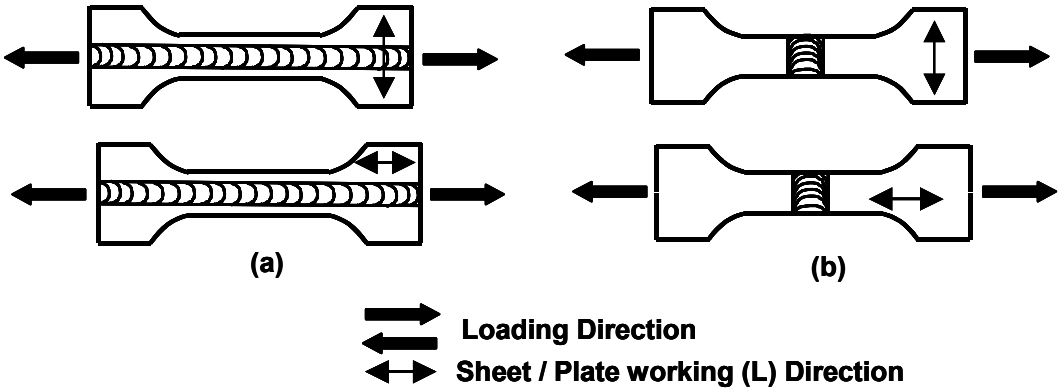

Figure 10: Tensile testing with respect to weld orientation in sheet and plate stock.
(a) Longitudinal weld orientation. Weld ∥ Loading Direction.
(b) Transverse weld orientation. Weld ⊥ Loading Direction

5.3 Joint Profiles & Weld Zones

The generalized profile of a butt joint, as proposed by TWI, [10] is an inverted trapezoid displaying four zones (Figure 11a). The first is the unaffected base metal, where no microstructural or property changes took place. The second is the heat-affected zone (HAZ), where the material experienced no plastic deformation but was influenced by the heat of welding, leading to some microstructural changes. The third is the thermo-mechanically affected zone (TMAZ), where the material has deformed and was also influenced by heat. Forth is the nugget, which is the recrystallized region of the TMAZ. The zones identified by TWI are by no means standardized throughout the community. For example, some authors [22] identify the nugget as the stir zone (SZ), while others [23] refer to it as the dynamically recrystallized zone (DXZ). Another example is the TMAZ, which is variedly referred to as the HDAZ (heat and deformation affected zone) [24] and the PRZ (partially recrystallized zone); [25] PRZ signifies that the zone contains both recrystallized and deformed but not recrystallized grains. TWI is in favor of classifying the TMAZ and the region under the shoulder as separate zones. Some authors, [26, 27] however, consider the region under the shoulder to be a region of rotation and, as such, they classify it as a part of the SZ, while others [28] seem to consider that the SZ consists of the nugget, TMAZ and the region under the shoulder.

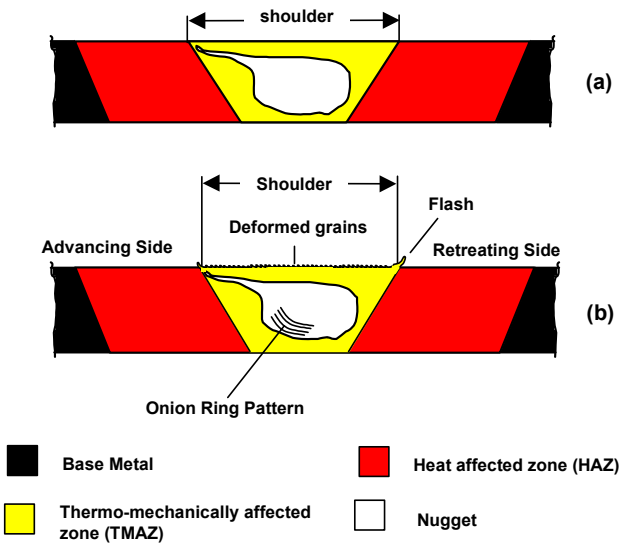

Figure 11: Generalized butt joint profile.
(a) Proposed by TWI.
(b) Modified by authors cited in the text.

Figure 11b incorporates some important features, reported by various authors, into the TWI-proposed joint profile. Specifically, these features are the deformed grains or swirl marks under the shoulder, [29] identification of the advancing and retreating sides, [30, 31] the weld flash [32] and the onion ring pattern. [30, 33] The figure now indicates the asymmetry of the nugget in that it extends more towards the advancing side. Although not depicted in Figure 11b, the widths of the TMAZ and HAZ on the advancing and retreating sides are typically not equal. Figure 11b also shows that the onion ring pattern is more prominent on the advancing side. Some authors, [34] however, report the onion ring pattern throughout the nugget. The onion ring pattern is simply a manifestation of banded microstructures brought about by the use of threaded pins; [30, 35, 36] the various types of pins are discussed in section 5.4.2. Some authors [30] indicate that the onion ring pattern has no effect on properties, while others [36] believe that it influences fracture. The swirl marks and weld flash depicted in Figure 11b can adversely affect fatigue performance and, as such, their removal may be required for some applications. Low plasticity burnishing has been proposed [37] as a means for this removal and, at the same time, to induce favorable residual stress fields.

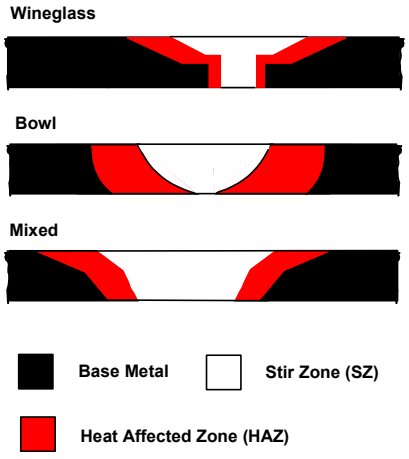

Figure 12: Other joint profiles reported by the authors cited in the text.

The inverted trapezoidal profile of the joint, shown in Figure 11, is brought about by tool geometry and the presence of the backup plate. [38] The broad base of the trapezoid corresponds to shoulder heating, whereas the narrow base corresponds to pin heating, as modified by the heat sink effect of backup plate. As will become evident later in this document, this type of joint profile has been reported for a wide range of alloys, particularly aluminum and magnesium alloys. Other profiles, however, have been reported in the literature. To illustrate, reference is made to Figure 12, which schematically depicts the bowl, wineglass and mixed joint profiles reported by Okada *et al*. [28] The joint profiles discussed here are, in principle, equally applicable to other types of joints. In fact, bowl type profiles have been reported in lap joints. [14, 39] It is important to note that in FSW, tool geometry has a profound effect on joint profiles and on the features within the weld zones; in fact, tool geometry can some times be gleaned from joint profile. This fact, in and by itself, makes it difficult to propose standardized joint profiles.

In some materials, such as alloy steels and most titanium alloys, the heat of welding can cause polymorphic changes. These phase transformations can in and by themselves cause recrystallization without strain. As a result, any TMAZ that might have formed will tend to recrystallize and, consequently, the HAZ / TMAZ boundary would become difficult to discern. Some materials, notably aluminum alloys and austenitic stainless steels, do not experience polymorphic changes and, as such, the TMAZ is frequently easy to discern. There is one case, [32] however, where no TMAZ was observed in an aluminum alloy.

5.4 Processing Variables

Joint profiles, microstructures and properties are governed by the thickness and material of the stock being welded and by choice of processing variables. Processing variables include the weld parameters (speeds, tilt, etc.), tool design (configuration and materials) and, in butt joints, even by the material and thickness of the back plate. Weld parameters and tool design, respectively, are discussed in 5.4.1 and 5.4.2. For more specific information, the reader is urged to consult TWI, their licensees or the various users listed in the publications cited in this document.

5.4.1 Welding Parameters

In reviewing the publications cited in this document, a multitude of welding parameters could be identified. These include rotational speed (rpm), travel speed, normal force, lateral force, tool attitude (tilt angle), shoulder plunge, penetration ligament (butt joints), penetration into the bottom member (lap joints); some of these parameters were defined in 5.2. Welding parameters are generally considered proprietary and, as such, are often fully or partially restricted from publication. Of those publications that disclose some weld parameters, only a handful mentions penetration ligament, shoulder plunge or tilt. The most widely disclosed and investigated parameters are the rotational and travel speeds. In general, slower travel speeds and lower rotational speeds are used for harder alloys or thicker sections. Increasing the rotational speed or decreasing travel speeds tends to increase heat input and welding temperatures. However, extremely high or low travel and rotational speeds can adversely affect properties. Nevertheless, the quest for increased travel speeds is relentless, due to economic pressures. The travel speeds quoted in this document do not exceed 51.18 in. / min. It is said, however, that machines capable of up to 100 in. / min are available on the market. In practice, weld parameters have to be adapted / optimized for the particular alloy type and condition / heat treatment, thickness of the stock being welded and the type of joint being produced. In this document, every effort will be made to quote whatever weld parameters published by the various authors cited.

5.4.2 Tool Design & Materials [4, 5, 12, 17, 20, 40]

In the early days of FSW, one-piece steel tools were used, and the pin was just a simple cylinder. This pin shape generated only limited material flow and mixing, and, as a result, the welding speeds had to be low. Tool design progressively evolved at TWI. Threaded pins were found to assist in ensuring that the plastically deformed workpiece material is fully delivered around the pin, and from the upper parts of the joint to the lower parts and vise versa. This enhanced mixing enables the use of higher speeds and results in better quality, void free welds. Threaded and fluted pins and frustum pins with flats were also found to enable higher speeds, more thorough mixing and better quality welds. It was also found that scrolled shoulders enable welding without tilting the tool and workpiece with respect to each other, which facilitates welding around corners. [17, 40] The scroll shoulder is also said to eliminate weld surface undercutting and the flash that extrudes under the tool shoulder, [12] and that it facilitates executing nonlinear welds. [40] It was TWI that introduced the frustum shaped pin and the use of grooves (flutes) or flats in addition to the thread forms, to assist in improving joint quality, especially for thick sections. [40] Other TWI improvements include the introduction of flat ended pins, [17] for better stirring action and weld penetration in butt joints, cooling of the tool, to increase its life and also improve weld quality in some applications, [40] the threaded conical pin [12] and the two-piece tool. [17, 41] The two-piece tool allows the use of pin materials suited for specific applications; e.g., a high temperature pin material to weld thick stock and / or high melting alloys [17] or a pin material that is resistant to embrittlement by Zn from 7xxx series aluminum alloys. [41] Figure 13 is a schematic depicting some pin and shoulder configurations from the various references cited herein. TWI has also introduced pins with a variety of sections other than circular (oval, paddle, etc.) to increase the volume of stirred material and improve weld properties. [12]

From one-piece steel tools to the two-piece design, progress continues into more advanced materials. Sorensen *et al*. [42] indicate that tools for FSW materials with high melting temperatures should resist physical and chemical wear, possess sufficient strength at elevated temperatures and effectively dissipate the heat carried to the tool during welding. The authors report that polycrystalline cubic boron nitride (PCBN) appears to be capable of meeting these requirements, since tools made from that material have been successfully used in FSW of AISI 316L and AISI 310 stainless steels and Alloy 600, a nickel-base alloy. PCBN is a super abrasive wear product primarily used for machining Ni-base superalloys, high strength ferrous materials and cast irons. It is made from

hexagonal BN under ultra-high temperature and pressure conditions. The resulting powder is consolidated by powder metallurgy techniques. Due to size and cost limitations, it is desirable to design the tools with PCBN shoulder and pin inserts, rather than fabricating the entire tool from PCBN.

Tool design (materials and configuration) is one of the most important factors that influence joint profile, microstructure and properties. Tool materials, apart from having to satisfactorily endure the welding process, affect friction coefficients, hence heat generation. The same is true for any coatings that might be applied to tool surfaces. Tool configuration influences joint size and profile. In general, pin length needs to be optimized around stock thickness. Furthermore, there appears to be optimal pin diameter / pin length and pin diameter / shoulder diameter ratios for each application. Pin length, configuration and diameter as well as shoulder diameter and configuration tend to dictate joint profiles and sizes and to also influence microstructures and properties. Tool design is probably the most guarded secret in FSW. Authors are generally reluctant to disclose tooling information. Every effort will be made in this document to list whatever tooling information disclosed by the various authors cited.

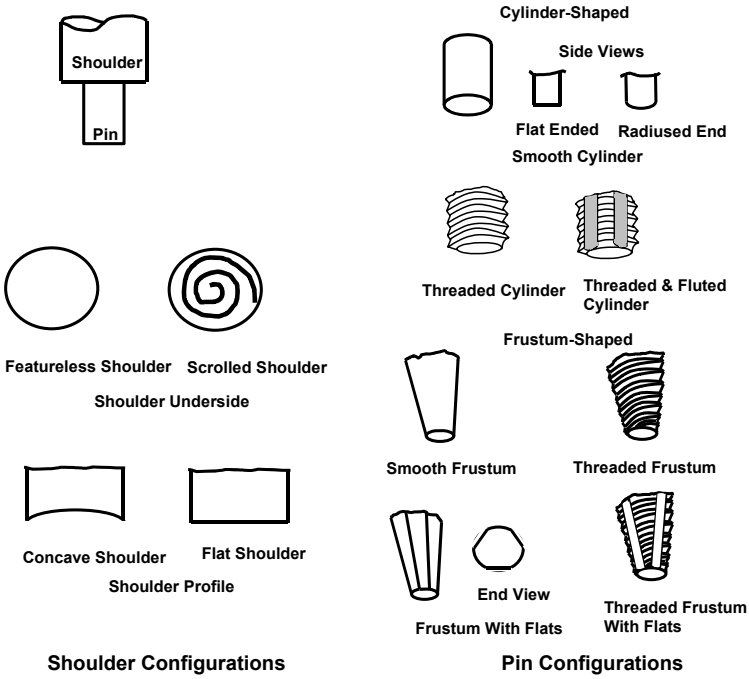

Figure 13: Some shoulder and pin configurations reported by the various authors cited in text.

5.5 Joint Microstructures

One of the key factors that control joint microstructures is the temperature generated during welding. Therefore, temperature determination in the weld joint is of interest in understanding joint microstructures and properties. Surface temperature measurements can be made by pyrometers; in FSW steels, visible color changes can be observed by the unaided eye. Surface and interior temperature measurements can be made by using thermocouples attached to the surfaces or interior; the attachment method is usually by insertion through drilled holes. In locations such as the nugget and region under the shoulder, where metal movement / flow takes place, it is not possible to directly measure temperatures by thermocouples. Pyrometers are of no use here either, since these locations are obstructed from view either by the shoulder or by other metal layers. As a result, researchers revert to computer modeling. The problem is that the models used generally assume that temperature distribution at the advancing and retreating sides are symmetrical. Actual measurements, however, reveal that the temperatures of the advancing and retreating sides are not the same. It makes sense to assume that greater heat inputs, hence higher temperatures, are generated at the retreating side of the weld, due motion in opposite directions. Maeda *et al*., [43] however, indicate that whether the retreating or advanced side would be hotter depends on welding conditions. This aside, the peak temperatures measured tend to increase with increasing the rotational speed, [44] decreasing the travel speed [44, 45] and decreasing section thickness. [45]

The information presented in the publications reviewed in this document indicate that, FSW generates sufficiently high temperatures, at least in some locations, to affect austenitizing in steels or re-solutionizing of the hardening phases in heat treatable nonferrous alloys. These temperatures are also thought to be sufficiently high to cause recovery and recrystallization. It is said that FSW involves dynamic recrystallization (DRX) and / or dynamic recovery (DRV); the term dynamic signifies that the process is coincident with deformation. There is debate, however, as which process is operating in which zone or region, and some authors even argue that superplastic forming is involved. This aside, as the tool passes away, the welded volume will cool to ambient temperature at a net rate that is controlled by the surrounding base metal and atmosphere, the back plate in butt joints, as well as by the back heating by the tool. During cooling, some tempering / aging can take place due to back heating and, in addition, static recrystallization (SRX) and recovery (SRV) can also become operative; the term static signifies that no deformation is involved. The matter is further complicated by the fact that the recrystallization and recovery processes are not controlled only by temperature, but also by the strain and strain rate. Lienert *et al*. [46]

cited several investigations that indicate that the strains, strain rates and temperatures experienced at the nugget are higher than those experienced at the TMAZ; the HAZ experiences the least temperatures and the least, if any, strains and strain rates. It reasonable to assume that the region under the shoulder experiences temperatures, strains and strain rates that are similar, if not higher, than those experienced at the TMAZ. Ultimately, for a given base metal stock, the temperatures, strains and strain rates are all controlled by the welding parameters and tool design.

The microstructures observed at room temperature will depend on a complex interaction between the aforementioned factors, parameters and processes. This is not all, however. There is one more complication brought about by the existence of temperature, strain and strain rate gradients, hence microstructural gradients, across the width, depth and length of the weld. In other words, rather than speaking of a typical microstructure within a zone, one should speak in terms of a typical microstructure at a given location within that zone.

Based on the above, it seems that the characterization of the flow processes, strains and strain rates involved in FSW is an important prerequisite to understanding the mechanics and dependencies of microstructural evolution throughout the joint. This said, there appears to be ongoing efforts to understand the flow / deformation behavior, using the embedded marker technique [11] and SEM orientation mapping by backscattred [33, 47] and secondary [30] electrons. It was not possible, however, to find publications regarding the characterization of strains and strain rates for the review presented herein. The situation was best summed up by Schneider and Nunes, [30] who state that, in FSW " the metal is subjected to thermomechanical processing in which the temperature, strain and strain rate are not completely understood."

5.6 Advanced FSW Concepts

There is considerable interest in executing circumferential welds, for civil, space and military applications. Orbital welding equipment and procedures have been developed for just such purpose. [48, 49] Closure of the end keyhole has always presented a problem in this regard. There is also increasing interest in welding tapered sections and complex (3-dimensional) shapes. [18, 27] To address these issues, advanced processing concepts have been sought. These include the retractable pin tool (RPT) and the self-reacting tool.

An RPT was developed at NASA [20, 50] to automatically retract the pin at the end of the pass, so as to affect keyhole closeout. This tool would enable the execution of circumferential and tapered section butt welds and the performance of repairs in existing welds. A similar concept was developed independently, in Europe and used for spot welding. [51, 52] RPT aside, Sato *et al*. [53] report on a self-reacting tool, and indicate that the concept was introduced in the original TWI patent and that it was demonstrated by Boeing. The self-reacting tool employs two tool pieces; one tool piece is placed on one face, and the other on the opposite face. The tool pieces are rotated by the same spindle, in the same direction. The opposing forces balance, simplifying the backup tooling used for inner support in circumferential and longitudinal welds in tanks. The self-reacting tool is also effective in preventing kissing bonds, due to heat input from the backside. A start hole needs to be drilled, but that can be filled by a return pass. An end keyhole, however, remains at the end of the pass and it has to be filled by some means; e.g., plug welding.

Another novel FSW processing concept is laser assisted FSW (LAFSW). [54, 55] Here, the heat required for welding is supplied by a laser, rather than by friction. This is said to involve equipment that are less massive and less expensive than those used in conventional FSW. To conclude this section, it is noted that, due to the versatility and adaptability of FSW, it was evaluated as a potential repair method for existing welds by both Airbus [56] and TWI. [57]

5.7 Mechanical Testing of Welded Joints

Butt joints may be tested to generate tensile, fatigue, fracture mechanics, shear, bend, and impact data. Tensile and fatigue testing may be transverse or longitudinal with respect to the weld. Specimens may also be excised from certain regions to generate region-specific data. The term "joint efficiency," used in conjunction with the ultimate strength of butt joints had been defined in section 5.2. Testing to generate fracture mechanics data, such as crack growth rates, is performed using the compact tension specimen. The notch may be aligned with any direction of interest to generate region-specific data. Ultimate shear strength data can be generated by single-shear testing, using a specimen that contains side notches to guide fracture along a "shear path." This test is ideal for generating region-specific data, simply by placing the shear path at the desired location, along the direction of interest. Bend testing is used to provide qualitative information about longitudinal and transverse joint ductility. Impact data is typically generated using the Charpy (V-notch) specimen. Here, the notch may be aligned with any desired direction, to obtain region-specific information. Lap and spot joints may be tested by

tension-shear, to generate strength or fatigue data, or by peel to generate strength data. A brief account of weld joint mechanical testing is presented in the Appendix.

6.0 REVIEW OF BUTT JOINT PUBLICATIONS

The bulk (about 85%) of the publications reviewed in this document pertain to butt joints. Unless otherwise stated, all joints were square, i.e., without grooves or any other faying surface preparation. Furthermore, the majority of the publications reviewed investigate FS welded joints in the as-welded condition, without subsequent heat treatment. This is because post weld heat treatments that involve fast cooling / quenching are objectionable for most, if not all, applications, due to the associated distortion. Even heat treatments that involve no fast cooling / quenching, such as aging, tempering, annealing or stress relief may not be a practical choice for certain applications.

Sections 6.1-6.5 are each devoted to a particular alloy group. Specifically, section 6.1 is for aluminum alloys, section 6.2 for magnesium alloys, section 6.3 for ferrous alloys (steels), section 6.4 for titanium alloys, and section 6.5 for copper alloys. Section 6.6, by contrast, is devoted to dissimilar-metal group welding. As much as possible, the publications will be reviewed in chronological order. In general, the tensile properties obtained in the various investigations will be expressed in terms of their base metal counterparts. Specifically, joint ultimate strength will be expressed in terms of joint efficiency (defined in section 5.2), whereas joint yield strength and elongation will be expressed as percentages of their base metal counterparts. Joint fatigue, shear, hardness and other properties will be expressed in qualitative terms in comparison with the base metal. For dissimilar-metal group welding, the properties of the weaker metal of the couple will be considered as a baseline. The topic of mechanical testing of welded joints has been introduced in section 5.7 ad the Appendix.

6.1 Aluminum Alloys

Aluminum alloy sheet and plate stock up to 1 in. thick has been butt welded by FSW. It is reported that 3 in. thick plate stock was butt welded by FSW, using two passes (double-sided joint configuration, Figure 14). [5] It is also reported that a machine exists that is capable of welding 2 in. thick plate in one pass. [58] Based on the arguments in section 5.5, it is reasonable to assume that FSW generates temperatures around those required for solution heat treatment of heat treatable alloys, especially in the nugget and TMAZ. Subsequent cooling, if sufficiently fast, can lead to the retention of supersaturated solid solutions that can naturally age. Even if some aging occurs during cooling, the remaining supersaturated solid solution would still naturally age at ambient temperature. As indicated in section 5.5, post weld heat treatments are generally objectionable or impractical. Thus, the majority of publications reviewed here investigate joints in the as-welded condition, without subsequent heat treatment. This would present a problem for 7xxx and certain other alloys, due to their tendency to naturally age for extended periods of time (see section 4.3). Every effort will be made here to flag potential natural aging concerns in the various publications.

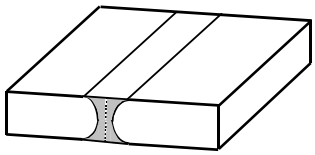

Figure 14: Double-sided joint configuration. Joint is welded with 2 passes, one from each side.

In what follows section 6.1.1 will focus on same-metal welding; i.e., welding of a given aluminum alloy to itself. The various alloys are arranged according to their particular group; viz., 2xxx alloys (6.1.1.1), 5xxx alloys (6.1.1.2), 6xxx alloys (6.1.1.3), and 7xxx alloys (6.1.1.4). The work pertaining to each particular alloy is presented under a separate heading. Section 6.1.1.5 reviews those publications where the authors investigated same-metal welding of more than one alloy in the same work, with the specific intent of comparison. Finally, section 6.1.2 deals with work on dissimilar aluminum alloy welding.

6.1.1 Same-Metal Welding

The discussions presented in section 5.5 indicate that it is reasonable to assume that the weld nugget will display recrystallized microstructures. This would be true for heat treatable and non-heat treatable alloys. In addition, for heat treatable alloys, the FSW temperatures reached within the nugget and parts of the TMAZ will cause at least partial dissolution of the hardening phases. Ordinarily, therefore, some softening within the nugget should be expected in heat treatable alloys that were welded in -T tempers. Some grain coarsening and softening could also take place in the HAZ. The microstructure of the HAZ should transition the base metal into the TMAZ, which, in turn, should transition the HAZ into the nugget. The trends just indicated would tend to give rise to a W-shaped hardness distribution, across the joint profile (defined in 5.2), with minima in the HAZ around the HAZ / TMAZ interface, as shown in Figure 15 (a). Here, the nugget hardness, depending on the alloy and temper, could range from just above the HAZ minima to values approaching that of the base metal. In some cases, depending on the

welding conditions, the reported hardness distributions display nugget hardness values higher than anywhere else, including the base metal, Figure 15 (c). It appears that whether the nugget hardness is below, close to, or above that of base metal is a function of temperature, strain, strain rate and the onset of aging, during cooling to ambient temperature. Hardness distributions similar to those of Figure 15(a) and, to a lesser extent, Figure 15 (c) have been reported for the vast majority of 2xxx, 6xxx and 7xxx alloys welded in some -T temper and tested in the as welded condition. The same is true for the hardness distributions reported after natural or artificial aging of the joints. In the strain hardened tempers of the non-heat treatable alloys, such as 5083-H131, recrystallization in the nugget, during FSW, would eliminate some or all of the cold work effects. This, in turn, would lead to nugget softening and the development of as welded hardness distributions similar to that depicted in Figure 15 (b). The opposite is true for the annealed tempers of these alloys, such as 5083-O, where the grain refinement associated with recrystallization, would lead to increasing the nugget hardness and the development of as welded hardness distributions similar to that depicted in Figure 15 (d). This same type of hardness distribution has also been reported for 7050 that was re-solution heat treated and artificially aged to the -T74 temper. Here, it appears that the re-solution heat treatment and aging have obliterated the HAZ minima, while the grain refinement in the nugget led to some hardening. As such, the hardness distribution of Figure 15 (d) could be regarded as a special case of that depicted in Figure 15 (c). Finally, the seemingly odd hardness distribution depicted in Figure 15 (e) has been reported for 7075-T76, in the as welded condition. This distribution, however, could be regarded as a special case of that depicted in Figure 15 (b).

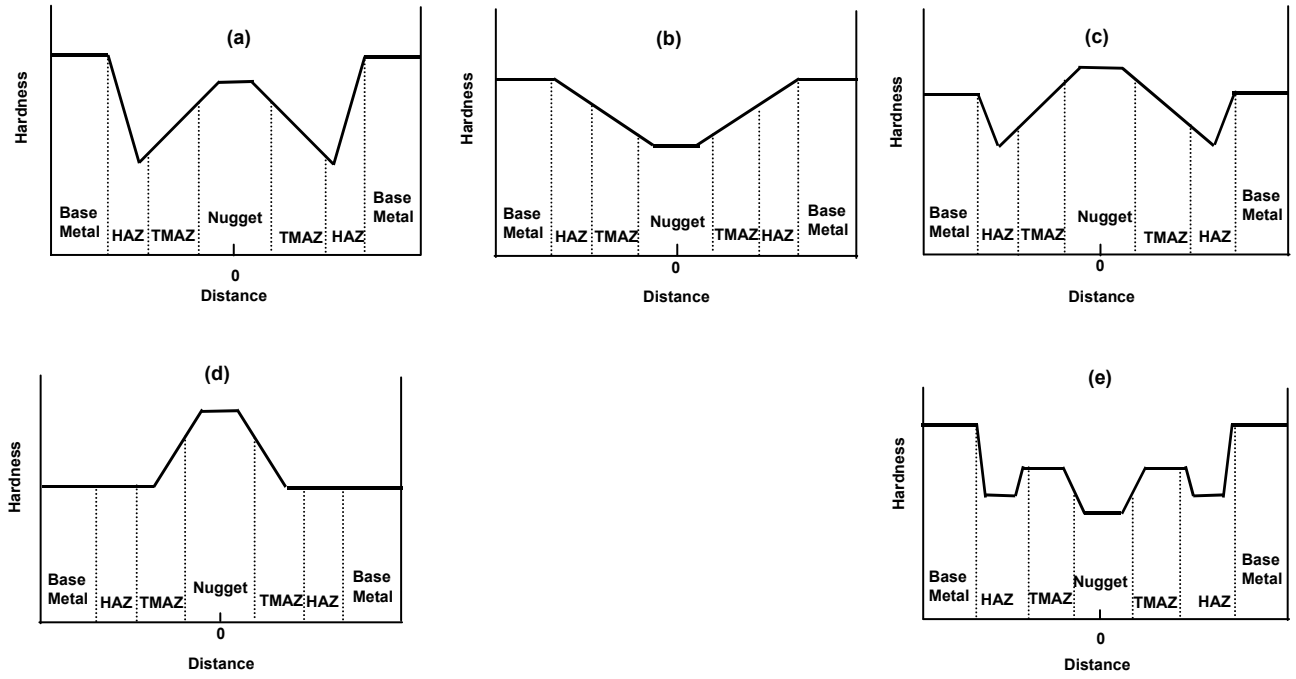

Figure 15: Hardness distribution trends across butt joint profiles. Zone boundaries are approximate.

Due to the asymmetry of the weld zones with respect to the weld centerline and mid-thickness plane, the hardness distribution is expected to vary with depth; i.e., the hardness distribution at the face of the weld would be different from that at mid-thickness or that at the root. It is important, therefore, to indicate the location of the distribution with respect to some fixed reference, such as mid-thickness, face or root. This is especially so when comparisons are being made. Frequently, however, authors fail to do so.

In general, the ultimate and yield strengths in the various zones duplicate the hardness trend. The % elongation, by contrast, displays the opposite trend. Butt joint tensile strength typically decreases with stock thickness. Tensile failures of butt joints usually take place at locations corresponding to hardness minima, such as those in the HAZ or nugget, if these exist. Failures may also occur around the weld centerline, due to thinning under to tool shoulder, or at defects or weld imperfections.

6.1.1.1 Aluminum 2xxx Alloys

This section contains data concerning alloys 2013, 2014, 2024, 2095, 2195, 2219 and 2519. Section 6.1.1.5 contains additional data on alloys 2014 and 2024.

(a) AA 2013

Tanaka *et al.* [59] investigated the effects of rotational speed on the properties of FS welded 0.16 in. thick AA 2013-T4511 sheet. The rotation speed was varied in the 500-3000 rpm range, while keeping the travel speed constant at 9.85 in. / min. No other processing details were disclosed, and the authors did not indicate the welding direction or publish a joint profile depicting the various zones resulting from FSW. After FSW, the material was aged at 383 F for 8 hr. [b] The temperatures generated during FSW were measured, apparently on the surface, at set intervals from the weld centerline; the specifics, however were not published. The peak temperature measured increased with rpm to a maximum of about 968 F at 2000 rpm, then dropped with further rpm increases. [c] The grains in the stir zone generally coarsened with temperature increase. The authors seem to indicate that the stir zone reached the solution treatment temperature, especially at the higher rpm values. Post weld aging increased stir zone hardness. The increase was more pronounced at rpm values > 1000 and mostly insignificant at rpm values ≤ 1000. At 1500 rpm, the peak stir zone hardness approached that of the base metal. Aging had little to no effect on HAZ hardness at all speeds. The authors indicate that the HAZ was overaged. In the aged condition, hardness distribution across the joint profile, at mid-thickness, was similar to Figure 15 (a). For welds performed at 1000 and 1500 rpm, tensile testing transverse to the weld resulted in HAZ failures, with joint efficiencies around 82%. Electrical conductivity generally decreased as the rpm increased, with peak conductivity occurring within the stir zone. Alloy microstructures were investigated, using TEM.

(b) AA 2014

Strangwood *et al.* [60] investigated FS welded 0.25 in. thick 2014-T6 plate (UK alloy similar to AA 2014). Welding was performed at 3.14-4.62 in. / min. No other weld parameters or tooling information were disclosed, and the authors did not indicate the welding direction was or publish a joint profile. After FSW, the material was aged at 320 F for various periods, up to 80 hr. The authors show hardness distributions, across the joint profiles, obtained after various aging times; the authors, however, did not report the locations were the microhardness data were obtained. Nugget hardness increased with aging time up to 18 hr, then decreased. Hardness minima existed in the HAZ. The published hardness distributions displayed considerable scatter and, as such, no trends could be reported here. Re-solutionizing and aging appeared to even out the hardness distributions. It should be noted that any hardness changes reported by the authors could be the result of location shift, rather than changes in aging time or temperature. Alloy microstructures were investigated, using TEM; a TEM study of alloy 7075 (similar to AA 7075) was also included.

(c) AA 2024

Biallas *et al.* [34] investigated the effects of travel speed on the tensile, fatigue, and corrosion properties of FS welded AA 2024-T3 sheet; 2024 is a European equivalent of AA 2024. Two thicknesses were investigated; viz., 0.063 and 0.16 in. The travel (v) and rotational (ω) speeds were varied in the 3.14-9.45 in. / min and 800-2400 rpm range, respectively, while maintaining a constant ω / v ratio of 10 (in SI units). No other weld parameters, tooling information or joint profile were published. It appears that welding was performed parallel to the working (L) direction for the 0.063 in sheet, and transverse to that direction (i.e., in the T direction) for the 0.16 in sheet. There were no post-weld heat treatments and it is presumed here that testing of the FS welded joints was performed after all natural aging had seized. Tensile and fatigue testing were performed transverse to the weld in all cases. The yield and ultimate strengths increased as both ω and v were increased at the constant ratio of 10. The authors explain this trend in terms of microstructure, as it is influenced by the temperatures attained during FSW and the cooling rates thereafter. Joint efficiencies of 90-98% were obtained for the 0.063 sheet, compared to 82-87% for the 0.16 sheet. [d] The yield strength of the FS welded joints ranged from 90-98% and 66-72% that of the base metal for the 0.063 and 0.16 sheets, respectively. The elongation of the joints ranged from 30-52% and 44-54% that of the base metal for the 0.063 and 0.16 sheets, respectively. Tensile failure locations were not clearly stated. Fatigue strength increased with increasing both v and ω at the constant ratio of 10. For the 0.16 in sheet, the endurance limit was about 80% of its base metal counterpart. The fatigue properties of the 0.063 in sheet appeared to involve lesser debit than the thicker one. The authors point out some geometric features that influence fatigue crack initiation. Specifically, in the 0.063 in sheet, FSW led to a reduction in sheet thickness

[b] *This would bring the –T4511 material to the –T6511 temper.*
[c] *The peak temperature measured is not necessarily the highest temperature developed during welding (see 5.5).*
[d] *The different joint efficiencies obtained for the two sheet stocks could, at least in part, be due to the fact that welding was performed in different directions.*

below the shoulder, whereas in the 0.16 in sheet, the material below the shoulder became thicker. In either case, steps formed at the advancing and retreating sides, Figure 16. Fatigue crack initiation in the 0.063 in sheet, took place at the location where thickness was reduced below the initial thickness. Crack initiation in the 0.16 thick sheet occurred at the higher of the two steps. Corrosion testing revealed that FSW leads to severe exfoliation corrosion in the weld region; it is assumed here that the weld region means the nugget, TMAZ and HAZ. The authors report that there was no increased stress corrosion cracking sensitivity as a result of FSW.

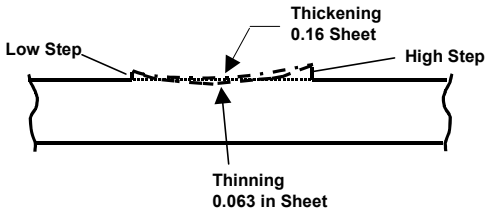

Figure 16: Surface geometry.

Talwar *et al.* [16] investigated the tensile properties of FS welded 0.08 in. thick AA 2024-T3 sheet. No weld parameters or tooling information were disclosed, and the authors did not indicate the welding direction. It is presumed here that testing was transverse to the weld and that it was performed after all natural aging had seized. The as welded joint efficiency was about 73%. The yield strength and elongation of the FS welded joint were about 91 and 10% their counterparts in the base metal. After machining 0.020 in off the root side, the joint efficiency increased to about 88% and the elongation also increased to about 41% of its base metal counterpart. The yield strength, however, remained essentially unchanged. The aforementioned percentages are based on the base metal properties published by the authors. Tensile failure locations were not disclosed.

Zettler *et al.* [26] investigated the effects of rotational speed on microstructure, hardness and tensile properties of FS welded 0.16 in. thick AA 2024-T351 sheet; 2024 is a European equivalent of AA 2024. These authors also investigated the peak temperatures generated during welding; the specifics of how this was done were not disclosed. Three travel speeds (3.94, 7.87 and 15.75 in. / min) were used, while maintaining the rotation speed fixed at 800 rpm. Two shoulder configurations, having the same diameter (0.59 in.) were used; viz., the concave shoulder (shoulder 1) with 2.5^{O} tilt and a normal force of 2698 lbf, and the scroll (spiral) shoulder (shoulder 2) with 0^{O} tilt and a normal force of 2023 lbf. Three pin designs were used; viz., frustum, frustum with threads and frustum with threads and flats. Figure 13 depicts illustrations of various pin and shoulder configurations. No welding direction was indicated. There were no post-weld heat treatments, and it is presumed here that testing of the joints was performed after all natural aging had seized. The data reported are generally for shoulder 1. Based on their temperature measurements, the authors argue that joint temperatures, whether the advancing side is hotter or cooler than the retreating side and, ultimately, microstructure and properties are not governed solely by the travel speed but also by pin configuration. The frustum pin produced a volumetric defect and also, at the lowest speed, some thinning. No volumetric defects or thinning were noted when using the other pin configurations. Lack of penetration, however, was noted when using the frustum pin with the threads, but only at the highest speed. The frustum pin with the threads and flats produced the largest and most symmetric nugget at all speeds, especially when used in conjunction with the scroll shoulder. Microhardness traverses across the joint profile, at various depths, generally show trends similar to that depicted in Figure 15 (a). Higher travel speeds generally gave rise to higher hardness values. For the frustum pin with threads, joint ultimate tensile strength and % elongation peaked at the intermediate speed. The yield strength, however, progressively decreased with increasing the speed. For the frustum pin with threads and flats, joint ultimate and yield strengths and the % elongation progressively increased with increasing the travel speed. The joint efficiencies reported by the authors were in the 68-97% range. The authors used computer tomography to study material flow via embedded markers technique.

Bussu and Irving [61] investigated the fatigue properties of FS welded 0.25 in. thick 2024-T351 plate; 2024 is a UK alloy similar to AA 2024. Welding was performed parallel to the rolling direction; no weld parameters or tooling information were disclosed. The joint profile was similar to that proposed by TWI, Figure 11 (a), except that the nugget was referred to as the dynamically recrystallized zone; weld flash was also present at the face of the weld, see Figure 11 (b). No post weld heat treatments were used, and it is presumed here that testing was performed after all natural aging had seized. Hardness distribution across the joint profile at mid-thickness was similar to that depicted in Figure 15 (a). Longitudinal and transverse fatigue samples were prepared and tested in axial fatigue (R=0.1). The samples were tested in the as welded condition and also after skimming, to remove about 0.020 in. from each of the face and root surfaces. S-N curves were generated; all curves showed a pronounced knee. The as welded samples exhibited significant degradation in fatigue performance, compared to the base metal, especially in the high cycle (low stress) regime. The longitudinal samples fared somewhat better than the transverse ones. Transverse sample fractures initiated at the weld flash, whereas longitudinal sample fractures initiated at the semicircular tool marks on weld face (Figure 6). Skimming removed all profile irregularities, including the tool marks and weld flash. The result was a dramatic improvement in fatigue performance. Performance of the transverse samples now was somewhat superior to that of the longitudinal ones, approaching that of the base metal. The skimmed transverse samples failed at the HAZ, near the hardness minima and oxide particles. The longitudinal samples failed in the parent metal and at the ends of the gage length.

Hannour *et al.* [62] investigated the corrosion behavior of FS welded 0.25 in. thick AA 2024-T351 plate, using the salt spray test (ASTM G 85) and immersion in various corrosive environments; no weld parameters or tooling information were disclosed. Microstructural characterization was performed using TEM and SEM-EDS. The authors report that the HAZ, adjacent to the TMAZ, was the most susceptible area to corrosive attack and that this attack was predominantly intergranular. The authors observed that an earlier study of FS welded 0.16 in. thick sheet [34] reported that the nugget and TMAZ were the most susceptible to corrosion. Based on that observation, the authors suggest a dependence of corrosion behavior on stock thickness.

In an investigation of dynamic compressive properties, Chao *et al.* [63] FS welded 0.374 in. thick AA 2024-T3 plate, using a tool made of tool steel, with a threaded pin. The following tool dimensions were disclosed: shoulder diameter, 1.1 in.; pin diameter, 0.394 in., and; pin length, 0.295 in. Welding was performed at 215 rpm and 4.4 in. / min travel speed. No post weld heat treatments were used. The hardness distribution across the joint profile was similar to that depicted in Figure 15 (a). The authors, however, did not disclose the location where the hardness readings were obtained, and it is presumed here that hardness testing was performed after all natural aging had seized.

Kumagai *et al.* [64] investigated the tensile properties of FS welded 0.16 in. thick extrusion of alloy 2024-T51 extrusion. The chemistry of the alloy, published by the authors indicates that it is similar to AA 2024 and it could very well be the Japanese equivalent, A 2024. The material was extruded in house and then solution treated, stretched and naturally aged to produce the -T351. FSW was performed using a tool with simple cylindrical pin, a rotation speed of 800 rpm and a travel speed of 4.9 in. / min. The authors did not disclose any other weld parameters or tooling information, and they did not indicate the welding direction. Following FSW, the samples were naturally aged for 96 hr. Tensile testing transverse to the weld indicated a joint efficiency of about 83%. The joint yield and elongation were, respectively, about 79 and 19 % those of their base metal counterparts. The aforementioned percentages are based on the base metal properties published by the authors. The study also includes some fatigue data that some readers might wish to review.

(d) Weldlite 2095

In a study of superplastic properties, Salem *et al.* [22] FS welded 0.064 in. thick Weldlite 2095 superplastic sheet; Weldlite 2095 is an Al-Cu-Li alloy, produced by Reynolds Metal Co. Welding was performed parallel to the rolling direction, using a threaded pin tool (pin and shoulder diameters 0.15 and 0.40 in., respectively), travel speeds in the 5-9.7 in. / min range, and a rotational speed of 1000 rpm. Four zones were reported: a stir zone that corresponds to the pin diameter, along the weld centerline; a swirl zone, within the stir zone, resulting from material flow between the threads, extending towards the advancing side; a TMAZ, and; a HAZ. [e] No elliptical nugget was reported, and the authors attribute that to the thin gage of the stock used. Welds performed at faster travel speeds (low heat input), referred to as cold welds, had finer grain structures.

(e) Alloy 2195

Alloy 2195 is an Al-Li alloy produced by Pechiney Rolled Products. Occasionally, unfamiliar temper designations are used with this alloy. For example, -T8P4 designates a plant-produced -T8 temper # 4. Similarly, -T8A3 designates heat treatment by the producer to the -T8 temper. Access to information pertaining to this alloy appears to be very restricted. Interest in this, and other Al-Li alloys, generated a need to investigate the FSW characteristics of these alloys.

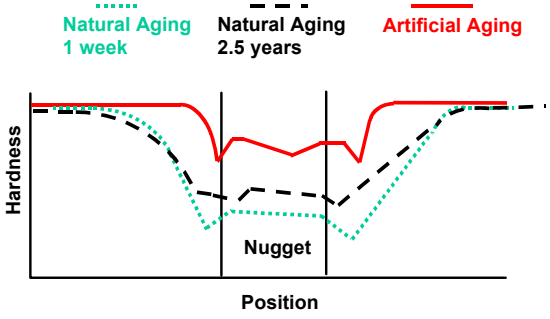

Figure 17: Hardness distribution across the joint profile after various aging treatments. AA 2195.

Litwinski [8] investigated the effects of travel speed and post-weld natural and artificial aging on the tensile properties of FS welded 0.25 in. thick alloy 2195-T87 (-T8A3) plate. No weld parameters, tooling information or weld direction were disclosed. After FSW, the joints were either naturally aged for various lengths of time, ranging from 1 hr to over 2 years, or artificially aged. It was reported that natural aging continues for as long as 2.5 years in this alloy. This is shown in the hardness distribution schematic of Figure 17, which reflects trends similar to that shown in Figure 15 (a). Tensile samples were prepared (presumably transverse to the weld) and then the root and face were skimmed, to remove 0.020 in, so as to eliminate weld flash, root notches and similar defects. In general, longer natural aging

[e] *The quality of the micrographs in the publication was such that it was not possible to discern the various zones for a schematic rendering here.*

times resulted in higher joint ultimate and yield strengths as well as higher % elongation values. Artificial aging further increased the strengths, but at a sacrifice to elongation. The ultimate and yield strengths, for both the naturally (3 months) and artificially aged joints increased with travel speed, but the effect diminished at the higher speeds. Higher speeds were also accompanied by an increased likelihood of a root notch defect. The improvement in strength with higher speeds was explained in terms of the increased cooling rates, associated with increasing the speed. The author argues that increasing the cooling rate limits the time spent at temperature, which, in turn, leads to the observed improvement in properties. To produce uniform properties across the joint profile, samples were re-solution treated and aged according to accepted procedures. The re-solution treatment, however, led to undesirable abnormal grain growth in the weld nugget. This growth was rationalized in terms of a critical amount of cold work, induced by FSW. [f] A proprietary process was used to increase the weld temperature and minimize the cold work and the attendant abnormal grain growth. In other results, it was found that increasing travel speed, in the range studied, had negligible effect on the peak temperatures measured; measurement locations, however, were not reported. One of the published micrographs shows an elliptical nugget with symmetrical onion ring pattern, contrasting the skew pattern shown in Figure 11 (b).

Colligan *et al.* [40] investigated the effects of rotational and travel speeds on the transverse tensile properties and hardness distribution in FS welded 0.72 in. thick alloy 2195-T8P4 plate. Two rotational speeds, 200 and 230 rpm, were used and the travel speed was varied in the 1.2- 3.7 in. / min range. Welding was performed using a 2-piece tool with an H13 tool steel shoulder and an MP159 pin. The pin was not cylindrical and it had a flat end; possibly, a frustum pin was used. The tool was not tilted during welding, suggesting that a scroll shoulder was used. Some shoulder and pin configurations are depicted in Figure 13. No other weld parameters or tooling information were disclosed, and the authors did not indicate a welding direction. There was no heat treatment subsequent to welding. The joint profile reported depicts a nugget that is contacting the root side, a feature that was attributed to the flat-ended pin configuration. The tensile test results show that the ultimate tensile strength of the joint initially increases somewhat with increasing travel speed and then either levels out (230 rpm) or slightly decreases (200 rpm) with further increases in travel speed. The data presented suggest that joint efficiency ranged from 58-66%; the authors state that the joint strengths obtained are among the highest obtained for aluminum alloys. The yield strength of the joint increased with travel speed for both the rpm values used. In general, the effect of travel speed on the ultimate and yield strengths was not pronounced. The % elongation of the joint, while always lower than that of the base metal, increased or decreased with travel speed and no specific trends could be discerned. It is stated that most tensile specimens fractured along the plane of maximum shear on the retreating side. The exceptions were those specimens welded at the highest and lowest travel speeds at 200 rpm, which fractured across the face of the weld. The authors, however, did not provide sufficient information or any graphics to assist in visualizing fracture locations. The hardness distribution across the joint at various depths, Figure 18, reflects the trend shown in Figure 15 (a). Figure 18 also shows that moving closer to the face of the weld, the harness minima in the HAZ are pushed outwards, as a result of the weld being wider at the face than at the root. Clearly, a hardness gradient exists not only across the weld profile but also through the thickness (depth) of the joint.

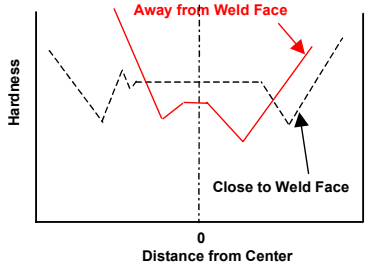

Figure 18: Hardness distribution across the joint profile close to and away from the weld face. AA 2195.

Schneider and Nunes [30] investigated metal flow during FSW of 0.323 in. thick alloy 2195-T81 plate, using grain orientation (orientation image mapping). This is a simpler technique than the commonly used marker method [11] which is tedious to execute and often difficult to interpret. Welding was performed along the rolling direction, at 200 rpm and 6 in. / min, using a tool with a 1.2 in. diameter shoulder and a threaded cylindrical pin that is 0.312 in. long and 0.5 in. in diameter. The tool was tilted at a 2.5^{O} angle. The resulting joint profile was similar to that proposed by TWI, Figure 11 (a). The authors here did not use the terms stir zone and nugget interchangeably. Rather, the stir zone is said to include the nugget, which is referred to as the dynamically recrystallized zone. As to what else constitutes the stir zone is not clear, but it could be the region under the shoulder; the authors consider the TMAZ a separate zone. The nugget was shown to display the onion ring pattern, which is a series of concentric bands or rings that are more pronounced on the advancing side than on the retreating side, Figure 11 (b). The authors indicate that ring spacing is typically the same as the distance traversed during a single tool revolution. The authors further indicate that the onion ring pattern tends to disappear at higher rpm, and that its

[f] *Small amounts of residual strains, remaining after FSW, could lead to abnormal grain growth by secondary recrystallization, during subsequent soaking at elevated temperatures, such as those used for solution treatment. In such cases, only a few grains would experience grain growth to exceptionally large sizes. Increasing the FSW temperature would reduce residual strains, thereby decreasing the likelihood of abnormal grain growth during subsequent solution treatment.*

presence does not affect properties. The authors conclude that the rings (bands) represent two distinct regions of fine recrystallized grains, the first having random orientation and the second having a preferred orientation.

Oertelt *et al.* [23] investigated the macro / microstructure and hardness distribution in FS welded 0.23 in. thick alloy 2195-T8 plate. FSW was performed at 3.75 in. / min travel speed and 200-250 rpm rotation speed, using a tool with pin and shoulder diameters of 0.43 and 1.1 in., respectively, a pin height of 0.31 in. and a penetration ligament (see 5.2) of 0.007 in. No other processing or tooling information were disclosed. A joint profile and weld zones similar to those proposed by TWI, Figure 11 (a), were reported, except that the nugget was referred to as the dynamic recrystallization zone (DXZ). The hardness distribution across the joint profile was similar to that depicted in Figure 15 (a); the authors, however, did not indicate the location where the hardness readings were obtained. The as welded microstructure of the DXZ displayed fine equiaxed grains, with evidence of supersaturation (i.e., as in the solution treated and quenched condition). The authors believe that some precipitation took place during FSW; the authors most likely mean that precipitation took place during cooling to ambient temperature. The TMAZ displayed elongated grains. The effect of thermal cycling on the DXZ was studied. Microstructural characterization was performed using OM, SEM-EDS and TEM.

(f) AA 2219

To generate data for welding of tanks using the self-reacting tool mentioned in section 5.6, Sato *et al.* [53] used FSW to join two 0.25 in. thick AA 2219-T87 plates. No weld parameters, tooling information or weld direction were disclosed. To execute the weld, a hole was drilled at mid-length of the butt-line, so as to set up the tool on the backside. The first weld was executed to one end of the butt-line, leaving an end hole. The second weld was started at the opposite end, without a start-up hole, and continued to overlap a segment of the first weld leaving an end hole; in actual applications, the end holes would be filled using friction plug welding. The resulting joint profile had an I-shaped profile, with the top and bottom surfaces representing the shoulder contacts; i.e., the joint profile with a self-reacting tool is similar to that obtained by a 2-sided weld, one from either side, using conventional tooling. Samples were prepared where the overlap region contained up to three passes. Joints produced by conventional tooling were included for comparison. There was no post-weld heat treatment, and it is presumed here that testing was performed after all natural aging had seized. Tensile testing, presumably transverse to the welds, found the properties of the single and multi-pass regions, produced by the self reacting tool, and those produced by conventional tooling to be very close. The joint efficiencies were around 78%, and the joint yield strengths and % elongation values were around 55% of their base metal counterparts; the FSW properties were superior to those obtained in GTAW joints. Schematics of the hardness distribution across the joint profiles produced by the self-reacting and a conventional tool are depicted in Figure 19; the locations of the hardness measurements, however, were not indicated. The shape of the hardness curve for the conventional tool is suggestive of the trend depicted in Figure 15 (a). For the self-reacting tool, it appears that heating from both sides lowered the hardness of the central region of the weld to the point where the HAZ minima were eliminated, and the hardness distribution approximated the trend depicted in Figure 15 (b).

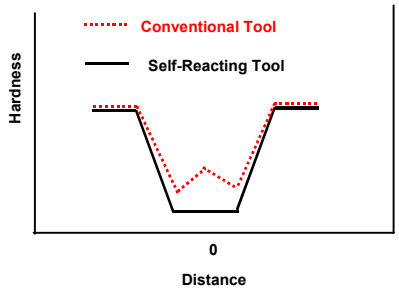

Figure 19:Hardness distribution in joints produced by conventional and self-reacting tools. AA 2219.

In another study, Cao and Kou [65] used 5/16 in. thick AA 2219-T851 plate to study liquation in FSW. The study was prompted by the results of earlier FSW modeling studies, which predicted that temperatures could reach the lower bound of the melting temperature range for such alloys as 6061, 7030 and 7075. AA 2219 was selected because of its clear lower bound of the melting temperature range; namely, the eutectic temperature (about 1015 F). The authors explain that constitutional liquation refers to the formation of liquid (L) in alloys with compositions less than the maximum solid solubility, under nonequilibrium conditions. Put differently, the A_xB_y compound would be present above the eutectic temperature, because the heating rate was too high for it to dissolve in the matrix by solid state diffusion. As a result, the eutectic reaction ($A_xB_y + \alpha \Rightarrow L$) would occur and cause liquation. In alloys with compositions greater than the maximum solid solubility, such as AA 2219, the reaction can occur under equilibrium and nonequilibrium conditions; i.e., the eutectic reaction (Al_2Cu [θ] + $\alpha \Rightarrow L$) would occur regardless of the heating rate. Put differently, liquation in this alloy would occur once the eutectic temperature is exceeded, regardless of whether FSW induces fast or slow heating. The study found no evidence of θ-induced liquation.

(g) AA 2519-T87

AA 2519-T87, known for its high strength and superior ballistic performance, is being used for armor plate applications, as a replacement for the mainstay aluminum armor alloy AA 5083-H131 (see section 6.1.1.2). AA

2519 butt joints produced by traditional arc processes, GMAW and GTAW, have not been capable of passing a certain ballistic test, due to low ductility. As a result, designs utilizing this alloy have to avoid butt joints and resort to other joint types that are complex and costly. FSW appears to offer a way out of this predicament.

Campbell and Stotler [66] investigated FSW of 1.25 in. thick plate of AA 2519-T87 to itself, using a double-sided joint configuration (Figure 14) in the following sequence. First, a partial-penetration weld, 0.75 in deep, was made on one side of the joint. This was followed by machining the weld face flat and turning the welded plates over. A second partial-penetration weld, 0.75 in deep, was then made; the overlap was intended to consolidate the roots of the first and second welds. Weld parameter optimization and tooling refinements ultimately led to butt joints with elongation values averaging about 11%, 1.5-2 times those produced by conventional GMAW. Plates FS welded as such passed the ballistic qualification test.

A similar result (14% elongation) was obtained by Colligan *etal.* [58] in FSW 1 in. thick AA 2519-T87 plate to itself in a single pass at 4 in. / min travel speed; the authors report the existence of a machine that can weld 2-in. thick plate in a single pass. The authors also investigated the effect of travel speed, in the 1.2-4 in. / min range, on joint tensile properties. Joint ultimate and yield strengths generally increased with increasing the travel speed, due to the reduced heat input. For the travel speeds investigated, the joint % elongation ranged from about 10-17%, but no particular trends could be discerned. In a subsequent publication, Colligan *et al.* [17] indicated that the tool used had a 2-piece design, with an H 13 tool steel shoulder and an MP 159 pin. The pin had a frustum shape with three flats and a flat end. Figure 13 schematically depicts the above shoulder and pin configurations. The authors indicate that transverse tensile failures of the joints, at travel speeds of 3 in. / min or less, took place in the HAZ. At higher speeds, however, the increased HAZ strength shifted the fracture location to the next weakest location, the stir zone (nugget). Both studies [17, 58] involved the development of weld parameters for corner joints (Figure 5) and two-pass butt welds (Figure 14). All joints passed the ballistic qualification test. However, no tensile data were published.

6.1.1.2 Aluminum 5xxx Alloys

This section contains data concerning alloy 5083. Section 6.1.1.5 contains data on alloys 5083 and 5005.

<u>AA 5083-H131</u>

AA 5083-H131 is an armor plate alloy; see section 6.1.1.1 (g) on AA 2519. Colligan *et al.* [40] investigated the effects of travel speed on the transverse tensile properties and hardness distribution across the joint profile of FS welded 1 in. thick AA 5083-H131 plate. The travel speed was in the 4.2-5.6 in. / min range, while the rotational speed was kept fixed at 250 rpm. Welding was performed using a 2-piece tool with an H13 tool steel shoulder and an MP159 pin, was used. The pin had a flat end, was not cylindrical and it had flats machined onto it; possibly, a frustum pin with flats (Figure 13) was used. No other weld parameters or tooling information were disclosed, and the authors did not indicate the welding direction. The authors show a nugget (also referred to as the stir zone) that contacts the root side, a feature that was attributed to the flat-ended pin configuration. The nugget displayed fine recrystallized grains (finer towards the TMAZ), contrasting the elongated grains of the base metal. The TMAZ was narrow, displaying grain distortion that was oriented downward on the advancing side and upward on the retreating side. Voids were detected at the advancing side, near the start and end of each weld. The tensile data show that joint ultimate strength increased gradually with increasing travel speed, reaching a maximum before dropping off with further increases in travel speed. The joint efficiency ranged from 82-89%, and the joint yield strength remained essentially unchanged, at around 56% that of the base metal, throughout the range of travel speeds studied. The joint % elongation ranged from about 153-250% that of the base metal, increasing with travel speed, reaching a maximum, before dropping off with further increases in travel speed. Notably, the % elongation and ultimate strength maxima did not occur at the same travel speed. The authors state that most tensile failures originated at the face of the weld and propagated through the stir zone (nugget) on a 45^{O} plane. They, however, did not provide sufficient information or any graphics to assist in visualizing fracture locations. The hardness distributions obtained across the joint profile displayed pronounced scatter. It appeared, however, than no hardness minima were present in the HAZ. Ignoring the scatter, Figure 20 schematically depicts the hardness distribution trends obtained at various depths; these trends are generally similar to that shown in Figure 15 (b). Clearly, a hardness gradient exists not only across the joint profile but also through the thickness (depth) of the joint.

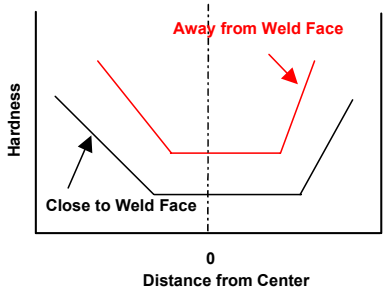

Figure 20: Hardness distribution across the joint profile close to and away from the weld face. AA 5083.

6.1.1.3 Aluminum 6xxx Alloys

This section contains data concerning alloys 6013, 6061, 6063, 6N01 and 6082. Section 6.1.1.5 contains additional data on alloys 6013, 6061 and 6063.

(a) AA 6013

Dalle Donne *et al.* [7] investigated residual stress distributions [g] in 0.16 in. thick 6013-T4 sheet welded to itself. Welding was performed in the rolling direction, using tools with shoulder and pin diameters in the 0.6-0.87 and 0.16-0.24 in. ranges, respectively. The travel and rotational speeds ranged from 11.8 to 39.4 in. / min and 1000 to 2500 rpm, respectively. No other weld parameters or tooling information were disclosed. There was no subsequent heat treatment after welding. Tensile testing, presumably transverse to the welds, was performed within 2 weeks after welding. In general, strength properties increased with increasing travel speed. Residual stress measurements were made using x ray and neutron diffraction. The longitudinal stresses were found to be higher than their transverse counterparts. A Typical residual stress distribution assumed an M-shape (Figure 21), with small compressive / tensile stresses at the butt line and high tensile stresses in the heat affected zone. Generally, residual stress distributions at the face and root were similar and close. Larger shoulder diameters widened the "M," i.e., increased the separation between the tensile peaks on either side of the butt line. The magnitudes of the tensile peaks generally decreased with decreasing the rpm. The data presented, however, makes it impossible to separate the effects of the travel speed since it was always increased when the rotational speed was increased. The peak magnitudes depended on the combination of parameters, being either higher on one side (advancing / retreating) or nearly equal. The residual stresses determined were mostly at the surface; through thickness profiles had not been completed at the time of publication. The authors learned later that natural aging continued for over one month. As such, the residual stress measurements were not performed on "stable" microstructures. This work also includes residual stress determination by the cut compliance method and cites several other investigations dealing with residual stress determination in FS welded joints. It is appropriate at this point to point out that the M-shaped residual stress distribution reported here should not be construed as typical of FSW in all aluminum alloys. Other authors report different shapes. The work of Sutton *et al*. [67] is a case in point. These authors used neutron diffraction to determine the distribution of residual stresses in the longitudinal, transverse and normal directions in FS welded 0.28 in. thick AA 2024-T3 plate. They published maps depicting the residual stress contours through the width and depth of the joints. Inspection of these maps at the face, root and mid-thickness of the joints indicate residual stresses that are mostly tensile, displaying W-shaped and inverted-U distributions; compressive stresses were only reported in the normal direction. One must then conclude that the magnitudes and distribution of residual stresses depend critically on the tooling, weld parameters and the type and temper of the alloy being welded.

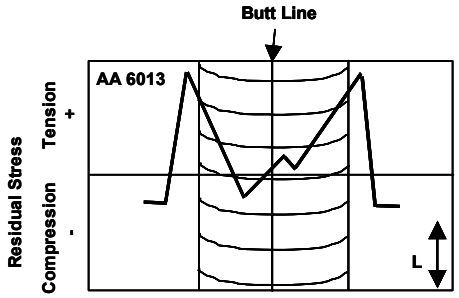

Figure 21: Longitudinal residual stress distribution (x rays) at the surface. Weld boundaries approximate.

(b) AA 6061

Chao and Qi [45] used a 3-D finite element analysis to model the temperature and residual stress fields in FSW. The model predicted that temperatures as high as 890 F [h] would be generated under the shoulder, and that the temperature increases with lower welding speeds and with thinner gage materials. The predicted temperatures are in general agreement with the data reported in similar investigations. [68, 69] The model was validated using 0.25 in. thick 6061-T6 plate, FS welded at 400 rpm and 4.7 in. / min travel speed, by placing thermocouples at 0.23 and 0.55 in. from the butt line. Residual stresses were modeled, but not validated by measurements. The model predicted that the transverse residual stress is the highest after welding and with the clamping / fixturing forces still acting. Once the clamping was released, the transverse residual stresses nearly vanished. While the longitudinal residual stress drops dramatically upon releasing the clamping forces, it remains significant at about 25% of the yield strength. Thus, in the end the longitudinal residual stress component will be higher than its transverse counterpart, in agreement with the results of Dalle Donne *et al.* on AA 6013. [7]

[g] *In FSW, residual stresses result from the rigid clamping, thermal effects and the mechanical work imparted.*
[h] *The solution treatment temperature for this alloy is around 990 F.*

In another study, Linert and Grylls [24] FS welded 0.25 in. thick 6061-T651 plate to itself, parallel to the rolling direction at 11 in. / min. travel speed; no other weld parameters or tooling information were disclosed. A joint profile similar to that shown in Figure 11 (a) was reported, except that the nugget, referred to as the stir zone, was elliptical in shape with concentric rings or bands (onion ring pattern) clearly visible, and that TMAZ was referred to as the HDAZ (heat and deformation affected zone). The microstructures in the various zones were studied, using TEM. The authors argue that the nugget, as FS welded, is in the solution treated condition. A hardness distribution similar to that depicted in Figure 15 (a) was reported; the authors, however, did not indicate the location where the hardness readings were obtained. Tensile testing transverse to the weld revealed an average joint efficiency of about 69%. The average joint yield strength and elongation were, respectively, 56% and 38% of their base metal counterparts. All samples failed in the HAZ.

(c) AA 6063 & 6N01

Alloys A6063 and 6N01 are listed as Japanese alloys that are similar to AA 6063; 6N01, however, has a somewhat higher Si content. Some of the studies on these extrusion alloys were performed using the -T5 temper. Quenching from the shaping temperature and then artificially aging at around 347 F develops the -T5 temper. A variant involves natural aging after quenching, to develop the -T1 temper, and then artificially aging to the -T5 temper.

In one study, Sato *et al.* [70] FS welded 0.24 in. thick A 6063-T5 plate; no weld parameters, tooling information or weld direction were disclosed. The joint profile published was such that it could not be adequately interpreted for schematic rendering here. The authors, however, discuss weld zones similar to those in Figure 11; however, the stir zone here appears to include the nugget and the region under the shoulder. The microstructures of the resulting zones were studied, in the as welded condition and after aging at 347 F, using TEM and OM. In general, the stir zone consisted of fine equiaxed grains with low dislocation density, indicating that recrystallization was the operating mechanism. The TMAZ was highly deformed with low dislocation density and high grain sub-boundary density, indicating that recovery was the operating mechanism. The parent metal displayed large grains with low dislocation density. In the as welded condition, the hardness distribution across the joint profile displayed a trend similar to that shown in Figure 15 (a). Hardness differences between the face, mid-thickness and root were insignificant. Aging at 347 F for 12 hr led to a hardness profile, at mid-thickness, similar to that shown in Figure 15 (c), with the nugget hardness higher than that of the base metal.

In another study, Hori *et al.* [71] compared single pass FSW to other welding processes for 0.47 in. thick 6N01-T6 plate. Those interested in the results of the comparison should consult the reference. Here the focus will be on FSW. Single pass FSW was performed at 4.9 in. / min and 315 rpm; no other weld parameters or tooling information were disclosed, and the welding direction was not indicated. The joint profile published was such that it could not be adequately interpreted for schematic rendering here. The main thrust of the work was to investigate the effect of cooling rate, after FSW, on hardness and strength in the as welded condition and also after aging (presumably at the -T6 aging temperature); specifically, air cooling and water cooling were compared. Water cooling increased the hardness of the HAZ and reduced its width, in comparison to air cooling. Nugget hardness, however, was not significantly affected by cooling rate. [i] These trends were observed in both the as welded and aged conditions. For both cooling methods, aging generally raised the hardness distribution above that of the as welded condition and also reduced the width of the HAZ. Hardness distribution across the joint profile generally reflected the trend shown in Figure 15 (a) for the as welded condition, regardless of the cooling method. The same trend was reported after aging, except that nugget hardness here approached that of the base metal. Tensile testing, presumably in the transverse to the weld, further revealed the beneficial effects of water cooling and aging on joint strength properties and its adverse effects on joint ductility. For air cooling, the as welded joint efficiency was about 64%; the joint yield and elongation were about 41% and 61%, respectively, of their base metal counterparts. After aging, the joint efficiency was about 73%; the joint yield and elongation were about 63% and 37%, respectively, of their base metal counterparts. For water cooling, the as welded joint efficiency was about 69%; the joint yield and elongation were about 49% and 54%, respectively, of their base metal counterparts. After aging, the joint efficiency was about 85%; the joint yield and elongation were about 81% and 29%, respectively, of their base metal counterparts. The aforementioned percentages are based on the base metal properties published by the authors. Tensile failure locations were not indicated, but it is thought that they have occurred in the HAZ. Based on a temperature of 752 F, measured 0.3 in. from the weld centerline, the authors concluded that the nugget must have been at high enough temperature to affect precipitate dissolution; thermocouples were embedded near the plate mid-thickness. The authors also investigated the effect of plate thickness, in the 0.47-0.79 in. range, on the tensile properties of water cooled joints. It is reported that joint strength decreased with increasing plate thickness, both in the as welded condition and also after aging. It is also

[i] *In the same study, water cooling was found to dramatically increase nugget hardness in A 6061 (Japanese alloy similar to AA 6061). The reason given is that AA 6061 is more quench sensitive than 6N-01.*

reported that the tensile properties of single pass welds were somewhat higher than their counterparts in two pass welds.

In a third study, Yun *et al.* [72] FS welded 0.24 in. thick 6N01-T5 plate at 21.7 in. / min travel speed and 1400 rpm; no other welding parameters, tooling information or weld direction were disclosed. The authors report a joint profile similar to that in Figure 11 (a), with weld flash, Figure 11 (b). The nugget, however, was elliptical, and there was more weld flash on the advancing side. In the as welded condition, the hardness distribution across the joint profile was similar to Figure 15 (a). The nugget hardness, however, recovered with aging at 347 F, reaching saturation after about 4 hr and then remained constant. Hardness distribution after aging for 12 hr was similar to that depicted in Figure 15 (c), with the nugget hardness slightly higher than the base metal; the authors did not indicate the locations where the hardness distributions were obtained. The work also involved a determination of the stress-strain curve for a FS welded joint.

(d) AA 6082

Svensson and Karlsson [73] conducted a microstructural study of FS welded 0.2 in. thick AA 6082-T6 sheet, in the as welded condition, using TEM, SEM and OM. Welding was performed at 29.5 in. / min; no other welding parameters or tooling information were disclosed, and the welding direction was not indicated. The authors reported a joint profile that was generally similar to that in Figure 11 (a), with an elliptical nugget and an onion ring pattern that was more pronounced on one (the advanced, most likely) side of the nugget, as shown in Figure 11 (b). The nugget displayed a fine recrystallized grain structure. The TMAZ was heavily deformed, but it displayed evidence of partial recrystallization and the grains were bent around the nugget. Beta double prime (Mg_5Si_6), the hardening phase in 6xxx alloys, was not present in nugget or HAZ. This would explain the softening in these zones with respect to the base metal, reported by the authors in earlier work (cited).

Ericsson *et al.* [74] investigated the mechanical properties of FS welded 0.23 in. thick AA 6082 plate in two conditions, -T6, as welded and -T4 aged to the -T6 condition after welding; the latter was referred to as the -T4 plus PWAT (post weld aging treatment) condition. Welding was performed at 1000 rpm and 13.8 in. / min, using a tool with 0.79 in. shoulder diameter. No other weld parameters or tooling information were disclosed, and the welding direction was not indicated. For the as welded -T6 condition, the hardness distribution across the joint profile was similar to that shown in Figure 15 (a). The authors indicate that for the -T4 plus PWAT condition, there was basically no difference between the HAZ and the base metal; however, no hardness distribution plot was published. The tensile and fatigue properties of the two conditions were also compared. Specimen configurations, however, were not published. Fatigue testing was performed transverse to the weld; test type (i.e., axial, etc.), however, was not indicated. No test direction was indicated for tensile testing, but it is presumed here that it was also transverse to the weld. The joint tensile ultimate and yield strengths for the -T4 plus PWAT condition were higher than their counterparts for the as welded -T6 condition; the % elongation values reported were more or less the same for both conditions. The fatigue data were in the form of S-N curves (R = 0.5), generated in the 10^5-10^7 cycle range (i.e., in the high cycle / low stress regime). The as welded -T6 samples displayed higher fatigue strengths than their -T4 plus PWAT counterparts, in spite of the fact that the latter possessed the higher tensile ultimate and yield strengths; no explanation for this was offered. Fatigue fractures of the as welded -T6 samples occurred around the weld / HAZ interface at the shear (advancing) side. For the -T4 plus PWAT samples, fracture occurred either near the center of the weld or halfway between that center and the HAZ, also on the shear (advancing) side. The authors, however, did not offer sufficient information or depictions to enable visualization of the fracture paths.

Hori *et al.* [71] investigated the hardness distribution and tensile properties of FS welded 0.79 in. thick alloy 6082 plate in the -T4 and -T6 tempers with and without subsequent aging to the -T6 temper. The chemistry of the alloy, as published by the authors, indicates that it is similar to AA 6082; the country of origin, however, could not be determined. Welding was performed at 4.9 in. / min and 315 rpm (single pass) or 550 rpm (two pass); no other welding parameters or tooling information were disclosed, and the welding direction was not indicated. Hardness distributions across the joint profiles were obtained for the as welded condition and after aging; the authors, however, did not indicate the locations where these distributions were obtained. For the as welded -T4 condition, the hardness distribution was similar to that shown in Figure 15 (c), with nugget hardness somewhat higher than that of the base metal. By contrast, the hardness distribution for the as welded -T6 condition was similar to that shown in Figure 15 (a), in agreement with earlier work. [74] Aging raised the hardness distributions to higher levels, compared with their as welded counterparts. The hardness minima for the aged -T4 condition were higher than their counterparts in the aged -T6 condition. The hardness distributions for the aged -T4 and -T6 conditions were similar to that shown in Figure 15 (c), with nugget hardness somewhat higher than that of the base metal. Tensile testing, presumably transverse to the weld, revealed a joint efficiency of 86% (single pass) and 96% (two pass) for the aged -T4 condition. These joint efficiencies are based on the base metal properties published by the authors.

6.1.1.4 Aluminum 7xxx Alloys

This section contains data concerning alloys 7010, 7050, 7075, 7349 and 7475. Section 6.1.1.5 contains data on alloys 7N01 and 7020, and additional data on alloys 7075 and 7475.

(a) AA 7010

Hannour *et al.* [62] investigated the corrosion behavior of FS welded 0.25 in. thick AA 7010-T7651 plate, using the salt spray test (ASTM G 85) and immersion in various corrosive environments; no weld parameters or tooling information were disclosed. Microstructural characterization was performed using TEM and SEM-EDS. The authors report that the HAZ, adjacent to the TMAZ, was the most susceptible area to corrosive attack and that this attack was predominantly intergranular. The authors further report that, compared to the base metal, the regions susceptible to corrosion were characterized by wider PFZ (precipitate free zone) at the grain boundaries as well as by coarser strengthening precipitates within the grains.

(b) AA 7050

Lumsden *et al.* [9] investigated the susceptibility of FS welded 0.25 in. thick 7050-T7451 plate to stress corrosion cracking (SCC), using the slow strain rate (SSR) test described in ASTM G129 and G49. In essence, the SSR test compares the failure loads and strains of specimens tested in air to those of specimens tested in a salt (3.5% NaCl) solution. Testing was performed transverse to the weld. No weld parameters, tooling information or welding direction were disclosed. The authors explain that alloy 7050 age hardens indefinitely at room temperature and it is because of this instability, FS welded samples had to be tested either as a function of post-weld time, to account for the effects of natural aging, or after artificial aging. Specifically, the SSR tests were performed either after natural aging (for 2 weeks or 5 months), or after artificial aging, at 212 F, for 1 week; the latter is a commonly used sensitizing treatment for simulating long periods of natural aging. Transverse SSR testing of the base metal in air and salt solution revealed equivalent failure loads and strains, indicating that the base metal is resistant to SCC. Testing in air, after FSW and natural aging for 5 months, indicated a reduction in failure load and strain, compared to their counterparts in the air tested base metal. The reduction in the failure load and strain were, respectively, attributed to the softening of the HAZ and the concentration of strain in the narrow soft HAZ. Failure here was transgranular in the HAZ. By contrast, testing of the equivalent specimen (FS welded + 5 months natural aging) in the salt solution produced an intergranular failure in the nugget and TMAZ on the advancing side. The failure load and strain were also reduced, compared to their counterparts in air, indicating susceptibility to SCC. Susceptibility to SCC was even greater for the specimen that was aged for only 2 weeks after FSW; here, failure in the salt solution was also intergranular in the nugget and TMAZ on the advancing side. Artificial aging restored resistance to SCC almost to the level of the base metal; failure in the salt solution was predominantly transgranular, within the HAZ. The beneficial effects of long-term natural aging and those of artificial aging on SCC resistance are clearly evident. Longitudinal SSR testing of specimens from within the weld nugget revealed the nugget to be susceptible to SCC after aging for 5 months and that artificial aging improved, but did not eliminate, that susceptibility. Furthermore, cracking in the salt solution was intergranular whereas that in air was transgranular. It is unfortunate that the authors did not publish typical joint profiles or any crack schematics / overall views that would aid in better visualizing the fractures involved with respect to the various weld zones; this was partially rectified in the subsequent work discussed below. This said, the reference includes some sustained load SCC test data (ASTM standards G 44 and G 49), for those interested.

In subsequent work, Lumsden *et al.* [25] investigated the corrosion properties of FS welded 0.25 in. thick 7050-T7651, plate. Welding was performed transverse to the plate rolling direction, using "conventional practices," 3.9 in. / min travel speed and 350 rpm rotational speed; no other weld parameters or tooling information were disclosed. Corrosion testing was performed after the FS welds were naturally aged for 5 months. The authors show a weld joint profile and zones similar to those depicted in Figure 11 (a), with a concentric onion ring pattern within the nugget. The TMAZ was referred to as the PRZ (partially recrystallized zone), to signify that that zone contains both recrystallized and deformed but not recrystallized grains. [j] Susceptibility to intergranular attack was determined per ASTM G 34. This revealed that the nugget / PRZ interface, the PRZ and the HAZ were all sensitized and susceptible to intergranular attack; the nugget / PRZ interface was by far the most susceptible. Pitting potentials were determined per ASTM G 61. The nugget was found to be most susceptible to pitting. It was not possible, however, to fabricate specimens that isolate the nugget / PRZ interface, so as to determine whether or not the culprit was that interface. Susceptibility to SCC was determined using the SSR test referred to earlier; testing was transverse to the weld (i.e., in the plate rolling direction), using several strain rates. Susceptibility to SCC was expressed in terms of a ductility ratio (the elongation obtained in testing in the salt solution / the average elongation value obtained in dry air testing). The results show that the ductility ratio

[j] *It seems that the authors define the advancing and retreating sides in a manner that contradicts the convention stated in section 5.2.*

decreased with decreasing the strain rate, reaching a constant value at the low end of the strain rates used. Fracture was transgranular for the samples tested in the salt solution at the highest strain rate used and also for the samples tested in air. These fractures occurred in the HAZ on the advancing side. For samples tested in the salt solution at the slower strain rates, fracture was intergranular, initiating in the area under the tool shoulder and propagating through the nugget at the nugget / PRZ (TMAZ) interface. TEM-EDS analysis of the microstructures revealed, among other things, the existence of a PFZ (precipitate free zone) near the nugget / PRZ interface. The authors indicate that they were unable to identify the chemical and / or microstructural culprits responsible for the increased sensitivity to corrosion, as a result of FSW. Hannour *et al.*, [62] however, working with AA 7010, made a correlation between the increased susceptibility to corrosion, on the one hand, and the presence of wider PFZ at the grain boundaries and coarser strengthening precipitates within the grains, on the other.

Talwar *et al.* [16] FS welded 2 in. thick 7050-T7451 plate in two passes, one from each side (Figure 14). No weld parameters, tooling information or weld direction were disclosed. The as welded material was very soft, and it remained so after aging, due to the overaging associated with the two passes. Solution treatment and aging, after welding, were performed as a possible means to improve strength; however, no heat treatment details were published. The authors report, without indicating the specifics, that tensile testing of bulk samples gave unsatisfactory results. The authors further report that thin specimen tests revealed weld regions with low ductility and others with low strength, and that further investigation was underway at the time of publication.

Bolser *et al.* [75] studied the tensile, shear, fatigue and fatigue crack growth properties of FS welded 0.25 in. thick 7050-T7451 strips. The strips were machined from a 3 in. thick plate, such that strip widths were in the short transverse (ST) direction. Welding of the strips was performed parallel to the longitudinal (L) direction; no weld parameters or tooling information were disclosed, and no joint profile was published. The joints were then aged at 250 F, for 24 hr, to stabilize the weld zone. This was followed by excising the test specimens and machining them, from the face side, to a thickness of 0.19 in. The above procedure was intended to simulate the design used in a specific application.

Tensile testing (ASTM E 8) was performed on base metal (L, ST), transverse-weld, longitudinal-weld and all weld (longitudinal from the center of the weld) specimens. The widths of the longitudinal-weld specimens were such that they included the nugget, TMAZ, HAZ and base metal on either side of the butt line. The base metal tensile ultimate and yield strengths in the ST direction were, respectively, around 96% and 93% of their counterparts in the L direction. Since the longitudinal-weld specimens were welded and tested in the L direction, the applicable joint tensile property comparisons should be expressed as percentages of the corresponding base metal properties in the L direction. This being so, the longitudinal-weld joint efficiency was about 91% and the joint yield strength was about 89% of its base metal counterpart. The all weld specimens displayed tensile ultimate and yield strengths that were, respectively, around 102 and 100% of their base metal counterparts; again these percentages are with respect to base metal tensile properties in the L direction. Since the transverse-weld specimens were tested in the ST direction, the applicable joint tensile property comparisons should be expressed as percentages of the corresponding base metal properties in the ST direction; note that welding here and in all the other specimens was in the L direction. This being so, the transverse-weld joint efficiency was about 85% and the joint yield strength was about 77% of its base metal counterpart. The elongation values of all specimens were close, except that of the transverse-weld specimen, which was about 41% of its base metal counterpart. The highest Young's modulus was that of the base metal in the L direction. The lowest (at about 75% of the highest) was that of the longitudinal weld.

Single shear testing was performed per ASTM B 831. The specimens were prepared such that the shear path (plane) would be in the base metal, weld metal center, the advancing side HAZ and the retreating side HAZ. The shear paths were always parallel to the L direction; refer to the Appendix for specimen configuration. The results indicate that the ultimate shear strength of the retreating side and advancing side HAZ, respectively, were about 89 and 93% that of the base metal. The ultimate shear strength of the weld was about 123% that of the base metal.

Fatigue testing was performed per ASTM E 466 (axial, constant amplitude); specimen axes were parallel to the L direction. S-N curves were obtained for longitudinal specimens of the base metal, weld metal center, the advancing side HAZ and the retreating side HAZ. The results show that, at the high stress (low cycle) regime, the fatigue lives of the weld center and HAZs were lower than that of the base metal. At the low stress (high cycle) regime, however, the fatigue lives of the HAZs and weld approached that of the base metal. In general, the advancing side HAZ performance was inferior to those of the retreating side HAZ and weld center.

Fatigue crack growth testing was performed per ASTM E 647, using compact tension specimens of the base metal, weld metal center, the advancing side HAZ and the retreating side HAZ. The notches were oriented in the ST direction, perpendicular to the welds. The results show that, at lower ΔK values, crack growth rates were higher at the advancing and retreating sides of the HAZ than in the base metal. Growth rates at the retreating side, however, were somewhat lower than their counterparts at the advancing side. At higher ΔK values, the crack growth curves converged. Crack growth behavior of the weld center was

inconsistent and, as such, no trends could be presented here.

Kumagai *et al.* [64] FS welded 0.16 in. thick alloy 7050 extrusion, using a tool with simple cylindrical pin, a rotation speed of 800 rpm and a travel speed of 4.9 in. / min; no other weld parameters or tooling information were disclosed, and the authors did not indicate the welding direction. The chemistry of the alloy, published by the authors indicates that it is similar to AA 7050; the country of origin, however, could not be determined. The material was extruded in house and then solution treated and stretched to produce the -T_51. Two groups of samples were tested. The applicable tensile property comparisons presented below are based on the base metal properties published by the authors.

a) One group of samples was left as is. [k] Following FSW, this group of samples was artificially aged using the thermal cycle required to produce the -T7451 temper. Transverse tensile testing indicated a joint efficiency of about 77%. Joint yield strength and elongation were, respectively, about 72% and 20% of their base metal counterparts. The authors report a hardness distribution across the joint profile that is similar to that shown in Figure 15 (a), with the nugget hardness approaching that of the base metal; the authors, however, did not indicate where the hardness readings were obtained. The welded joints here were characterized by high resistance to stress corrosion cracking (SCC).

b) The remaining samples, following stretching, were artificially aged to produce the -T7451 temper. After FSW, the samples were divided into two subgroups.

- **The samples of one subgroup were naturally aged for one month. [l] Tensile testing indicated a joint efficiency of about 89%. Joint yield strength and elongation were, respectively, about 74% and 40% of their base metal counterparts. The authors report a hardness distribution across the joint profile that is similar to that shown in Figure 15 (a), with the nugget hardness approaching that of the base metal; the authors, however, did not indicate where the hardness readings were obtained. The welded joints were characterized by low resistance to SCC; intergranular cracks initiated at the stir zone.**
- **The samples of the other subgroup were re- solution treated and aged to the -T7451 temper. The authors report a hardness distribution across the joint profile that is similar to that shown in Figure 15 (d), with the HAZ minima obliterated and the nugget hardness exceeding that of the base metal; the authors, however, did not indicate where the hardness readings were obtained. Tensile testing indicated a joint efficiency of about 95%. Joint yield strength and elongation were, respectively, about 93% and 30% of their base metal counterparts. While these properties are impressive, the authors dismissed re-heat treatment as impractical due to the excessive distortion that results from quenching.**

The study also includes fatigue data that some readers might wish to review.

(c) AA 7075

Mahoney *et al.* [36] investigated the tensile properties of FS welded 0.25 in. thick AA 7075-T651 plate. The authors list the tensile properties of the alloy, but do not indicate whether these were in L or T direction; however, the tensile property comparisons presented below will be based on these properties. Welding was performed at 5 in. / min travel speed, using a threaded pin; no other weld parameters or tooling information were disclosed, and the welding direction was not indicated. The authors report a joint profile similar to that shown in Figure 11 (b), with weld flash and deformed grains under the shoulder. The nugget, however, was elliptical and the onion ring pattern appeared to consist of concentric rings. Using embedded thermocouples, the authors measured and reported temperatures around 900 F, just outside the nugget, during FSW. Higher temperatures would be expected within the nugget; temperature measurements within the nugget are not possible due to extensive stirring. Longitudinal (within the nugget) and transverse tensile properties were determined in the as welded condition [m] and after performing the standard -T6 aging treatment (250 F / 24 hr / air). The resulting microstructures and fractures were characterized by TEM, SEM and OM; Strangwood *et al.* [60] conducted a similar microstructural study of the same alloy.

The longitudinal data indicate that, in the as welded condition, the ultimate strength, yield strength and elongation of the nugget, respectively, were about 84%, 64% and 103% of their base metal counterparts. After post-weld aging, the nugget ultimate strength dropped to, and nugget yield strength increased to, about 80% of their base metal counterparts. Nugget elongation after aging dropped to about 24% that of the base metal. The authors seem to attribute the results to the presence of PFZs in the aged specimens and their absence in the as welded specimens. The authors also point out that the decrease in ductility, resulting from artificial aging indicates that, in the absence of that artificial aging, there could be embrittlement of the weld nugget during long term natural aging.

---

[k] *The authors refer to the resulting temper after solution treating, quenching and stretching as -T451. The author of this document is not aware of a -T4 type temper in 7xxx alloys. -W51 would be a more appropriate designation.*

[l] *It is not certain that one month is sufficient to complete all natural aging. 7xxx alloys tend to naturally age for extended periods of time.*

[m] *Since alloy AA 7075 naturally ages for extended periods of time, the term as welded is meaningless without indicating the time elapsed between welding and testing.*

resulting from artificial aging, indicates that, in the absence of that artificial aging, there could be embrittlement of the weld nugget during long term natural aging.
The transverse data indicate that, in the as welded condition, the ultimate strength, yield strength and elongation of the joint, respectively, were about 75%, 55% and 52% of their base metal counterparts. After post-weld aging, the joint yield strength remained unchanged, whereas the joint ultimate strength dropped to about 72% of its base metal counterpart. Joint elongation after aging dropped to about 24% that of the base metal. The authors report that transverse failures occurred in the HAZ and attribute this to the presence of coarse (overaged) precipitates in the HAZ, especially after artificial aging, and to the generally coarse grain size of that zone. The authors also discuss the concentration of strain in the narrow soft HAZ and how such concentration can influence joint strength and elongation.

Lumsden *et al.* [38] studied the susceptibility of FS welded 0.25 in. thick AA 7075-T651 plate to intergranular (IG) attack (ASTM G 34). Welding was performed at 5 in. / min travel speed; no other weld parameters or tooling information were disclosed, and the authors did not indicate the welding direction. No post-weld heat treatments were used. Embedded thermocouples were used to measure the temperatures at various locations during FSW. A joint profile, similar to that reported by Mahoney *et al.* [36] was reported here as well. The study found that the hottest regions of the HAZ (about 650-790 F) were the most susceptible to IG attack. The deformed grains of the TMAZ and the nugget were also susceptible to IG attack, but to a lesser extent. The increased susceptibilities were discussed in terms of sensitization, PFZs and pitting potentials; Hannour *et al*. [62] made an association between PFZs and the increased susceptibility to corrosion. It should be noted that, in this work, [38] ranking of the susceptibilities of the various zones was based on immersion in corrosive environment for various lengths of time. Furthermore, it is known that solution treated AA 7075 naturally ages for extended periods of time. Therefore, it may be that the susceptibilities of the nugget and some TMAZ areas to IG attack were brought about, at least in part, by natural aging, rather than by the increased immersion times. The same authors also studied corrosion in AA 7050. [9, 25]

Talwar et al. [16] reported on the tensile properties of 0.08 in. thick Alclad AA 7075-T6, sheet; no weld parameters or tooling information wee disclosed, and the authors did not indicate the welding direction. Tensile testing, presumably transverse to the weld, revealed an as-welded joint efficiency of about 74%, and the joint yield strength and elongation were, respectively, about 69 and 14% of their base metal counterparts. [n] The poor elongation was attributed to the root alclad layer extending into the weld along the advancing side of the nugget. Machining 0.02 in. from the root side raised joint elongation to about 33% that of the base metal; joint efficiency was about 84% and the joint yield strength was about 71% that of the base metal. Aging at 250 F / 24 hr after machining further increased the joint efficiency to 89% and the joint yield strength to 86% that of the base metal. Joint elongation, however, was somewhat decreased by aging to about 29% that of the base metal. The aforementioned percentages are based on the base metal properties published by the authors.

Karlsen *et al.* [47] studied the microstructure of FS welded 0.06 in. thick 7075-T6 sheet (similar to AA 7075, probably of European origin); no weld parameters or tooling information were disclosed, and the authors did not indicate the welding direction. Microstructural characterization was by OM, SEM backscatter diffraction and pole figures, in as welded and after high temperature annealing at about 932 F / 1 hr. In addition to the base metal, the authors recognize four distinct zones in the joint profile; viz., the nugget, the shoulder contact zone, the TMAZ and the HAZ. The main focus of the study, however, was the nugget. The authors report that, in the as welded condition, the nugget and shoulder contact zone were characterized by severe deformation. The nugget had a fine grain structure, with texture varying from one region to the other. Each region of the nugget had two or more texture components, with high angle grain boundaries dominating the microstructure. Based on these findings, the authors conclude that the nugget was dynamically recrystallized. After annealing, the fine nugget grain structure was replaced by coarse irregular grains with texture components that are different from those present in the as welded condition. The base metal, however, appeared unchanged. The authors attribute the resulting coarse grains in the nugget to secondary recrystallization, where a fine-grained alloy experiences abnormal growth of only a few grains during soaking at elevated temperatures; see the work of Litwinski [8] on alloy 2195.

In another microstructural characterization study, Shibayanagi and Maeda [33] FS welded 0.2 in. thick A 7075-T 761 sheet; A 7075 is a Japanese alloy similar to AA 7075. There were no post-weld heat treatments, [o] and there appears to be no indication of a welding direction. No tooling information was disclosed, except that the tool was tilted 3^{O} and that a 0.4 in. thick SUS 304 (equivalent to AISI 304) back plate was used. The authors listed different travel and rotational speeds in the abstract, experimental procedure and in one of the figure captions. As a result, it is not possible to the appropriate speed(s) to be quoted here. No other welding parameters or tooling information were disclosed. Microstructural characterization was by OM, SEM backscatter diffraction and pole

---

[n] *Since alloy AA 7075 naturally ages for extended periods of time, the term as welded is meaningless without indicating the time elapsed between welding and testing.*
[o] *Since alloy AA 7075 naturally ages for extended periods of time, the authors should have indicated the time elapsed from welding and until testing was performed.*

figures. The joint profile depicted was unconventional in that the stir zone, as identified by the authors, consisted of three regions. These are: a heterogeneously stirred region at the face side of the weld, an elliptical region with concentric onion ring pattern at the center, and an insufficiently stirred region containing a kissing bond at the root side. Microstructural characterization focused mainly on the central (elliptical) region and the results appear to be in good agreement with the findings of Karlsen *et al.* [47] This aside, the authors reported a color map, depicting the hardness distribution across the joint width (profile) and depth. The map suggests a hardness distribution similar to that depicted in Figure 15 (e), with the central region of the weld displaying lower hardness than anywhere else, including the HAZ.

In an investigation of dynamic compressive properties, Chao *et al.* [63] FS welded 0.374 in. thick AA 7075-T7351 plate, using a tool made of tool steel. The tool had a threaded pin and the following tool dimensions: shoulder diameter, 1.1 in.; pin diameter, 0.394 in., and; pin length, 0.295 in. Welding was performed at 215 rpm and 4.4 in. / min travel speed. No other weld parameters or tooling information were disclosed, and there were no post weld heat treatments. The hardness distribution across the joint profile was similar to that depicted in Figure 15 (a); the authors, however, did not disclose the location where the hardness readings were obtained. Again, due to the fact that 7xxx alloys tend to naturally age for extended periods of time, the authors should have indicated elapsed from welding until testing was performed.

In a study of the effects of rotational and travel speeds on defect formation, Maeda *et al*. [43] FS welded 0.2 in. thick sheet of A 7075-T651 (Japanese alloy similar to AA 7075). Welding was performed using a tool made of SKD61 steel (Japanese steel similar to H13 tool steel). The tool had a threaded pin and it was tilted 3^{O}. The following tool dimensions were disclosed: shoulder diameter, 0.6 in.; pin diameter, 0.24 in., and; pin length, 0.19 in. The backing plate was 0.4 in. thick SUS 310 stainless steel (Japanese steel similar to AISI 310). The rotational speed ranged from 1200-2400 rpm and the travel speed from 4.7-11.8 in. / min. Temperature measurements were also made, by placing thermocouples at the face and root sides of the weld, on the advancing and retreating sides, 4.7 in. from the weld start point, at predetermined intervals. Defect free welds were obtained within a window of travel and rotational speeds, Figure 22. At 1800 rpm at 5.9 in / min travel speed, the measured temperature, 0.4 in. away from the weld centerline was about 613 and 432 F, at the advancing and retreating sides, respectively. The isothermal contour maps published by the authors seem to show that the advancing side was hotter than the retreating side along the entire length of the butt line; readers are urged to inspect the maps and draw their own conclusions. Without elaborating, however, the authors state that by changing the welding conditions, the retreating side could be made hotter than the advancing side.

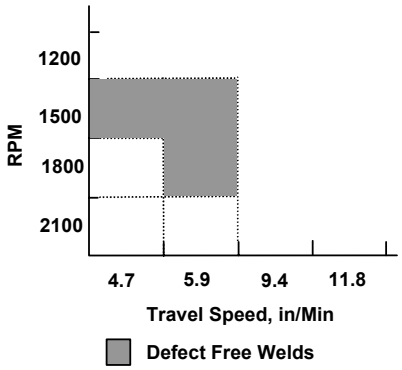

Figure 22: Window for defect free welds. A 7075-T651.

(d) Alloy 7349

To investigate the effects of rotational and traveling speeds on compressive yield strength, Marie [41] FS welded 0.4 in. thick alloy 7349-T6511 extrusion; [p] no weld parameters or tooling information were disclosed. No post weld treatment was used, since the intended application would not allow it. A joint profile similar to that shown in Figure 11 (a) was reported. The hardness distribution at mid-thickness reflected the trend depicted in Figure 15 (a). The results indicated that the compressive yield strength increases with travel speed. Again, due to the fact that 7xxx alloys naturally age for extended periods of time, the authors should have indicated elapsed from welding until testing was performed. Furthermore, the effects of this continued aging on the intended application need to be assessed.

(e) AA7475

Kumagai *et al.* [64] FS welded 0.16 in. thick AA 7475 extrusion, using a tool with simple cylindrical pin, a rotation speed of 800 rpm and a travel speed of 4.9 in. / min; no other weld parameters or tooling information were disclosed, and the authors did not indicate the welding direction. The chemistry of the alloy, published by the authors indicates that it is similar to AA 7475; the country of origin, however, could not be determined. The material was extruded in house and then solution treated and stretched to produce the -T_51. Two groups of samples were tested. The applicable tensile property comparisons presented below are based on the base metal properties published by the authors.

[p] *Alloy 7349 is produced by Pechiney Rolled Products, formerly Reynolds Aluminum.*

a) One group of samples was left as is. [q] Following FSW, this group of samples was artificially aged, using the thermal cycle required to produce the -T7451 temper. Transverse tensile testing indicated a joint efficiency of about 88%. Joint yield strength and elongation were, respectively, about 92 and 25% those of their base metal counterparts.

b) The remaining samples, following stretching, were artificially aged to produce the -T7451 temper. After FSW, the samples were naturally aged for one month. [r] Transverse tensile testing indicated a joint efficiency of about 94%. Joint yield strength and elongation were, respectively, about 85 and 40% those of their base metal counterparts.

The study also includes fatigue data that some readers might wish to review.

6.1.1.5 Multiple Aluminum Alloys

Hashimoto *et al.* [44] investigated the effects of varying the rotational speed / travel speed ratio on the tensile properties of same-metal FS welded joints of 0.157 in. thick sheet stock of A 5083-O, A 2024-T6 and A 7075-T6; the subject alloys are Japanese and they are similar to AA 5083, AA 2024 and AA 7075, respectively. The temperature generated during welding was measured by means of a thermocouple that was inserted 0.08 in. below the surface, through a hole, near the pin. The ranges of rotational (ω) and travel (v) speeds investigated were, respectively, 500-2500 rpm and 3.93-51.18 in. / min. No other weld parameters or tooling information were disclosed, and the authors did not indicate the welding direction. Furthermore, the authors did not indicate whether tensile testing was longitudinal or transverse. There were no post weld heat treatments. The results indicate that the peak temperature generated, at the selected location, during welding increased with increasing ω / v. For the same ω / v ratio, the peak temperature was highest for 5083-O, followed by 2024-T6 and 7075-T6, in that order. The peak temperature reported for all alloys and all the ω / v ratios investigated ranged from about 752 to 1112 F. The joint tensile strength increased with increasing the ω / v ratio, until some ω / v value, dependant on the alloy, was reached. At that point, the strength leveled out at some peak value. For 5083-O, the strength remained level for the remainder of the ω / v range investigated. For 2024-T6 and 7075-T6, the joint strength, after leveling out, started decreasing upon reaching some ω / v value that depended on the alloy. The peak joint strength for the 5083-O indicates a joint efficiency of about 99%. Those for 2024-T6 and 7075-T6 indicate joint efficiencies around 78%. Failure locations were not disclosed. In other results, the authors reported on some of the joint profiles and weld defects observed during FSW AA 2024-T6. It is recalled here that there were no post weld heat treatments. For the A 2024 joints, one may presume that mechanical testing was performed after all natural aging had seized. As to the A 7075 alloy, the authors should have indicated the time elapsed from welding until mechanical testing was actually performed; this is because 7xxx alloys tend to naturally age for extended periods of time.

Von Strombeck *et al.* [76] investigated the microstructure, hardness and the tensile and fracture toughness properties of same-metal FS Welded joints of 0.12 in. thick 5005-H14 and 0.20 in. thick 2024-T351, 6061-T6 and 7020-T6 sheet. It is assumed here that the alloys were of European manufacture, and that they are similar to their AA counterparts. No weld parameters or tooling information were disclosed, and the welding direction was not indicated. No post weld heat treatments were used.

Macro / Microstructure: Weld joint profiles similar to that shown in Figure 11 (a) were reported for all alloys investigated. In the precipitation hardenable alloys, the nugget displayed fine equiaxed grains, with a finer grain size than the other zones, due to dynamic recrystallization. Bending of the grains was observed in the TMAZ. It appears that the authors define the weld region as consisting of the nugget, TMAZ and HAZ. There was no discussion of the macro / microstructure of alloy 5005.

Hardness: Microhardness traverses were performed across the joint profiles in three locations; viz., near the face, at mid-thickness and near the root. In general, the hardness profiles of the precipitation hardenable alloys displayed trends similar to that shown in Figure 15 (a). The hardness distribution in the 7020 alloy, however, was noticeably flatter than those of the other two alloys. No hardness distribution for alloy 5005 was reported.

Transverse tensile specimen testing: The authors state that all joints failed in the weld region, without indicating exactly where. For the 5005 alloy, the joint efficiency was about 75%. Joint yield strength and elongation were, respectively, about 50 and 100% of their base metal counterparts. For the 2024 alloy, the joint efficiency was about 83%. Joint yield strength and elongation were, respectively, about 77 and 27% of their base metal counterparts. For the 6061 alloy, the joint efficiency was about 79%. Joint yield strength and elongation were, respectively, about 58 and 46% of their base metal counterparts. For the 7020 alloy, the joint efficiency was about 84%. Joint yield strength and elongation were, respectively, about 74 and 33% of their base metal counterparts. The reduced ductility of the precipitation hardenable alloy joints was attributed to strain localization within the lower strength weld region. It is noted here that

---

[q] *The authors of the cited reference refer to the resulting temper after solution treating, quenching and stretching -T451. The author of this document is not aware of a -T4 type temper in 7xxx alloys; -W51 would be a more appropriate designation.*

[r] *It is not certain that one month is sufficient to complete all natural aging, since 7xxx alloys tend to naturally age indefinitely.*

the aforementioned percentages are based on the base metal properties published by the authors.
Micro-flat tensile specimen testing: To determine the tensile properties of the various zones, micro-flat specimens were extracted, parallel to the weld direction. The tests were limited to alloys 2024 and 6061. The trends obtained are schematically depicted in Figure 23. In general, the ultimate and yield strengths duplicated the hardness trend of Figure 15 (a). The elongation, by contrast, displayed the opposite trend, with the nugget displaying somewhat higher (2024) or significantly higher (6061) % elongation than that of the corresponding base metal. Typically, the maxima and minima in property values did not occur at the same locations.
Fracture toughness: Standard compact tension specimens were extracted with the fatigue precracks oriented along the nugget and the HAZ / TMAZ region parallel to the weld. Base metal specimens were included for comparison. The face and root of the joints were not machined off before testing. The nuggets in the 5005, 6061 and 7020 joints displayed higher fracture toughness values than their respective base metals. The same was true for the TMAZ / HAZ region in the 5005 and 6061 joints; TMAZ / HAZ testing of the 7020 joints was not complete at the time of publication. By contrast, the nugget and TMAZ / HAZ region in the 2024 joints displayed lower fracture toughness values than the base metal. Higher fracture toughness values indicate higher resistance to stable crack growth. R-curves were reported for the four alloys.

It should be noted that there were no post weld heat treatments. For the 2024 and 6061alloys, one may presume that mechanical testing was performed after all natural aging had seized. As to the 7020 alloy, the authors should have indicated the time elapsed from welding until mechanical testing was actually performed; this is because 7xxx alloys tend to age for extended periods of time.

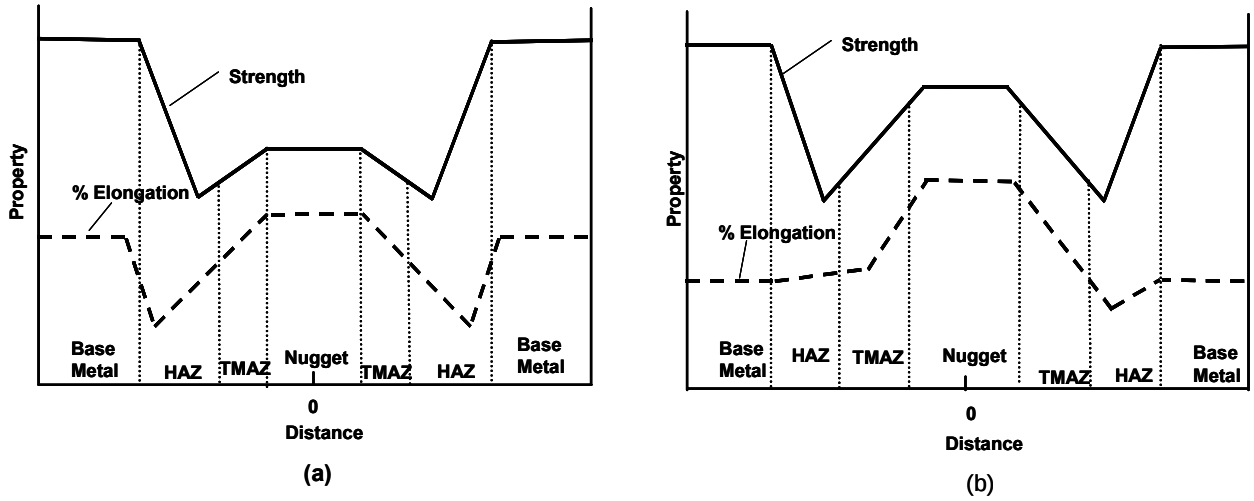

Figure 23: Simplified strength and % elongation trends. As welded condition.
(a) 2024-T351.
(b) 6061-T6.

Leonard [77] investigated the microstructure and hardness distribution of same-metal FS welded joints of UK aluminum alloys 2014A-T651 (a modified version of AA 2014) and 7075-T651 (similar to AA 7075) plates; the stock thicknesses were, respectively, 0.24 and 0.25 in. Welding was performed parallel to the rolling direction, at 3.3 and 3.9 in. / min for the 2014 and 7075 alloys, respectively. No other welding parameters or tooling information were disclosed. The temperatures generated during welding were measured by means of thermocouples inserted in small holes drilled at the face of the weld. During welding, peak temperatures in the 842-932 F were generated 0.24 in. from the weld centerline; these temperatures are close to (2014) or in excess of (7075) the solution treatment temperature. Within about 2 in. from the weld centerline, the peak temperatures were in excess of those required for aging to the -T6 temper. Both alloys displayed joint profiles similar to that shown in Figure 11 (a), with a concentric onion ring pattern and more weld flash at the advancing side. The author indicates that the nugget is a dynamically recrystallized region of the TMAZ and argues that the onion ring pattern is a result of grain size variations, which, in turn, result from variations in the distribution of fractured constituent particles. Hardness distributions were obtained after naturally aging the joints for 2 hr, 5 days, 2 months and 9 months. The 2 hr aging was considered as near to the as welded condition as was practicable; to minimize natural aging effects after the 2 hr aging, the joints were refrigerated to - 4 F and maintained at that temperature until hardness testing. The as welded and the naturally aged hardness profiles reported for both alloys displayed trends similar to that shown in Figure 15 (a). The hardness minima in alloy 2014A were at the HAZ / TMAZ interface (peak

temperature 667-932 F). Compared to 2014A, the hardness minima in 7075 were farther removed from the weld centerline, occurring well within the HAZ (peak temperatures > 716 F). With increasing the aging time, the hardness in the nugget, TMAZ and HAZ generally increased, while remaining below that of the base metal. Furthermore, the hardness minima moved away from weld centerline. The author reports that natural aging in both alloys was essentially complete two months after welding was completed. For the 7020 alloy, this conclusion contradicts the commonly held notion that 7xxx alloys tend to naturally age for extended periods of time. It may be that hardness is not a sensitive enough indicator of the cessation of natural aging.

Magnusson and Kallman [78] investigated the macrostructure and mechanical properties of same-metal FS welded joints of aluminum alloy sheet stock. The sheet alloys investigated were: 0.08 in. thick 2024-T3, 0.063 in. thick 6013-T4 and 0.08 in. thick 7475-T7. It is assumed here that the alloys were of European manufacture, and that they are similar to AA 2024, AA 6013 and AA 7475. Welding was performed in the LT direction (i.e., perpendicular to rolling direction), using a "standard tool" with a 0.16 in. pin diameter. The rotational and travel speeds used were 1180 rpm and 4.3 in./ min (2024), 2000 rpm and 8.2 in. / min (6013) and 950 rpm and 4.3 in. / min (7475). No other weld parameters or tooling information were disclosed.

Macrostructure: The joint profiles reported were generally similar to the mixed type, depicted in Figure 12, with a concentric onion ring pattern faintly visible. Some weld defects were reported in the AA 7475 joints.

Tensile Testing: Tensile testing was performed transverse to the welds, i.e., parallel to sheet rolling direction. Base metal properties, however, were not published. For 2024, an as welded joint efficiency of 90% was reported. Fracture occurred at the retreating side of the weld; no specific locations were indicated. After solution treatment and aging, joint efficiency was reported to have remained unchanged at 90%; presumably, aging was natural, to develop a stable -T4 / -T3 temper. Joint yield strength and elongation, however, were somewhat lower than their as welded counterparts. Furthermore, fracture location moved to the nugget. For 7475, an as welded joint efficiency of 92% was reported. Fracture occurred at the retreating side of the weld; no specific locations were given. After solution treatment and aging, joint efficiency was reported to have increased to 97%; presumably, aging was artificial, to develop the -T76 temper. The joint yield strength was significantly higher, and the joint elongation lower, than their counterparts in the as welded condition. Fracture locations were not indicated. The 6013 joints were tested only after artificial aging to the -T6 temper and the reported joint efficiency was 75%. Fracture location was not indicated. The authors indicate that the joint efficiencies of FS welded 2024 and 7475 were superior to those obtained by conventional GTAW. The FS welded 6013 joint efficiency, on the other hand, was similar to those obtained by conventional GTAW.

Bend Testing: Bend testing was performed over a 120^{O} angle, using a 0.63 in. diameter mandrel. The tests were performed transverse to the welds, with the face and root on the tension side. Cracking was noted on the face and root specimens of the reheat treated 2024 and 7475 joints. All other specimens were free of cracks.

Fatigue Testing: Constant amplitude, presumably axial, fatigue testing (R=0.1) was performed only for the as welded condition. Testing was performed transverse to the welds (i.e., parallel to the rolling direction), using dog-bone specimens, to generate S-N curves. The 2024 and 7075 joints were tested in the as welded condition and after machining to remove 0.4-0.6 in. from the face side of the welds. Machining improved fatigue performance and raised the SN curve closer to that of the respective base metal; the improvement was more noticeable in the 7475 joints. The 6013 joints were tested in the as welded condition and after machining both the root and face sides. Machining improved fatigue performance and raised the SN curve closer to that of the base metal; the improvement, however, was less significant in the low cycle (high stress) regime. In all three alloys, fatigue crack initiation in the as welded condition was at the face side of the weld. Face side machining in the 2024 and 7475 joints caused root side initiation to occur as frequently as face side initiation. With face and root machining in AA 6013, crack initiation still occurred at the face side. The authors did not publish schematics or overall photos of fracture locations.

Hardness: Microhardness traverses were performed across the as welded 2024 and 7475 joints, and the post weld aged 6013 joints. In all cases, the hardness profiles reported displayed trends similar to that shown in Figure 15 (a); the authors, however, did not indicate the locations where the hardness readings were obtained.

It should be noted that here, the authors report on the as welded properties of alloys 2024 and 7475. For the 2024 alloy, one may presume that mechanical testing was performed after all natural aging had seized. As to the 7475 alloy, the authors should have indicated the time elapsed from welding until mechanical testing was actually performed; this is because 7xxx alloys tend to naturally age for extended periods of time.

Dalle Donne *et al.* [41] investigated the effects of weld defects (pores) and residual stresses on fatigue crack propagation (FCP) rates in same-metal FS welded joints of 0.16 (5/32) in. thick 2024-T3 and 6013-T6 sheet stock. It is assumed here that the alloys, possibly of European manufacture, are similar to AA 2024 and AA 6013, respectively. A simple tool (tool A) was used to produce welds with pores near the root side, whereas a tool with

a threaded pin (tool B) was used to produce the defect-free welds. The authors explain that the presence of a thread, rotating in the proper direction, affects rotational flow and effectively eliminates pores. A byproduct of the threaded pin tool is the formation of the onion-ring pattern within the nugget; welds produced by the simple tool lacked the onion-ring pattern. Welding was performed parallel to the rolling direction. However, for 2024 joints welded with tool A, welding was in the transverse direction. The authors list some weld parameters and the resulting transverse tensile properties of the joints, as well as hardness distributions across joint profiles at midthickness. Unless otherwise stated, testing was performed in the as welded condition, presumably after all natural aging had seized. For both alloys welded with tool A (simple), the hardness distribution was similar to that depicted in Figure 15 (a) with the maximum nugget hardness lying within the hardness band of the base metal. For 2024 welded with tool B (threaded), the hardness distribution was similar to that depicted in Figure 15 (c), with the maximum nugget hardness somewhat higher than the base metal hardness range. For 6013 welded with tool B (threaded), the hardness distribution was similar to that depicted in Figure 15 (a), with the nugget hardness significantly lower than the base metal. FCP tests were carried out in the as welded condition, except those for alloy 6013 produced by tool A, which were artificially aged to the -T6 temper after FSW. Most of the tests were performed on compact tension specimens (ASTM E 647); some tests utilized center cracked specimens. The notches / cracks were oriented along the center of the weld. A simple approach, based on the cut-compliance method, was used to incorporate residual stress effects in crack growth data. The results indicated that the presence of pores had limited effect on da/dN- ΔK behavior of the welds, and that the effect of residual stresses was the more significant. Accordingly, the authors warned that ignoring residual stresses could lead to nonconservative estimates of FCP behavior.

A group of authors [28, 79-81] reported on a four-part study of same-metal FSW of 0.12 in. thick sheet stock of three aluminum alloys. One important aspect of the study was to examine the effects of changing material suppliers and FSW processors. The alloys investigated were A 5083-O, procured from two sources (#51 and #52), 6N01-T5, procured from three suppliers (#61, #62 and #63) and 7N01-T5, also procured from three sources (#71, #72 and #73). A 5083, 6N01 and 7N01, respectively, are Japanese alloys similar to AA 5083, AA 6063 and AA 7004. FSW was performed by four licensed processors, each using his own tools and welding parameters. Of these, three (#1, #2 and #4) used conventional processing with tilted tools and one (#3) used zero tilt; a zero tilt suggests that a scroll shoulder was used (Figure 13). The authors did not disclose any other weld parameters or tooling information, and the weld direction was not indicated. No post weld heat treatments were used. Part 1 of the study deals with NDI and imperfections, part 2 with metallurgical features, part 3 with tensile properties and part 4 with formability. The work includes comparisons with GMAW and GTAW that will be excluded here.

<u>Part 1, NDI</u>: Oiwa *et al.* [79] used the ultrasonic phased array method to image the cross-section (D-scan) and the face and root (C-scan) of the welds. This was supplemented by metallography, to ascertain the type and extent of each defect detected by the scans. It is reported that the flash on the weld face resulted in noise signals and interference. As such, removal of that flash is recommended, if only face scans were to be used. If removal is not carried out, then the welds should be scanned from both the face and root sides. Using this ultrasonic phased array method, the authors indicate that it was possible to detect subsurface cavities that are undetectable by radiography or penetrant inspection. The method was also capable of detecting opening lack of penetration, where an actual separation (gap) exists; in this regard, the method would be similar to penetrant inspection. Finally, the method enabled the detection of closed imperfections, such as the closed lack of penetration and the kissing bond defects. The authors seem to refer to closed lack of penetration defects as kissing bonds, and classify both as occurring near the root side of the weld, as a result of large penetration ligaments (defined in 5.2). It is appropriate at this point to review some NDI work by other authors. Lamarre and Moles [82] investigated the use of the ultrasonic phased array method for the inspecting FS welded aluminum alloy sheet and plate in the 0.2-0.4 in. thickness range. The defects inspected for were lack of penetration, wormholes, kissing bonds, and faying surface and root defects; unfortunately, no metallographic or schematic depictions of these defects were published. In general, the method was capable of detecting all defects. Figure 24 shows the three basic scan directions defined by the authors; it is noted that the D-scan direction is different from that indicated by Oiwa *et al.* [79] In related work, Oosterkamp *et al.* [21] discussed the parallel between the kissing bond phenomenon in FS welds and extrusion welds of aluminum alloys, and performed SEM analyses of kissing bond fracture surfaces. The authors argue that the major cause for kissing bond formation in FSW is the insufficient stretch of the material caused by sliding, rather than sticking, friction on the pin; the authors indicate that the work of Colligan [11] supports their arguments.

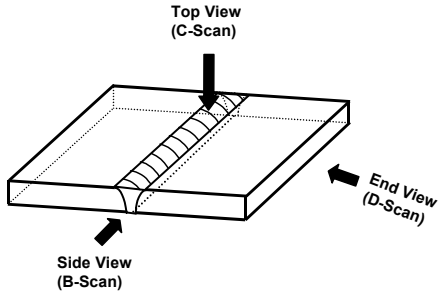

Figure 24: Basic scan directions.

Part 2, Metallurgical Features of FSW: Okada *et al.* [28] looked at the metallurgical features of the FS welded joints of the three aluminum alloys investigated. They reported features such as weld flash on the advancing and retreating sides, the onion ring pattern, inclusions, underfill and undercut. The authors, however, appear to define the stir zone as encompassing the region under the shoulder, the nugget and the TMAZ; a reasonable definition. With this in mind, the authors identify three basic stir zone shapes (Figure 12); viz., the wineglass, bowl and mixed (nearly trapezoidal) shapes. The authors computed the FSW heat input, Q, using the yield strength of the alloy in question, the travel and rotational speeds and the shoulder radius of the tool. Some observations were then noted regarding the effect of Q on the shape of the stir zone and on the onion ring pattern. The authors argue that low Q values give rise to the wineglass stir zone shape, whereas high Q values generally give rise to the bowl or mixed stir zone shape. Also at high Q values, the onion ring pattern, thought to be the result of some sort of solute banding, either disappeared or became difficult to discern. The surface width of the weld and its cross sectional area increased with increasing Q. The same trends were observed for all three alloys, regardless of the alloy source or FSW processor. The authors propose that the stir zone, initially having an I-shape (square butt), develops into wineglass then the bowl shape, with increasing heat input. Hardness distributions across the joint profiles were determined at mid-thickness for A 5083 and 7N01 joints. Alloy A 5083 displayed a hardness distribution similar to that depicted in Figure 15 (d), with the peak hardness at the nugget dependent on the alloy source and FSW processor. Depending on the alloy source and FSW processor, alloy 7N01 displayed one of three hardness distributions. The first was a uniform hardness distribution. The second was a distribution similar to that of Figure 15 (a), with the nugget hardness lower than that of the base metal. The third was a distribution that is similar to Figure 15 (c), with the nugget hardness higher than that of the base metal. The differences were attributed to the degree of natural aging between cooling and testing. [s] The authors suggest that certain weld dimensions could be useful in predicting hardness distribution.

Part 3, Tensile Properties: Hori *et al.* [80] determined the transverse tensile properties of the FS welded joints of the three alloys. For comparison purposes, this was preceded by a determination of the longitudinal and transverse tensile properties of the stock obtained from each alloy source. The resulting data (listed in part 2 of the study) indicate that tensile properties tend to vary from one alloy source to the other and that the property scatter bands were noticeably more pronounced for alloys 7N01-T5 and 6N01-T5, compared to those of alloy A 5083-O. The ultimate and yield strength scatter bands for alloy 7N01-T5 were somewhat wider than their counterparts for alloy 6N01-T5, whereas the % elongation scatter band for alloy 6N01-T5 was significantly wider than its counterpart for alloy 7N01-T5. The tensile properties of the FS welded joints were influenced by base metal properties; i.e., joint properties depended on alloy source. The joint efficiency, however, remained essentially the same for each alloy, regardless of alloy source. In general, joint efficiencies in A 5083 were higher than those in 7N01, which, in turn, were higher than those in 6N01. To determine the effect of processing, one alloy source was selected for each alloy; viz., # 52 for A 5083, # 61 for 6N01 and # 71 for 7N01. For A 5083, the changes in FS welded joint properties from one processor to the other were within 10% for the ultimate strength, 7% for the yield strength and 85% for the % elongation. Joints FS welded by # 1 and # 2 processors failed within the stir zone, due to thinning effects. Joints FS welded by # 3 processor (0 tilt) failed at the edge of the stir zone, due to stress concentration effects. Joints FS welded by # 4 processor failed at the base metal. For 6N01, the changes in FS welded joint properties from one processor to the other were within 20% for the ultimate strength, 23% for the yield strength and 40% for the % elongation. Joints FS welded by all four processors failed in HAZ, at the weld interface, due to thinning and to strain localization within the HAZ. For 7N01, the changes in FS welded joint properties from one processor to the other were within 10% for the ultimate strength, 8% for the yield strength and 130% for the % elongation. Joints FS welded by # 1 and # 2 processors failed within the stir zone. Joints FS welded by # 3 (0 tilt) and # 4 processors failed in the HAZ. It is recalled here that there were no post weld heat treatments. In view of the tendency of 7xxx alloys to naturally age for extended periods of time, the authors should have indicated the time elapsed from welding until tensile testing was actually performed on the 7N01 joints. The same concerns apply to the hardness data reported for alloy 7N01 in part 2 of the study.

Part 4, Formability: Hashimoto *et al.* [81] assessed formability transverse to the weld joints by a plunger-type bend test, without removal of the weld flash. Both face and root bend tests were used, and formability was expressed in terms of (bend diameter / 2) x thickness. Base metal (alloy source) and processing details (processor) had some effect on 6N01, but not on the other alloys. Formability of 5083 was better than the other two alloys. Correlations were made between formability and local tensile %

[s] *It is thought that there are additional potential culprits here. First is that the exact elemental constitution of any given alloy is likely to vary from one material source to the other. Minor compositional differences can influence how the alloy reacts to FSW, thereby affecting microstructure and hardness. Second is the fact that different FSW processors use different tooling and different processing parameters. These differences are likely to lead to different temperatures, strains and strain rates, which, in turn, would lead to different microstructures, hence different hardness distributions.*

elongation in the various zones across the weld profiles, determined from tensile testing; formability was also correlated with the overall tensile % elongation. Interested readers may wish to consult the reference.

6.1.2 Dissimilar Aluminum Alloy Welding

Larsson *et al.* [31] investigated dissimilar FSW of AA 5083-H12 and AA 6082-T6 sheet stock, 0.2 in. thick; these joints were referred to as I-joints. Two orientations were used: (a) AA 5083 on the advancing side and AA 6082 on the retreating side, and; (b) AA 6082 on the advancing side and AA 5083 on the retreating side. The authors also investigated similar metal FSW, using consumable inserts of the other alloy; these joints were referred to as strip-joints. Welding was performed at 6.8-19.7 in. / min; no other weld parameters or tooling information were disclosed, and the authors did not indicate the welding direction or publish the tensile properties of the base metals. No post-weld heat treatments were used.

Macro / Microstructure: Weld profiles similar to that shown in Figure 11 (b) were reported for all I and strip-joints. The flow and mixing were easy to observe, due to the different etching characteristics of the two alloys. As such, the onion ring pattern, consisting of alternating bands of the two alloys was clearly visible. SEM-EDS analysis of these bands revealed only the composition of the two alloys, and no intermediate compositions were detected. This was considered as evidence for lack of mixing; bonding, however, appeared to be intimate. The authors indicate that mixing in the nugget appeared to be more homogeneous in I-joints with AA 6082 on the advancing side. The authors report that mixing in the nugget appeared easier to achieve in AA 5083 strip joints with AA 6082 strips than the other way around. However, adding a second FSW run to AA 6082 strip joints with AA 5083 strips significantly improved mixing in the nugget. The surface layer (under the shoulder) in all joints consisted of AA 6082, regardless of which alloy was on which side (I-joints) or the type of strip used (strip-joints).

Hardness: Hardness distribution across the joint profile was determined at mid-thickness for one I-joint, with AA 5083 on the advancing side; the hardness of the base metals were more or less the same. A simplified schematic rendering is shown here in Figure 25. A notable hardness minimum was present on the AA 6082 side. The authors indicate that this minimum was in the TMAZ; the HAZ is another distinct possibility. The hardness within the nugget fluctuated, probably reflecting the various bands encountered.

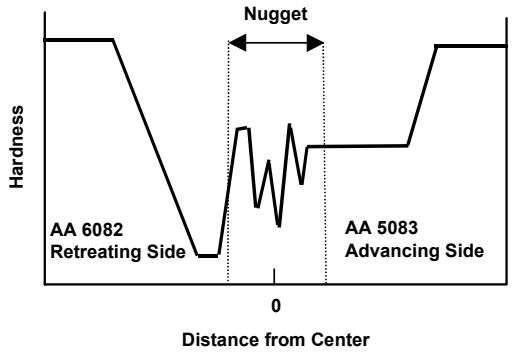

Figure 25: Hardness distribution at midthickness. AA 5083-H12 / AA 6082-T6 joint. As welded. Zone boundaries are approximate.

Tensile Properties: Tensile properties were determined transverse to the welds. For I-joints, the ultimate joint strength did not significantly change by changing alloy orientation. Specifically, joints with AA 5083 on the advancing side displayed strengths in the 29.4-30.7 ksi range. Somewhat higher strengths (31.2-32.5 ksi) were obtained for those joints with AA 6082 on the advancing side. In general, higher travel speeds resulted in higher joint ultimate strength values. All I-joints failed in the TMAZ, at the location of the hardness minimum on the AA 6082 side. The joint ultimate strength of strip-joints showed a noticeable dependence on the strip alloy used. For AA 6082 joints with AA 5083 strips, the strength was in the 29.6-31.9 ksi range. Adding a second weld run did not significantly affect strength. The strength of AA 5083 joints with AA 6082 strips was in the 42.8-42.9 ksi range. In general, higher travel speeds resulted in higher joint ultimate strength values. The strip joints failed either in the TMAZ, weld center or off weld center; however, no specifics were published.

Bend Testing: I and strip-joints were root and face bend tested, through a 120^{O} angle in the longitudinal and transverse directions. Failures / cracking occurred more frequently in root bends than in than in face bends.

The authors conclude that, the material with lower hot strength should be placed at the advancing side in I-joints, and used as the consumable strip in strip-joints. In both cases, higher welding (travel) speeds are preferable.

Ouyang and Kovacevic [29] investigated dissimilar FSW of AA 6061-T6 and AA 2024-T3 plate stock, 0.5 in. thick. For comparison purposes, same metal joints of 0.5 in. thick AA 6061-T6 plate stock were also investigated. Welding was performed using a tool steel tool with a threaded pin, a travel speed of 5.2 in. / min and a rotational speed of 416 rpm (same metal welding) or 637 rpm (dissimilar alloy welding). No other welding parameters or tooling information were disclosed, and the authors did not indicate the welding direction. There were no post weld heat treatments. This is basically a macro / microstructural study, using metallurgical sections in three perpendicular

directions; viz., transverse (joint profile), longitudinal at mid-thickness and longitudinal at weld centerline. Hardness distributions across the joint profiles were also determined. The authors, however, did not reveal the locations where hardness measurements were made.

In same metal AA 6061 joints, the authors show a joint profile that is generally similar to that shown in Figure 11 (a). The nugget, also referred to as the stir zone, displayed fine equiaxed grain structure that the authors attribute to a combination of hot working and dynamic recrystallization (DRX) or dynamic recovery (DRV). At the center of nugget (longitudinal section-weld centerline), there was "zigzag bonding," a feature that was attributed to action of the threaded pin. The authors indicate that the presence of this feature suggests that, while bonding between the two plates was perfect, mechanical mixing was far from complete. The surface under the tool shoulder was heavily deformed, and the TMAZ displayed the presence of flow lines, referred to as vortex structures, attributed to the stirring action. The hardness distribution across the joint profile was similar to that shown in Figure 15 (a), with the hardness minima being near the TMAZ / HAZ interface.

Typical joint profiles in dissimilar AA 2024 / AA 6061 welds displayed the familiar zones (nugget, TMAZ and HAZ) in a more complex manner; the macrograph published was not sufficiently clear to enable schematic rendering here. The nugget displayed three regions; viz., the MMR (mechanically mixed region) on the AA 6061 side, the UMR (unmixed region) outboard of the MMR, closer to the AA 6061 base metal, and the SPFR (stirring-induced plastic flow region) on the AA 2024 side. A distinct interface existed between the nugget and the AA 2024 alloy at the root of the weld. The UMR displayed fine equiaxed AA 6061 grains and its microstructure was similar to that of the nugget in same metal AA 6061 welds. The MMR consisted of dispersed particles of the different alloy constituents. The SPFR displayed alternate, vortex like lamellae of the two alloys, with visibility of the lamellae enhanced by the different etching characteristics of the two alloys. The authors conclude that the nugget features indicate that bonding was complete whereas mutual mixing, while intimate, was far from complete. A simplified rendering of the hardness distribution across a typical joint profile is schematically depicted in Figure 26. As was the case in the work of Larsson *et al.*, [31] depicted in Figure 25, the hardness contrast between the two alloys and the hardness fluctuations are evident. Unfortunately, the authors here did not indicate which alloy was on the advancing side and which was on the retreating side. It appears, however, that AA 2024 was on the advancing side. In other results, the authors studied the effects of changing the travel and rotational speeds on microstructure. It is reported that increasing the rotational speed and, to a lesser extent, reducing the travel speed tend to enhance material flow; the authors published representative microstructures.

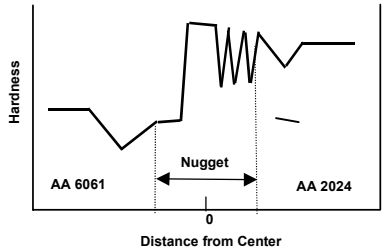

Figure 26: Hardness distribution. AA 6061-T6 / AA 2024-T3 joint. joint. As welded. Nugget boundaries not indicated in reference.

In a study of the effects of rotational and travel speeds on defect formation, Maeda *et al.* [43] FS welded 0.2 in. thick A 5083-O and A 6061-T651 sheets, using a tool made of SKD61. [t] The tool had a threaded pin and it was tilted 3^{O}. The following tool dimensions were disclosed: shoulder diameter, 0.6 in.; pin diameter, 0.24 in., and; pin length, 0.19 in. A 0.4 in. thick 310 stainless steel backing plate was used. The rotational speed ranged from 1200-2400 rpm and the travel speed from 4.7-11.8 in. / min. No other weld parameters or tooling information were disclosed. Temperature measurements were also made, by placing thermocouples at the face and root sides of the weld, on either side of the butt line, 4.7 in. from the weld start point, at predetermined intervals. The temperature measurements were used to construct thermal contour maps. In one set of specimens, the A 6061 alloy was placed on the advancing side and the A 5083 alloy on the retreating side. The situation was reversed in another set of specimens. In either case, defect free welds were obtained within a window of travel and rotational speeds. The window, however, was considerably narrower when A 6061 was placed on the advancing side, Figure 27. For example, using 1800 rpm and 5.9 in. / min produced defect free welds, when A 6061 was placed on the advancing side. These same conditions, however, produced weld defects, when A 5083 was placed on the advancing side. The thermal maps at 1800 rpm and 5.9 in. / min indicate that the isothermal contours expand to

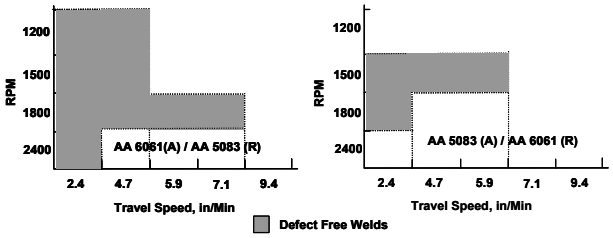

Figure 27: Window for defect free welds. A 5083 / A 6061. (A) and (R) after alloy designation signify the advancing and retreating sides, respectively.

[t] *A 5083 A 6061 are Japanese alloys similar to AA 5083 and AA 6061. SKD61 is a Japanese steel similar to H13 tool steel.*

the advancing side when A 6061 is placed on the advancing side, and to the retreating side when A 5083 is placed on the advancing side. In this latter arrangement, the advancing side may be hotter or colder than the retreating side, depending on location along the butt line. Readers are urged to study the isothermal contour maps to formulate their own conclusions. This work and that of Larsson *et al.* [31] clearly demonstrate that, in FSW dissimilar aluminum alloys, it matters as to which alloy is placed at the advancing side and which at the retreating side.

6.2 Magnesium Alloys

Fusion welding of magnesium and its alloys, especially the cast alloys, results in the formation of porosity in the fusion zone. Furthermore, the fairly high coefficients of thermal expansion, typical of these alloys, tend to cause objectionable distortion of the weldments. As such, fusion welding is not a commonly used joining practice for magnesium and its alloys. Rather, adhesive bonding and mechanical fastening are the preferred joining practices. FSW offers an attractive option for welding these alloys. The work reviewed here involves only same-metal welding that was performed in Japan.

Nakata *et al.* [83] studied same metal FSW of 0.08 in. thick thixomolded [u] AZ91D alloy. Rather than indicating a temper, the authors indicated an ultimate tensile strength range of 32.5-36.7 ksi and an elongation of about 4%. Welding was performed using a tool with a threaded pin, travel speeds in the 2-20 in. / min range and rotational speeds in the 880-1750 rpm range. The following tool dimensions were disclosed: shoulder diameter, 0.47 in.; pin diameter, 0.12 in., and; threaded pin length, 0.08. No other weld parameters or tooling information were disclosed, and the authors did not indicate a welding direction. No post-weld heat treatments were used. The study involved a determination of the optimum welding conditions, macro / microstructural characterization by OM, hardness measurements and a determination of the tensile properties.

> **Developing Optimum Welding Parameters: The authors varied the rotational and travel speeds in order to determine the optimum conditions for producing defect-free welds. Subsurface cavities (voids) and / or lack of bonding at the advancing side of the stir zone were observed at lower rpm or higher travel speeds. Increasing the rpm and / or decreasing the travel speed resulted in an improvement in weld quality. This was explained in terms of the increased heat input and temperature, and the attendant enhancement of alloy formability; increased heat inputs, however, were accompanied by generally coarser structures. Thus, optimum FSW conditions were limited to a narrow rpm-travel speed window, a behavior that is caused by the inherent poor formability of the alloy, which is attributed to its as cast structure.**
>
> **Macro / Microstructure: Using the optimum conditions referred to above, the authors report zones similar to those observed in aluminum alloys; viz., stir zone (SZ), TMAZ, HAZ and base metal. The macrograph published, however, did not lend itself to schematic rendering here. The base metal displayed large spherical α-Mg islands in a fine $\alpha + \beta$ ($Al_{12}Mg_{17}$) matrix that was formed by eutectic reaction during nonequilibrium cooling. The SZ displayed a fine grain structure, resulting from dynamic recrystallization, and it was characterized by partial or full re-solution of the β phase into the α phase.**
>
> **Hardness: The hardness distribution across the profile of a joint, obtained under optimum conditions, was determined at mid-thickness. The hardness displayed large fluctuations and, as a result, it was not possible to discern any trends, for schematic rendering here.**
>
> **Tensile Properties: A joint, produced under optimum conditions, was tested transverse to the weld. Fracture occurred at the base metal and, accordingly, the joint properties were those of the base metal (F_{tu}, 34.8 ksi, about 4% elongation). Testing of a small longitudinal specimen excised from the SZ Indicated an F_{tu} of about 49 ksi and an elongation of about 5%. The superior properties of the SZ are evident.**

Katoh and Tokisue [84] studied same metal FSW of 0.25 in. thick AZ31 plate. Rather than indicating a temper, the authors indicated an ultimate tensile strength of 35.4 ksi and an elongation of about 16.8%. Welding was performed parallel to the rolling direction, using a carbon steel (SK105) tool with a smooth (unthreaded) conical pin; the tool was tilted 3^{O}. The travel speeds were in the 1.2-11.8 in. / min range and the rotational speeds in the 582-1332 rpm range. No other weld parameters or tooling information were disclosed, and the authors did not indicate a welding direction. The study involved macro / microstructural characterization by OM, hardness measurements, tensile and impact testing, and measurements of temperature and welding force.

> **Macro / Microstructure: The authors indicate that the shape of the stir zone (SZ) generally reflected the shape of the probe and they seem to indicate that the TMAZ was narrow and that the onion ring pattern, an outcome of threaded pins, was not observed. The authors also discuss the stirring action of the shoulder; it appears that they classify the region under the shoulder as part of the stir zone. The SZ had finer grain structure than the base metal and it became finer with increasing the travel speed and / or decreasing the rpm, as a result of the lower temperatures associated with these conditions. The width of the SZ decreased with increasing the rotational speed. The authors did not refer to a HAZ in the macro /**

[u] *Thixomolding is a semi-solid processing method.*

microstructures discussed. It is unfortunate that the macrographs presented did not lend themselves to schematic rendering of the weld zones here.

Hardness: The hardness distribution across a joint profile was determined at mid-thickness. The hardness appeared to be more or less uniform and close to the hardness of the base metal. No hardness minima were observed in the HAZ or TMAZ, and the authors indicate that this behavior was also observed in friction welding and GTAW of AZ31.

Tensile Properties: Tensile testing was performed transverse to the welds. Before testing, the specimens were machined from the face and root to a thickness of 0.16 in. The properties obtained depended on the travel and rotational speeds used, but no consistent trends could be discerned, as schematically depicted in Figure 28. Joint efficiencies ranged from 82-103% and joint elongation ranged from 35% to 70% that of the base metal; these percentages are based on the base metal tensile properties published by the authors. All fractures, regardless of the welding conditions, occurred by dimple rupture, near the SZ / base metal boundary on the advancing side. Joints with low elongation values fractured at 45^{O} angle to the tensile axis. Joints with high elongation values had V-shaped fractures, initiating at the face and root sides. Typical macrographs of the fractures were published.

Impact: Notched impact specimens were prepared, with the notch cut at the center of the SZ. Before testing, the specimens were machined from the face and root to a thickness of 0.2 in. All specimens showed impact values that were higher than the base metal; the highest value reported was 183% that of the base metal impact value published by the authors. The impact value obtained depended on the travel and rotational speeds used, but no consistent trends could be discerned, as schematically depicted in Figure 29.

Other Results: The temperatures resulting from welding were measured at mid-thickness, using thermocouples inserted at predetermined positions along the weld line, 0.24 in. from the weld centerline. The temperature profiles obtained at each position showed the temperature rise as the tool approached that position, the peak temperature reached and the temperature decay as the tool moved away. Peak temperatures of almost 900 F were reported. The authors also measured the welding force as a function of time and welding parameters; interested readers may wish to consult the reference in that regard.

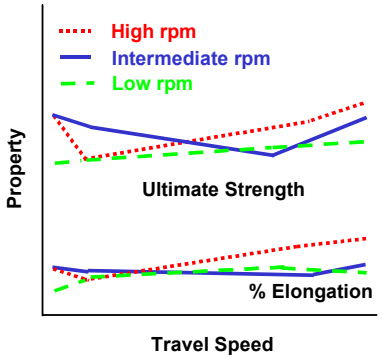

Figure 28: Variation of tensile properties with travel and rotational speeds. AZ31.

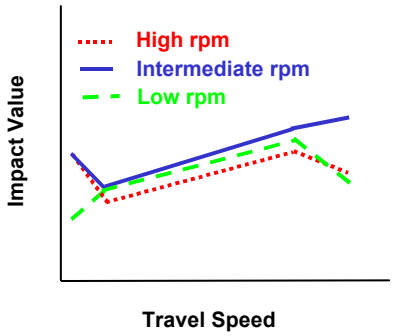

Figure 29: Variation of the impact value with travel and rotational speeds. AZ31.

Saito *et al.* [85] studied same metal FSW of Mg-6Al-2Ca sheet in the 0.03-0.08 in. thickness range. Rather than indicating a temper, the authors indicated an ultimate tensile strength range of 35.5-38.3 ksi. This aside, the authors pointed out that Mg-6Al-2Ca is noncombustible alloy, with high ignition temperature, brought about by the addition of Ca, which also acts as a grain refiner and a strengthener; there appears to be no US equivalent for this alloy. Welding was performed at rotational and travel speeds in the 1500-6000 rpm and 2-39.4 in. / min, respectively. No other weld parameters or tooling information were disclosed, and the authors did not explicitly indicate a welding direction. The study involved a determination of the optimum welding conditions, macro / microstructural characterization by OM and TEM, a determination of the susceptibility to corrosion and tensile testing. FSW is compared to laser welding and GTAW.

Developing Optimum Welding Parameters: The rotational and travel speeds were varied in order to determine the optimum conditions. The authors reported that the optimum welding speed- rpm window for Mg-6 Al-2 Ca is narrower than that for AZ31, due to the lower formability of former. The authors further reported that the optimum travel and rotational speeds decreased with increasing stock thickness.

Macro / Microstructure: The authors report a nugget / stir zone (SZ) that is identical in shape to that depicted in Figure 11 (a), and displaying a concentric onion-ring pattern. There was Weld flash on the advancing side. The authors indicate that there was no TMAZ, between the SZ and base metal and no mention is made of a HAZ, even in laser and GTAW joints. Both the base metal and the SZ displayed

equiaxed grain structures, with that of the SZ being much finer. The authors argue that the SZ had experienced dynamic recrystallization (DRX), followed by static grain growth after passage of the tool. Al-Ca particles were detected on the grain boundaries of the SZ and base metal; those in the SZ were much finer. The authors also reported the macro / microstructures observed in laser joints and GTAW for those interested readers.

Corrosion: Susceptibility to corrosion was determined by immersion of the joints in 3.5% NaCl solution for 24 hr, and measuring the resulting weight-loss. The base metal was found to be more susceptible to corrosion than the SZ.

Tensile Properties: Tensile testing was performed transverse to welds. The authors reported joint efficiencies in 91-94% range, with the fractures occurring in the weld (SZ). The corresponding joint efficiencies for laser welding and GTAW were, respectively, 86% and 46%.

6.3 Ferrous Alloys-Steels

The steels investigated in the work reviewed in this section can be divided into four categories. The first is the low carbon 12 % Cr steel and dissimilar 12% Cr / plain low carbon steel. The second is plain low carbon steels (AISI 1010 and AISI 1018). The third is HSLA (high strength low alloy) [v] and low carbon high strength steels (HSLA-65 and DH/EH-36, respectively). The fourth is stainless steels (Al-6XN, 304 and 304L). Unless otherwise stated, no post-weld heat treatments were used. It is recalled here that steel experiences polymorphic transformations, and these can mask the presence of some of the weld zones typically observed in aluminum and magnesium alloys. It is felt that these polymorphic changes are the reason for the conflicting reports, soon to be evident, about the presence or lake thereof of the TMAZ, HAZ and nugget / stir zone.

Thomas [86] conducted one of the earliest feasibility studies on FSW of steels. He studied same-metal (12% Cr steel) and dissimilar steel (low carbon 12% Cr steel / low carbon steel) welding of 0.47 in. plate stock. He observed that, unlike most nonferrous alloys, which show little or no color change resulting from temperature increase during FSW, a color change occurs during FSW steel. The tool shoulder developed a bright orange color (over 1800 F) within seconds of contacting the plate. As the tool traveled, the weld track immediately behind it appeared orange / bright red (1650-1830 F). This color changed to a darker cherry red (about 1100 F) a short distance (about 1 in.) from the tool. The tool maintained its bright orange color through out. The temperature increased with increasing the rotational speed. The study focused on two-sided welds; i.e., a weld pass from one surface followed by another pass from the opposite surface. In same-metal (12% Cr steel) welding, the author reported a TMAZ, and a HAZ. The TMAZ experienced recrystallization and grain growth; the author did not recognize a nugget / stir zone. The HAZ showed evidence of some transformation, but only near the weld, and there was no evidence of grain growth. Macrographs depicting typical joint profiles in same metal and dissimilar steel joints were presented.

In another feasibility study, Lienert and Gould [87] investigated same-metal FSW of 0.25 in. thick AISI 1010 steel plate. Welding was performed parallel to the rolling direction, using a travel speed of 1 in. / min. No other weld parameters or tooling information were disclosed. The authors list two weld zones, the stir zone (SZ) and the HAZ, in addition the base metal; however, the actual joint profile showing these zones was not published. Contrasting the work of Thomas, [86] the authors here reported no TMAZ. The SZ underwent DRX and it displayed a "swirl pattern" consisting of alternate bands of fine and coarse grains of a very fine ferrite / carbide aggregate with polygonal and Widmanstatten ferrite. The HAZ displayed three regions, a coarse grained region surrounding the SZ, a fine grained region encompassing the coarse grained region, and an intercritical region near the base metal. The constituents found in the coarse and fine grained regions of the HAZ were similar to those encountered in the SZ. Using a thermal model, the authors surmise that the grain coarsened region experienced peak temperatures well above A_3 (about 1625 F), leading to appreciable grain growth of the austenite. During subsequent cooling, this coarse austenite transformed to coarse ferrite-carbide mixtures. The grain refined region experienced temperatures just above A_3 and, accordingly, the austenite grains remained fine in size, since no appreciable grain growth would take place. During subsequent cooling, this fine austenite transformed to fine ferrite-carbide mixtures. The intercritical region experienced temperatures between A_3 and A_1 (about 1300 F) and, as such, no austenite transformations took place. The model predicts that most of the weld would experience temperatures above about 1832 F. Hardness measurements revealed that the SZ was harder than the base metal and the various HAZ regions. Within the SZ, however, there were wide hardness fluctuations, depending on the phases (bands) present. In transverse tensile testing, the authors reported a joint efficiency over 100%. The joint elongation and reduction in area were, respectively, 55% and 140% of their base metal counterparts. The aforementioned percentages are based on the tensile properties of the base metal published by the authors. Tensile failure was in the coarse grained region of the HAZ; however, no photographs or schematics of failure locations were published. The joints also passed the 180 ^{O} root and face bend test. Based on this work, the authors concluded that FSW of steels is feasible.

---

[v] *HSLA steels are micro-alloyed steels with high strength properties.*

In follow up work, Lienert *et al.* [46] investigated same-metal welding 0f hot rolled 0.25 in. thick AISI 1018 steel plate. Welding was performed parallel to rolling direction, using Mo and W-Based tools, 1 in. / min travel speed, rotational speeds in the 450-650 rpm range, and 4200 lbf axial tool force. The following tool dimensions were disclosed: shoulder diameter, 0.75 in., and; pin length, 0.25 in. A shielding gas was used to protect against oxidation. No other weld parameters or tooling information were disclosed. It is reported that during welding, the tool and the flash around the tool glowed a reddish-orange color, suggesting temperatures of at least 2012 F. Temperatures of about 1814 F were measured near the shoulder / workpiece interface. The authors surmise that temperatures as high as 2192 F, well in the austenite phase field, could be reached elsewhere in the stir zone where measurements are not possible. The authors report three main zones in the welded joints; viz., the stir zone (SZ), the HAZ and the base metal. As before, [87] no TMAZ is reported; the authors here refer to the TMAZ as HDAZ (heat and deformation affected zone). The absence of a HDAZ / TMAZ was attributed to the polymorphic transformations, in the steel, which tend to obliterate flow lines and similar features that distinguish the HDAZ in aluminum alloys. The HAZ was reported to consist of four regions; viz., grain coarsened (CGHAZ), grain refined (FGHAZ), intercritical (ICHAZ) and subcritical (SCHAZ). Using the above descriptions and the sketch and partial macrograph published by the authors, an approximate schematic of the joint profile was constructed and is depicted in Figure 30.

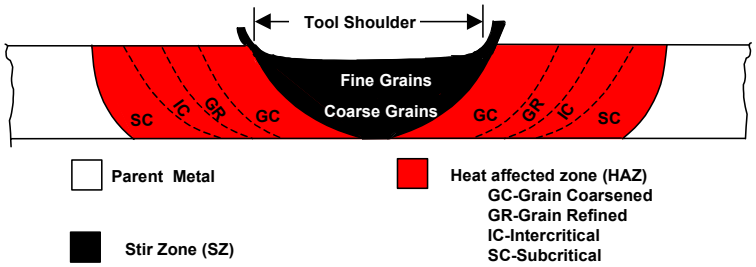

Figure 30: The SZ and various HAZ regions. AISI 1018.

<u>Microstructural characterization</u> was performed using OM and SEM-EDS. The SZ displayed the presence of proeutectoid (grain boundary) ferrite, ferrite / carbide aggregate (fine pearlite or bainite) and what appears to be Widmanstatten ferrite with aligned second phases (possibly carbides). [w] The authors clearly classify the region under the shoulder as a region of the SZ and report that this region had a generally finer grain structure than that observed at the center of the SZ. The microstructure of the SZ was indicative of hot working at temperatures well into the austenite phase field. The authors reported evidence of Mo (from the tool) in the SZ. The microstructures observed in the HAZ regions were rationalized in terms of the temperatures experienced and the Fe-C phase diagram, as shown in Figure 31. The CGHAZ experienced temperatures well above A_3, leading to austenite grain growth and the subsequent transformation of that austenite, during cooling, to coarse ferrite and pearlite constituents. The microstructure in this region was very similar to that of the SZ. The FGHAZ experienced temperatures just above A_3 (not sufficiently high for grain growth). Upon cooling, this fine austenite transformed to fine products; viz., fine proeutectoid ferrite and fine pearlite. The ICHAZ experienced temperatures within the austenite + ferrite phase field (i.e., temperatures between A_3 and A_1). As in the FGHAZ, the resulting microstructure consisted of ferrite and fine pearlite, except that here the ferrite appeared to have mixed grain size. [x] The SCHAZ experienced temperatures below A_1, leading to spheroidization of the carbides in the pearlite. The base metal is reported to consist of fine equiaxed ferrite grains and a fine pearlite mixture. In general, the various microstructural features reported in the SZ and HAZ seem to be similar to those described the previous work. [87] The various operating mechanisms, in the SZ (DRX and DRV) and the roles of, stress / strain, strain rate and stacking fault energy are discussed. The authors point out that microstructural evolution in the SZ is not as easy to interpret as that of the HAZ. This is because the HAZ experiences a thermal

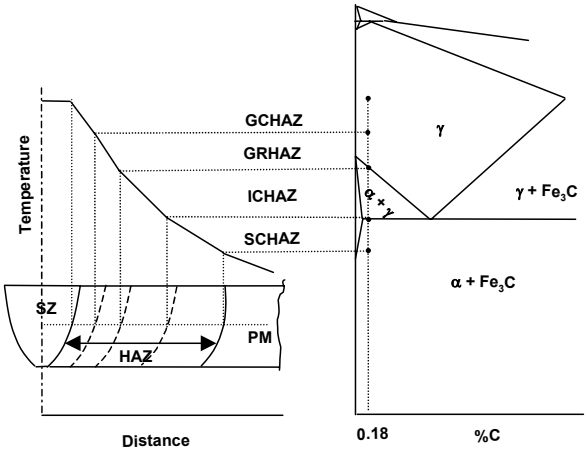

Figure 31: The microstructures of the SZ and HAZ regions rationalized in terms of the Fe-C phase diagram. The abbreviations are explained in Figure 29. AISI 1018

[w] *This description is that of the author of this document.*
[x] *Note that within the austenite + ferrite phase field, the austenite will have much higher C% than the nominal 0.18% of the steel. As such, there is a possibility that the new austenite could transform to martensite or to constituents that are not ordinarily expected in AISI 1018.*

cycle only, whereas the SZ experiences both thermal and mechanical cycles. This, however, may not be entirely accurate, since a TMAZ is likely to have formed, only to be obliterated by polymorphic transformations, thereby making it appear as a part of the HAZ or the nugget / stir zone. A schematic of the hardness distribution across the joint is depicted in Figure 32; the authors, however, do not indicate the location where the measurements were made. The welded samples passed a 3T bend test (15 % strain in outer fiber). The authors also list the joint tensile properties published in the previous work. [87] The failure location here, however, was in the base metal, not in the CGHAZ as was the case in the previous work. The authors argue that the tensile data indicate that the SZ and HAZ have greater yield and ultimate tensile strengths than the base metal. This and the good bend ductility indicated that FSW is suitable for welding mild steel.

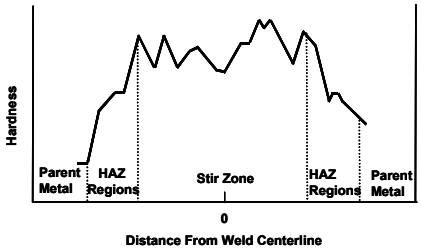

Figure 32: Hardness distribution across joint profile. AISI 1018.

FSW of HSLA steels is of interest to the US Navy in developing advanced ship-hull design concepts. Working towards that end, Konkol *et al.* [88] investigated same metal FSW of HSLA-65 [y] steel plate stock; the thicknesses used were 0.5 and 0.25 in., with the latter machined from the 0.5 in. thick plate stock. The 0.25 in. plates were welded in one pass, whereas the 0.5 in. plates were welded in two passes, one from each of the "top" and "bottom" surfaces. Prior to welding, a starting hole was drilled in the plates to be welded and both the tool and plates were heated to 575 F, above the ductile-brittle transition of the tool material. Welding was performed using a truncated cone (AKA, frustum of a cone) tool made of tungsten, rotational speeds in the 400-450 rpm range and travel speeds in the 3.9-5.5 in. / min range. The following tool dimensions were disclosed: pin diameter, 0.24 in. (for 0.25 in. plate) or 0.31 in. (for the 0.5 in. plate). During welding, argon was used for shielding; an exception was made for those specimens intended for corrosion studies. No other processing details were disclosed by the authors.

Macro / Microstructure: In either of the thicknesses welded, the authors identified a stir zone (SZ) and a HAZ, with no TMAZ evident. Approximate schematics of the joint profiles are presented in Figure 33. The weld faces (weld track) exhibited deep concentric gouges (ripple), with scale rolled within them; the ripple is schematically depicted in Figure 6. The authors indicate that this ripple, which results from motion of the tool shoulder, can adversely affect fatigue performance and, as such, it should be eliminated by grinding. The base metal displayed fine equiaxed ferrite with a small amount of pearlite in the form of bands. The HAZ displayed equiaxed ferrite and randomly distributed pearlite packets; the ferrite here appeared somewhat finer than its counterpart in the base metal. The authors indicated that the HAZ was heated above A. The SZ displayed coarse grained ferrite, Widmanstatten ferrite and small pockets of a ferrite + carbide aggregate.

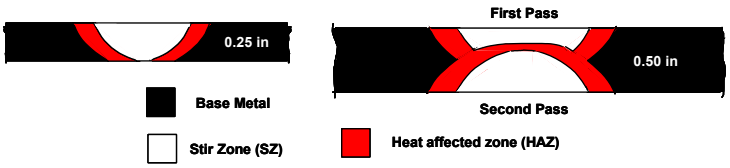

Figure 33: Joint profiles in 0.25 (single pass) and 0.50 in. (two pass) thick HSLA-65 plate stock.

Mechanical Properties: Two 0.5 in. and two 0.25 in. weld joints were tensile tested transverse to the welds. All fractures took place in the parent metal. Instead of obtaining the actual tensile properties of the plate stock, the authors opted for listing the minimum values of the steel specification. The joint ultimate strength of all four joints exceeded the corresponding minimum value. The same is true for the yield strengths of three of the joints; one 0.25 in. joint, however, displayed lower yield strength than the specification minimum. Inasmuch as the joint elongation is concerned, the 0.5 in. joints exceeded the specification minimum, whereas the 0.25 in. joints fell slightly below. [z] Based on these data, joint tensile properties were deemed acceptable. Two root and two face 120^{O} bend tests were performed on joints from each plate thickness, after machining from both surfaces; the bend factors were 2 and 2.5, respectively, for the 0.25 in. and 0.5 in. joints. Note that, for the 0.5 in. joints there is really no root, since the plates were welded in two passes (one pass from each surface). All the 0.5 in. joints passed, whereas the two root bends of the 0.25 in. joints failed (cracked). The failures were attributed to the smaller bend factor (higher strain) used with the 0.25 in. joints, the fact that the 0.5 in. joints did not really have a root and to some differences in the bend test details. Charpy V-Notch (CVN) specimens were machined from the 0.5 in. joints, such that the notch axis was at the SZ centerline, normal to the plate surface. For comparison, CVN specimens were also machined from the base metal. Impact testing was performed at - 20 and - 40 F. Toughness of the SZ, while considerably lower than that of the base metal, was considered

[y] *The major constituents of the steel, in weight %, were C, 0.1; Mn, 1.4; Si, 0.2, and; Cu, 0.22. The steel is covered by ASTM A945.*
[z] *While fracture took place in the base metal, the strain would tend to be localized in some of the weld zones. This apparently influenced the yield strength and elongation of some joints, causing them to fall below their respective specification minima.*

adequate for ship hull construction. Hardness distributions across two joints, one 0.25 in. and the other 0.5 in., were determined at mid-thickness and close to the bottom (i.e., root of 0.25 in. joint and face of second pass in 0.5 joint); refer to Figure 33. In both locations of the 0.25 in. joint, the SZ was harder than base metal and HAZ and the hardness minima appeared to be in the HAZ. The SZ and HAZ hardness values on the retreating side appeared to be generally higher than their counterparts on advancing side. In the 0.5 in. joint, the SZ at mid-thickness (close to the roots of both passes) was harder than the base metal or the HAZ, and the hardness minima appeared to be in the HAZ. Near the bottom (that is the face of the second pass) hardness peaks could be seen in or near the HAZ and the SZ appeared to be harder than the base metal but softer than the HAZ. It is thought that this unconventional behavior was brought about by the application of two passes.

Corrosion Behavior: Salt spray testing revealed no difference in corrosion rates between the SZ, HAZ and base metal.

As a part of the aforementioned US Navy effort, Posada *et al.* [89] reported on the results of FSW studies of DH/EH-36, [aa] HSLA-65, AL-6XN, [bb] and AISI 304L steels.

DH/EH-36 Steel: The authors indicate that 0.25 and 0.5 in. thick plates of this steel have been successfully FS welded. They published a macrograph showing a weld joint profile and identifying a stir zone (SZ), a swirl region within the SZ, a dark etching TMAZ and a HAZ; the applicable plate thickness, however, was not explicitly indicated. An approximate schematic of these zones is depicted in Figure 34 (a). The authors also published a hardness map that indicates that the SZ was harder than HAZ, which, in turn was harder than the base metal. The map also indicates that the swirl region was the hardest in the SZ. The authors indicate that increasing the travel speed decreased the widths of the SZ and HAZ and increased peak hardness and joint ultimate and yield strengths. The data presented show lower heat inputs with higher travel speeds.

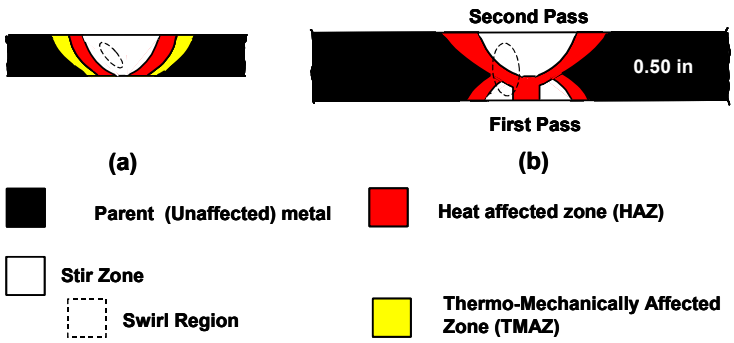

Figure 34: Joint profiles.
(a) DH/EH-36. Plate thickness not indicated.
(b) HSLA-65. 0.50 in. plate.

HSLA-65: The authors indicate that plate stock of this steel in the 0.25-0.5 in. thicknesses range has been FS welded. They published a macrograph showing a weld joint profile and identified a stir zone (SZ), a swirl region, with evidence of vertical flow, within the SZ, and an HAZ; no TMAZ was identified. An approximate schematic of these zones is depicted in Figure 34 (b). The authors also published a hardness map that indicates that the SZ was somewhat harder than the base metal and that some softening occurred in the HAZ. The authors report that the joint tensile ultimate and yield strengths were comparable to their base metal counterparts. The authors further report that HSLA-65 joints, while not as strong as their DH/EH-36 counterparts, they are tougher. A post weld distortion study was performed to compare FSW to conventional welding, using 0.25 in. plate stock. The FS welded plates displayed significantly lower angular distortion than the conventionally welded plates.

AL-6XN: The authors indicate that 0.25 and 0.5 in. thick plates of this steel have been FS welded. They report that the hardness distribution across the joint profile was similar to that in the DH/EH-36 steel, with the hardness increasing from the base metal through the HAZ and into the SZ. They further report that the strength properties of the SZ overmatched (exceeded) their base metal counterparts, with a significant reduction in elongation. Centerline sigma phase was observed in the 0.25 in. joints but not in the 0.5 in. joints. Evidence of the tool pin material (W) was found in the swirl zone. No joint profiles or hardness distribution maps were published.

AISI 304L:The authors report that FS welds made with this steel were similar those of DH/EH-36 and AL-6XN; evidence of the tool material (W) was found in the weld. They report that the hardness distribution across the joint profile was more or less uniform, and that the tensile strength properties of the SZ across the joint profile was more or less uniform, and that the tensile strength properties of the SZ exceeded

---

[aa] *This is one of the high strength steels of ASTM A131, with higher C, Ni and Cr than HSLA steels. The letter D refers to the ASTM grade; the grades are designed to meet various toughness requirements. The letter H designates the higher strength versions of the steels. The main alloying elements in this steel (% wt.) are: C, 0.18; Mn, 0.90-1.60; Si, 0.1-0.5, and; Al, 0.025 min.*

[bb] *This is a nitrogen-modified super austenitic stainless steel with superior mechanical and corrosion properties than standard 300 stainless steels. The nominal contents of the main alloying elements in this steel (%wt.) are: Cr, 21; Ni, 25; Mo, 6.5, and N, 0.2.*

those of the base metal, while maintaining high ductility. No joint profiles or hardness maps were published.

Beach *et al.* [90] and Czyryca *et al.* [91] discussed other facets of the above US Navy program. The work pertaining to aluminum armor alloys, AA 2519 and AA 5083, reviewed in sections 6.1.1.1 (g) and 6.1.1.2 of this document, respectively, is also a part of the US Navy's effort.

A group of authors [92, 93] investigated FSW of 304 stainless steel [cc] flat stock, 0.08 and 0.24 in. thick. Welding was performed using a PCBN (polycrystalline cubic boron nitride) tool, tilted 3.5°. The travel and rotational speeds were 10.6 in. / min and 1300 rpm for the 0.08 in. stock and 3.1 in. / min and 550 rpm for the 0.24 in. stock. A pin length of 0.19 in. was used for the 0.24 in. stock; pin length for the 0.08 in. sheet was not published. No other weld parameters or tooling information were disclosed, and the authors did not indicate a welding direction. Microstructural characterization was performed using OM, orientation image microscopy, SEM-EDS and TEM. The authors, however, did not report on the microstructure of the base metal.

Kokawa *et al.* [92] reported on macro / microstructural findings. For the 0.08 in. joint, the authors identified a stir zone (SZ) and a TMAZ, but did not mention a HAZ. Furthermore, they indicate that the SZ did not take the form of an elliptical nugget or exhibit the onion ring pattern. The joint macrograph published was such that it was not possible to discern the SZ from the TMAZ; no HAZ could be identified either. Figure 35 is an approximate schematic rendering depicting the combined SZ-TMAZ and showing what the HAZ and base metal zones might have looked like. The SZ and TMAZ had finer grain sizes than the base metal. The SZ displayed somewhat lower hardness than the TMAZ, but higher than the base metal. The hardness distribution across the joint profile indicates that the TMAZ on the retreating side was much wider than its counterpart on the advancing side. The authors argue that the SZ was dynamically recrystallized, since some grains displayed low dislocation density. The TMAZ, by contrast, displayed high dislocation and subgrain boundary densities, suggestive of dynamic recovery. "Tunnel-type defects" were observed at the SZ / TMAZ interface, on the advancing side. Evidence of δ- ferrite was found around said defects, at the advancing side of the SZ and at the weld centerline; the δ- ferrite was predominantly located at the austenite grain boundaries. The authors indicate that the microstructural features of the SZ and TMAZ in the 0.24 in. joint were similar to those described above, except in two aspects. The first was that σ phase, not δ- ferrite, was observed at the weld centerline and the advancing side; the tunnel shaped defects were not specifically mentioned. The second was that bands, similar to the onion-ring pattern, containing the σ phase were observed at the advancing side of the SZ. No σ phase was detected at the retreating side and no δ- ferrite was detected anywhere. No macrograph depicting joint profile was published, and, again, there was no mention of the HAZ.

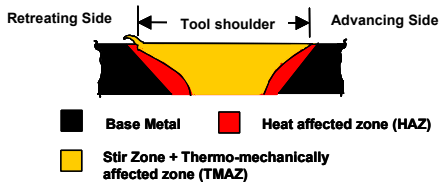

Figure 35: Joint profile. 0.08 in. stock. 304 stainless steel. The HAZ was not identified by the authors.

Park *et al.* [93] conducted a comparative corrosion study of the 0.24 in. FS welded joint and a similar GTAW joint. They show a joint profile that is similar to Figure 11 (a), with more weld flash on the advancing side. On that joint profile, the authors identified a SZ and a HAZ; no TMAZ was identified on the joint profile or mentioned in the text. Figure 36 is an approximate schematic depiction of the joint profile reported by the authors, with a TMAZ inserted. Corrosion resistance was evaluated by exposure to ferric sulfate-sulfuric acid mixture for 72 hr. The advancing side of SZ was most susceptible to corrosion. This was followed by the sensitized region of HAZ of the GTAW joint, sensitized region of the HAZ of the FSW joint, the base metal and the remainder of SZ, in decreasing order of susceptibility. The authors argue that the increased susceptibility of the SZ advancing side to corrosion was due to the presence of grain boundary σ phase, and the attendant Cr-depletion. The authors further argue that in the remaining SZ regions, dissolution of residual ferrite and carbides, during FSW, resulted in a decreased susceptibility to corrosion.

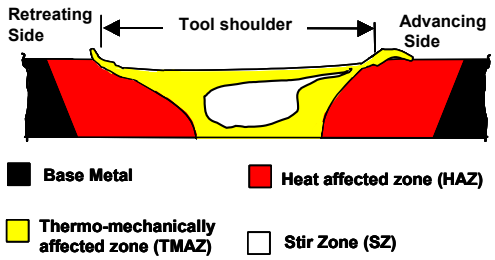

Figure 36: Joint profile. 0.24 in. stock. 304 stainless steel. The TMAZ was not identified by the authors.

[cc] *Japanese steel similar to AISI 304.*

Klingensmith *et al*. [94] investigated the macro / microstructure and hardness distribution in FS welded 0.25 in. thick AL-6XN steel plate stock. A double-sided joint configuration, with root overlap, was used. The authors indicate that a groove preparation was used. Welding was performed using a W-base tool, 150 rpm, a travel speed of 2 in. / min, and a normal force of 18000 lb_f. No other welding parameters or tooling information were disclosed. Microstructural characterization was carried out using OM, TEM-EDS and SEM-WDS (wavelength dispersive spectroscopy, AKA electron probe microanalysis or EPMA). The authors identified the familiar zones, nugget, TMAZ and HAZ, in addition to the base metal. They also reported that it was difficult to distinguish the HAZ from the base metal by microscopy. An approximate schematic rendering of the reported joint profile, without the HAZ, is depicted in Figure 37; the HAZ, however, could not be discerned in the macrograph published by the authors. The base metal displayed equiaxed austenite grains with annealing twins. Near plate mid-thickness, σ phase, appearing as streaks, was observed. The nugget displayed fine recrystallized grains, with a stream of W inclusions (swirls), mainly on the advancing side, resulting from tool wear. For each pass, the grains became smaller towards the root. Banding was also reported, but deemed the result of differences in austenite etching response as opposed to an onion ring pattern, which consists of alternating ferrite and austenite layers. Near plate mid-thickness and also near the TMAZ, σ phase, appearing as fragments (not streaks), was observed. The HAZ displayed large austenite grains with smaller recrystallized austenite grains present at their grain boundaries. The authors suggest that the fine grains were brought about by a combination of residual strains (from plate working) and FSW temperatures. No evidence of the σ phase was found in the HAZ. The TMAZ transitioned the nugget microstructure to one that is very similar to the base metal. Microhardness data indicate that the nugget was generally harder than the base metal, with the TMAZ and HAZ transitioning the two. It must be noted, however, that the hardness traces in all zones and in the base metal displayed noticeable fluctuations.

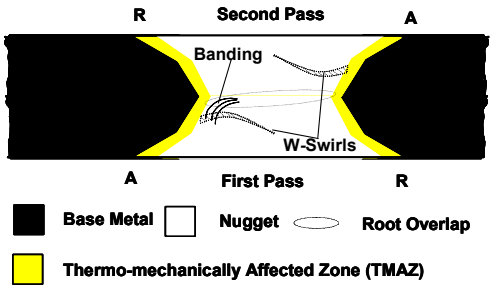

Figure 37 : Joint profile in double-sided FS weld joint. The HAZ could not be discerned. "A" and "R" indicate advancing and retreating sides, respectively. 0.25 in. thick AL-6XN steel plate.

6.4 Titanium Alloys

Juhas *et al.* [95] conducted a microstructural survey of FS welded Ti-6Al-4V flat stock, using OM and TEM. The authors indicate that welding was performed at EWI (Edison Welding Institute) and that they have no knowledge of the welding parameters, tooling data or initial material condition (heat treatment); stock thickness was not indicated. No macrograph of the joint profile was reported. The authors report that the most striking observation was the absence of a distinct TMAZ. As such, the stir zone (SZ) lies adjacent to what appears to be a relatively coarse undeformed structure that the authors refer to as the HAZ / TMAZ. The base metal consisted of Widmanstatten (α / β) with coarse equiaxed α grains along the prior β grain boundaries. The authors state that this microstructure is indicative of heating below the β transus, followed by relatively slow cooling. The microstructure near the top of the SZ displayed fine equiaxed α grains and fine α / β colonies. A similar but coarser microstructure was observed near the center of the SZ. The TMAZ / HAZ displayed even finer arrangements of these same constituents. Hardness distributions across the joint profile were obtained near the face, at mid-thickness and near the root. These distributions, however, displayed wide fluctuations that tended to mask any trends that might have existed. The authors propose that the differences between the microstructures at the top and center of the SZ were brought about by slower cooling at the center. The authors indicate that the presence of α / β colonies in the SZ is the result of moderately slow cooling from temperatures above the β transus. By contrast, the mechanism for the formation of the equiaxed α is unclear, although DRX, nucleation and growth and /or superplastic behavior may have played a role. The authors did not address the TMAZ / HAZ microstructure in any depth.

In follow up work, Juhas *et al.* [96] investigated the microstructure, hardness and residual stress distribution in FS welded Ti-6Al-4V 0.24 in. thick plate. Two initial material conditions were investigated, mill annealed (30 min at 1350 F) and β annealed (1899 F / 30 min followed by stabilization anneal 1350 F 2 hr / air cool). The plates were grit blasted and pickled in an HF / HNO_3 acid mixture. Welding was performed using rotational and travel speeds of 275 rpm (counterclockwise) and 3.74 in. / min, a shoulder plunge depth of 0.005 in., and argon gas shielding. No other welding parameters or tooling information were disclosed, and the authors did not indicate a welding direction or publish any joint profile. No temperature measurements were made. Microstructural characterization was by OM, and the authors indicate that future efforts will include TEM analyses. The hardness data collected were in the form of contour maps, generated for longitudinal sections surrounding the retracted pin. When a longitudinal section through the weld centerline is prepared, the SZ would be on the trailing edge of the tool, whereas the TMAZ, HAZ and base metal would be on the leading edge. Longitudinal and transverse (respectively,

// and ⊥ to the weld) residual stresses were measured by means of x-ray diffraction, first at the face of the weld and then after removing 0.01 in. of the material from the face, by electropolishing.

Mill Annealed: The base metal displayed coarse equiaxed α grains and α / β colonies (transformed beta). The SZ displayed Widmanstatten structure, with fine α grains on some of the prior β grain boundaries; this is a refined version of the β annealed microstructure described below. The authors state that the presence of the Widmanstatten structure indicates that temperatures in excess of the β transus were encountered during welding; this, however, contradicts the statement made in the earlier work [95] reviewed above. The TMAZ consisted of two regions. The first region, a band next to the SZ, displayed fine equiaxed α, and the second region, close to the base metal, displayed coarse equiaxed α grains; presumably, α / β colonies were present in both regions. The authors argue that the fine-grained region must have deformed at temperatures within the α / β phase field, and that grain coarsening was inhibited by either a fast cooling rate or a relatively low temperature. The hardness contour map shows that the SZ was harder than the base metal; the TMAZ hardness appeared to be close to that of the SZ. Peak hardness was reported around the shoulder and bottom of the pin. An approximate schematic rendering of the residual stress data obtained is depicted in Figure 38. It is seen that the longitudinal stresses are tensile in nature, whereas those in the transverse direction are, for the most part, compressive. The authors attribute this to the downward force, which causes the plate to elongate slightly in the welding direction, thereby creating local tensile stresses, balanced by compressive stresses acting normal to the tensile axis. [dd] Figure 38 further shows that residual tensile stress peaks occur near the TMAZ, with the retreating side displaying somewhat higher residual stresses. Finally, as would be expected, grit blasting resulted in significant compressive residual stresses in the base metal, in both the longitudinal and transverse directions, at the surface. The effect, however, tended to disappear below surface.

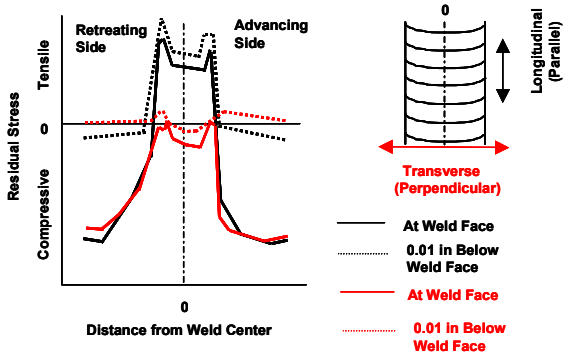

Figure 38: Residual stress distribution in the longitudinal and transverse directions. Mill annealed Ti-6Al-4V.

Beta Annealed: The base metal displayed Widmanstatten structure at the grain interiors, with α grains decorating the prior β grain boundaries; the micrograph published indicates a fairly coarse β grain size. The SZ experienced temperatures in excess of the β transus and it displayed Widmanstatten structure with α grains on the prior β grain boundaries. The TMAZ, adjacent to SZ, displayed a band of fine equiaxed alpha, as was the case in the mill annealed weld. Away from the SZ, the TMAZ displayed a curved Widmanstatten structure, indicative of localized plastic deformation without recrystallization. The hardness contour map shows that the hardness of the β annealed base metal was generally higher and less uniform than its counterpart. The residual stress data obtained reflect trends similar to those observed in the mill annealed material (Figure 38). It appeared, however, that here the compressive component, brought about by grit blasting, was smaller than its counterpart in the mill annealed material. It is thought that this was due to the larger stress relief achieved at the elevated temperature used for β annealing.

It is worth noting that here, in contrast to the earlier work, [95] the authors identify a TMAZ. It is felt that the difficulty in identifying various zones in titanium alloys is brought about by the existence of polymorphic transformations. A similar situation exists in steels (6.3).

In reviewing the above two papers, it became very clear that identifying a unique deformation-thermal path based on microstructure only is very difficult. A determination of the temperature regimes and cooling rates involved (or the use of some validated model) would certainly be helpful in microstructural characterization. Even then, the issue would remain clouded by the vague (e.g., transformed beta) and interchangeable (e.g., Widmanstatten, acicular) terms used by the titanium technical community. Some standardization and definition of the terms used would be beneficial. If modeling of the stains and strain rates involved in FSW is at all possible, it will enable the use means similar to Prasad's processing maps to shed some light on the operating deformation mechanisms

---

[dd] *The measured residual stress distribution is a function of several factors, many of which are interrelated. These include the welding parameters (downward force, speeds, tilt, etc.), tool design (configuration and material), initial microstructure, the thermal effects associated with welding (heating, cooling and phase transformations), the strains / strain rates resulting from metal deformation, the clamping specifics, and the preexisting residual stress fields (grit blasting, heat treatment, etc.). It seems that some modeling would be required to understand how these factors might interact to produce the final observed residual stress field and how they might be modified to produce desirable effects.*

and the prevailing defects at different temperature-strain rate regimes. Figure 39 depicts approximate schematics of such maps for Ti-6Al-4V with equiaxed α + β (e.g., mill annealed) and lamellar (e.g., β annealed). Processing maps of this type have been developed for a range of alloys, metal matrix composites and aluminides.[97-103]

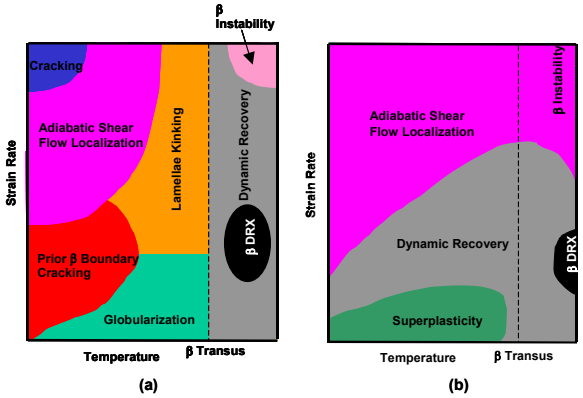

Figure 39: Processing maps. Ti-6Al-4V.
(a) Starting microstructure: equiaxed α + β.
(b) Starting microstructure: lamellar α + β.

6.5 Copper Alloys

Working on a program to construct canisters for storage of spent nuclear fuel, Andersson and Andrews[104] experimented with FSW of 0.4 and 2 in. thick oxygen free copper plate. In welding the 0.4 in. plates, they report that a pilot hole had to be drilled at the start point. The pilot hole was slightly undersize and it duplicated the tool tilt. To assist in pin penetration, the tool was fed slowly into the pilot hole, until the shoulder had just touched or penetrated the plate surface. A certain dwell time was then allowed for the temperature adjacent to probe to reach about 750 F. At that point, the tool was traversed, along the butt line, initially at 0.60 in. / min and increasing gradually to a steady state maintained to the end of the weld. Argon gas was used for shielding, to protect against oxidation. The authors indicate that, without the pilot hole, the tool prematurely fractured, or otherwise became damaged. Furthermore, a tool made of tungsten, sintered with a nickel-iron binder, had to be used, since conventional tool steels softened at the welding temperatures; a temperature of about 1200 F was measured 0.2 in. from the tool. The authors published a macrograph showing the profile of a joint that was produced at steady state travel speed of 2.2 in. / min. The various zones were faintly visible, but the profile appeared to reflect that shown in Figure 11 (b), with weld flash and the onion ring pattern. The authors reported that the central nugget displayed fine recrystallized grains. The TMAZ displayed larger grains that were subjected to some deformation. The HAZ displayed larger grains than the base metal. It should be noted, however, that the grain size and deformation effects reported by the authors could not be discerned in the published macrograph. Bend testing confirmed that the joints were of adequate quality. The authors indicate that tensile testing revealed uniform properties along the weld, with joint efficiencies around about 77%, and with fractures occurring at random locations. For FSW of thicker copper plate, the authors report that successful welding relied more on the effectiveness of the pin than the shoulder, to generate frictional heat. The authors published a macrograph showing a joint profile in a 2 in. plate. The most interesting feature here was the existence of an upper and a lower nugget, a result of the pin design used. Bend and tensile testing provided results that reflected those obtained in welding the thinner plate.

6.6 Dissimilar-Metal Group Welding

This section is concerned with welding metals and alloys of different groups. Specifically the articles reviewed here pertain to welding of aluminum to magnesium and to steel. This is different from welding of dissimilar alloys from the same group, such as dissimilar aluminum alloy welding (section 6.1.2) and dissimilar steel welding (section 6.3).

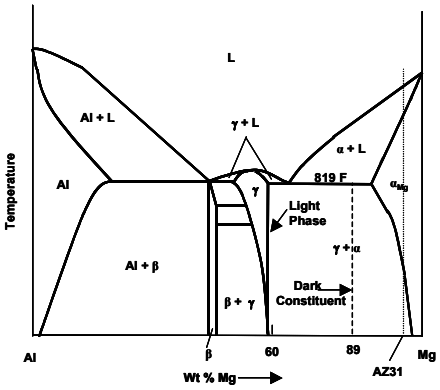

Figure 40: The Al-Mg phase diagram.

6.6.1 Aluminum-Magnesium

Michiuchi et al. [105] FS welded 0.24 in. thick plates of A 1050 and AZ31,[ee] using a tool tilt of 3°, a travel speed 0f 3.5 in. / min and a rotational speed of 2450 rpm (counterclockwise). No other weld parameters or tooling information were disclosed, and the authors did not indicate a welding direction or the tempers of the alloys welded. A 1050 was placed on the retreating side and AZ31 on the advancing. The authors published a macrograph showing the joint profile. There, the A 1050 side was light etching and the AZ31 was dark etching. A large irregular region, not connected to the face or root, appeared near the weld centerline. The region had some porosity, light etching equiaxed γ ($Al_{12}Mg_{17}$) grains and a dark etching constituent (the eutectic mixture, α + γ, where α is a Mg-rich solid solution. The phases and constituents were identified on the basis of EDS analyses and x-ray diffraction. Based on the Al-Mg phase diagram, Figure 40, the authors argue that the eutectic mixture must have formed due to

[ee] *A 1050 is a Japanese alloy similar to AA 1050. AZ31 is a US designation for a Mg alloy. The Japanese designation system does not appear to include AZ designations. As a result, the alloy is presumed to be the US AZ31. It is not clear, however, whether the authors refer to the A, B or C versions of the alloy; these versions differ somewhat in their Fe and Ca contents.*

liquation during FSW; i.e., the temperature must have locally exceeded the eutectic temperature (about 819 F). The authors cite other work that supports this contention. In other results, the hardness of the irregular region was found to be significantly higher than either the A 1050 or AZ31 base metals; AZ31 was somewhat harder than A1050. Furthermore, the weld interface at the weld face shifted from the centerline to the advancing (i.e., Mg) side. The authors state that reversing the positions of the alloys led to failure; they, however, did not explain what constitutes failure. It is interesting to note the work of Larsson *et al.* [31] and Maeda *et al*. [43] demonstrated the importance of alloy position (orientation) in FSW dissimilar aluminum alloys; see section 6.1.2.

In the Al-Mg FSW work just cited, the authors are of the view that the γ / $\alpha + \gamma$ microstructure, observed in the irregular region, was the result of liquation during FSW. There is an alternate explanation; viz., that these phases formed as a result of solid state diffusion. What we have here is basically an A 1050- AZ31 diffusion couple, with the butt line being the Matano interface. At any given temperature, interdiffusion will take place across the interface, as a result of the concentration gradients present; i.e., Mg (in AZ31) will diffuse to the A 1050 side, while Al (in A 1050) will diffuse to the AZ31 side. Diffusion will be by unequal exchange of various atoms, and this can lead to interface shift. This is the Kirkendall Effect. Here, it appears that Mg diffused faster than Al, leading to a shift of the (Matano) interface towards the AZ31 side, as reported by the authors, and the new interface is now referred to as the Kirkendall interface. The voids reported by the authors could very well be Kirkendall Voids. The ultimate aim of interdiffusion is to equalize the concentrations across the diffusion couple. In the process, composition bands would form, perpendicular to the diffusion direction, in the diffusion zone. These bands will eventually correspond to the single and multi phase fields on the Al-Mg phase diagram; second phase formation can also occur during soaking at the FSW temperature and / or during subsequent cooling. All of these reactions as well as the formation of voids can take place without involving the liquid (melt) phase. It is important to note that the temperatures at the face and the root of the weld would typically be different. This can cause the Kirkendall interface at the root and that at the face not to coincide. Temperatures aside, there would also be concentration and strain gradients throughout the width and the depth of a joint, and these can further influence diffusion. The above discussion was focused on butt joints of dissimilar metal group members. It is believed that the same diffusion aspects would be applicable to lap and spot joints of dissimilar metal group members. In fact, it is further believed that the arguments could be extended to include joints made between dissimilar alloys from the same group.

6.6.2 Aluminum-Steel

Welding of aluminum alloys to steel is of interest to the automotive industry. Fusion welding of these alloys, however, does not produce sound joints, due to the formation of brittle intermetallic compounds. FSW appears as a viable approach. Earlier experiments, however, showed that inserting the tool pin at the interface made it impossible to complete the weld, due to rapid pin wear. The welds could be successfully completed only when the pin was offset to the aluminum side, just penetrating steel. The work reviewed here was initiated by the Japanese automotive industry.

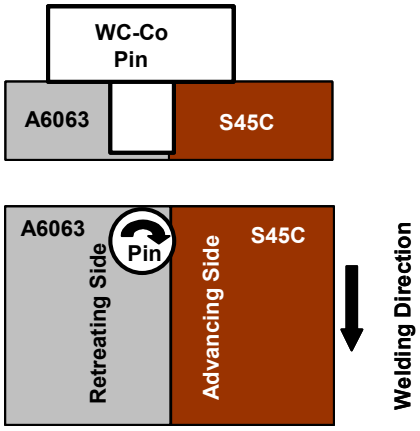

Figure 41: Dissimilar welding of A6063 Al and S45C steel.

Ishii *et al.* [106] and Shimoda *et al.* [107] studied dissimilar metal FSW of 0.24 in. thick plate stock of A 6063 aluminum alloy (hereinafter, Al) and S45C steel (hereinafter, steel). [ff] Welding was performed at rotational speeds up to 5000 rpm and travel speeds up to 39.4 in. / min, using a WC-Co cemented carbide tool with a straight-sided pin that was offset 0.08 in. to Al side, as shown in Figure 41. The following tool dimensions were disclosed: shoulder diameter, 0.8 in.; pin diameter, 0.16 in., and; pin length, 0.18 in. No other weld parameters or tooling information were disclosed, and the authors did not indicate the welding direction or the initial tempers / heat treatments of the base metals. Surface temperature at the face of the weld was measured by means of a thermocouple, placed some distance from the butt line, on the Al side; the temperatures reached at the interior regions of the weld would be higher than those measured. The exact location of the thermocouple, however, was not revealed. In a sort of a companion paper arrangement, Ishii *et al.* [106] reported on the temperature and torque findings, the optimum travel and rotational speed ranges for welding and on some aspects of the macro / microstructure. Shimoda *et al.* [107] reported on the remaining aspects of macro / microstructure, the nature of defects that form under less-than optimum weld conditions, hardness distribution and transverse tensile properties.

[ff] *A 6063 is a Japanese alloy similar to AA 6063 and S45C is a Japanese steel similar to AISI 1045. The authors cite earlier work where S45C was successfully welded to ADC12 (similar to 384.0 cast Al alloy).*

Ishii *et al*. [106] reported that the peak temperature measured increased somewhat with rpm at a constant travel speed. For example, at 7.9 in. / min travel speed, increasing the rotational speed from 2000 to 5000 rpm led to an increase in peak temperature from 354 F to 410 F. Peak temperature increased more dramatically with decreasing the travel speed at a constant rotational speed. For example, at 4000 rpm, decreasing the travel speed from 39.4 to 7.9 to in. / min led to an increase in peak temperature from 158 F to 358 F. The torque decreased with increasing the rotational speed or decreasing the travel speed. This was attributed to the increased plasticity / plastic flow, resulting from the higher heat inputs and temperatures associated with increasing the rotational speed or decreasing the travel speed. Optimum welding was achieved within a narrow window of rotational and travel speeds, as shown in the schematic depicted in Figure 42. The authors reported a large cavity that formed at the weld interface on the Al side, as a result of welding within the region of excessive plastic flow. The authors also seem to argue that degradation of mechanical properties, due to high heat input, can take place in that region. In the other regions, small root defects were reported. The authors report that EDS analysis did not reveal any evidence of intermetallic Al-Fe compounds at the weld interface. In fact, the macrographs published suggest that little, if any, mixing took place between the aluminum alloy and the steel; more on this below.

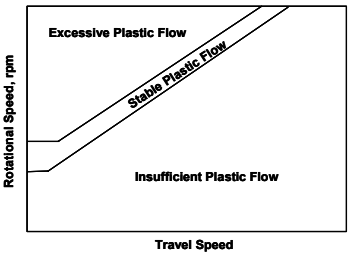

Figure 42: Acceptable A6063 Al-S45C steel welds were achieved in the stable plastic flow region.

Shimoda *et al*. [107] reported that, on the Al side, there existed a stir zone (SZ) containing steel debris, a TMAZ and a HAZ, in addition to the base metal. On the steel side, apart from the base metal, only a HAZ was present. No SZ or TMAZ were reported, since almost no stirring took place on the steel side. Figure 43 is a schematic of the joint profile, based on the information just described and the macrograph presented in the work cited. Weld flash (not shown in Figure 43) was reported on the retreating (Al) side. The authors reported that the weld track became narrower as travel speed increased at constant rpm. They also shed more light on the nature of the interface defects encountered outside the optimum widow of rotational and travel speeds, as shown in the schematic depicted in Figure 44. The authors published micrographs that some readers may wish to review. Hardness distributions across the joint were determined close to the face, near the root and at mid-thickness. On the Al side, it appeared that the SZ, TMAZ and HAZ were generally softer than the base metal, and there was a suggestion of a hardness minimum at the TMAZ / HAZ interface. On the steel side, the hardness at the interface was clearly higher than that of the base metal or HAZ, which appeared to be similar. Transverse tensile testing revealed a joint efficiency of 66%, with respect to the Al, and a joint elongation that was about 63% that of the Al. The above percentages are based on the Al properties published by the authors. The authors indicate that failure was in the HAZ at a location corresponding to the hardness minimum.

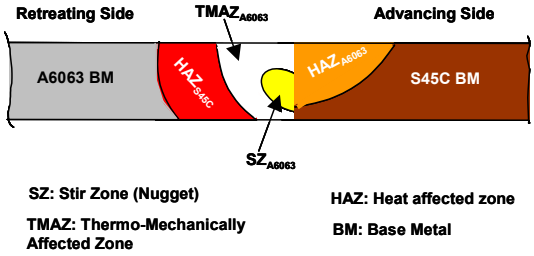

Figure 43: A6063 Al-S45C joint profile.

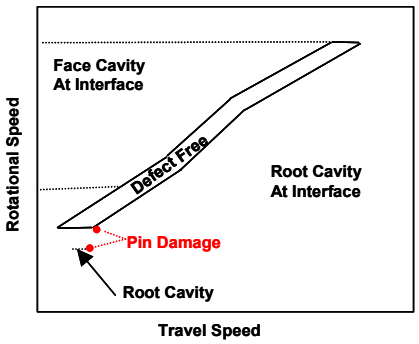

Figure 44: Defect types in the various regions of Figure 42.

Kimapong and Watanabe [108] studied dissimilar metal FSW of 0.079 in. thick sheet stock of A 5083 aluminum alloy (hereinafter, Al) and SS400 mild steel (hereinafter, Fe). [gg] The faying surface of each sheet was polished before welding. Welding was performed using a travel speed of 0.98 in. / min, rotational speeds in the 100-1250 rpm range and an SKH57 [hh] tool. The following tool dimensions were disclosed: shoulder diameter, 0.6 in.; pin diameter 0.079 in., and; pin length, 0.075 in. (unthreaded). No other weld parameters or tooling information were

[gg] *A 5083 is a Japanese aluminum alloy similar to AA 5083. The ultimate tensile strength for the stock investigated was 40 ksi. No listing for SS400 could be located in the international references available to the author of this document. The authors of the work cited did not indicate composition of the steel. They only indicate that it is a mild steel, presumably of Japanese origin, with an ultimate tensile strength of 66 ksi; the 400 designation probably indicates a minimum strength of 400 Mpa (about 58 ksi).*
[hh] *SKH 57 is a Japanese high-speed steel. The closest US match is M 44.*

disclosed. The Al was placed on the retreating side and the pin, rotating clockwise, was inserted in the Al then thrust towards the Fe faying surface. The authors define pin offset as the distance from the side of pin to the butt line; - in Al and + in Fe and 0 is when the pin side is just touching the butt line (Fe). Transverse tensile testing was used to determine the effects of the various welding parameters. The tensile property percentages listed below are based on the properties of the Al (A 5083) published by the authors.

Effect of rotational speed (rpm): First, the effect of rotational speed was investigated, at an offset of - 0.0079 in and the constant 0.98 in. / min travel speed. Joint strength increased with rpm, peaking at 250 rpm (joint efficiency 86%), and then decreased with further rpm increases. The low joint strength at 100 rpm was attributed to low heat generation and the attendant lack of Al plasticization. The authors report that, at 100 rpm, only a fraction of the weld length could be successfully executed; the rest was only welded at the face. Fracture here was along the Al / steel interface. The specimens welded at 100 and 500 rpm displayed the presence of Fe (SS400) fragments, in the welded Al. Fragment size increased with rpm. The fracture path here followed the interfaces between the Fe fragments and the Al matrix. At 1250 rpm the weld could not be completed, due to oxidation of the Mg (in the Al), and fracture occurred during machining to fabricate tensile specimens.

Effect of Offset: Based on the above data, a pin rotational speed of 250 rpm was selected to investigate the effect of pin offset on joint strength, at the constant travel speed on 0.98 in. / min. Offsets in the - 0.0079 to + 0.079 in. range were investigated. As the pin was moved from the Al (- offset) to contact (0 offset) and then penetrate (+ offset) the Fe, joint strength increased peaking at a + 0.0079 in. offset, and then decreased with further offset increases, as shown schematically in Figure 45; the data in the publication were utilized to construct this figure, which is not in the publication itself. The authors suggest that the low joint strength at negative offset is due to the insufficient removal of the oxide film from the Fe faying surface; fracture here was along the Al / Fe interface. As the offset became positive and joint strength increased, fracture shifted from the Al / Fe interface to the Al side. Here, the fracture path followed the interfaces between the Fe fragments and the Al matrix. The fragments became larger in size, and voids also formed, as the offset became more positive. The presence of the fragments and voids as well as rapid pin wear led to a progressive decrease in joint strength at the higher offset values.

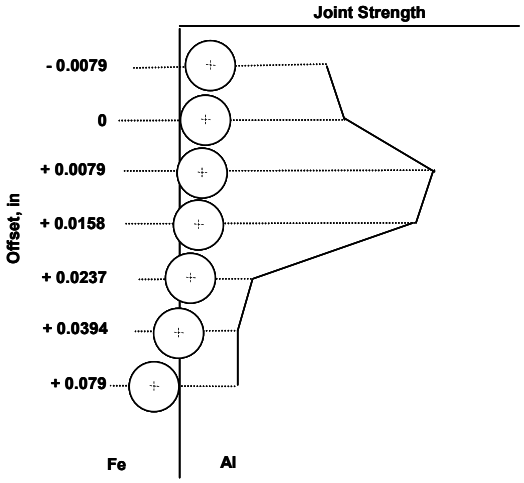

Figure 45: Effect of offset on A 5083 Al-SS400 steel joint strength.

Effect of Pin Diameter: Using the optimum conditions of 250 rpm, +0.0079 in. offset and the constant 0.98 in. / min travel speed, the effect of pin diameter was studied; the original pin diameter was 0.079 in. Using a smaller (0.039 in.) pin diameter led to rapid pin wear, and no sound joints could be produced. The strength of joints made with larger (0.12 and 0.17 in.) pin diameters were similar to those obtained with the original pin.

Effect of Rotation Direction: Using the optimum conditions of 250 rpm, +0.0079 in. offset and the constant 0098 in. / min travel speed, the pin was made to rotate counterclockwise; this would cause the Al to be the advancing side. The authors report that here, welding was confined to the face side with little evidence of bonding. They explain bonding and lack thereof by whether or not the pin could mechanically clean, hence activate, the Fe surface before stirred Al came in contact with it, as shown in Figure 46. The assumption here is that Al would bond to activated Fe but not to un-activated Fe.

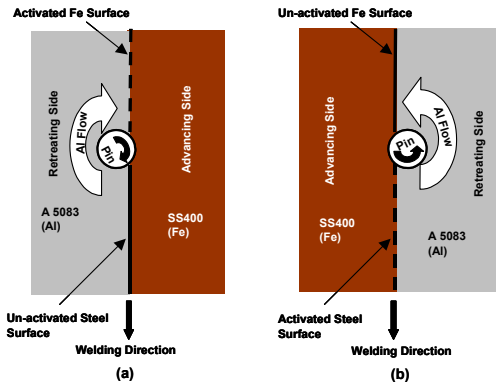

Figure 46: The effect of rotation direction on activation of the steel faying surface. Dissimilar A 5083-SS400 FSW.
(a) Clockwise rotation.
(b) Counterclockwise rotation.

Microstructure: The authors conducted a microstructural study of the joint with the highest strength, using OM and SEM. They report the presence of Al / Fe intermetallic compounds at the upper regions

(the face side) of the Al / Fe interface, and also around the Fe fragments. The authors indicate that these compounds were present along the fracture paths and that they had an adverse effect on joint strength.

7.0 REVIEW OF LAP JOINT PUBLICATIONS

The scope of lap joint applications is potentially very large, especially in the transportation industry in general and the aviation industry in particular. The problem, however, is that the level of confidence in FS welded lap joints does not match that in butt joints. This is due to the fact that the static and dynamic properties of lap joints can be seriously impaired by several factors that are peculiar to these joints. The subject factors include geometry of notch on either side of the joint, inadequate disruption of the oxides at the interface, inadequate penetration of the lapped (bottom) member and adverse interface reorientation (hooking). In lap joints, it is important to distinguish between the top and bottom members, since the former is in contact with the shoulder and, as such, is subject to the associated heating and deformation effects. FS welded lap joints may be tested in tension-shear or in tension-peel; the former is the most widely used. Due to the offset axes of the members, loading single-lap joints in tension-shear, without special provisions, gives rise to bending stresses that tend to increase the severity of the test. To balance the effect of the offset, packing pieces need to be used in the grip regions. All testing of the FS welded joints reviewed here was transverse to the welds. A detailed discussion of mechanical testing of welded joints is presented in the Appendix. The work reviewed here is presented in a generally chronological order.

Brooker *et al.* [14] FS welded lap joints of 0.094 in. thick details, machined from thicker 7075-T7351 [ii] stock. No weld parameters or specific tooling information were disclosed. The authors generally show weld joint profiles similar to those reported in butt FSW, except that here the joint does not typically penetrate the entire thickness of the bottom member. The lap joints were tension tested, transverse to the weld, in various locations along the length of the weld; presumably, the joints were of the single lap configuration, tested in tension-shear. Joint strengths ranged from 115-140% that of a bolted joint. The authors traced the lower end values to variations, outside the tolerance range, in the original sheet thickness. When the sheets with such variance were excluded, the results improved. Joint strength varied somewhat along the length of weld, probably due to variations in heat input. The authors explain that fracture took place at the upper sheet, bottom sheet or through the nugget. They published a macrograph with a hand drawn line indicating that failure at the bottom sheet initiated at the notch Figure 47 and indicate in the text that that failure was in the HAZ; no other failure figures were published. The authors assert that while lap joints may not be as strong as butt joints, they have adequate strengths to replace bolted joints. In other results, the authors report that if the proper tool design is not used, significant thinning of the top sheet can take place, due to metal movement in the direction of the top sheet. This thinning can adversely affect joint strength. The authors also report on early trials where clad materials were used. The presence of cladding at the interface led to joint contamination, inadequate bonding and lifting of the top sheet.

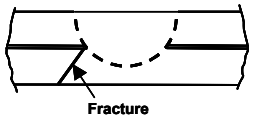

Figure 47:P Fracture in a lap joint, tested in tension-shear.

Cederqvist and Reynolds [15] FS welded lap joints of clad AA 2024-T3 (top) and AA 7075-T6 (bottom) sheet stock, Figure 48; in essence this is dissimilar aluminum alloy welding. The ultimate base metal tensile strengths were 69 and 86 ksi for the clad AA 2024-T3 and AA 7075-T6, respectively. Welding was performed using nine different tool configurations, all with unthreaded pins. In these configurations, the shoulder diameter ranged from 0.5 to 1 in., the pin diameter from 0.17 to 0.38 in. and the pin length from 0.12 to 0.16 in. The welds were made either in one pass (single pass) or two passes (double pass). Note that the term double pass here does not have the same meaning as that used in conjunction with butt welds; here, both passes are from the same side. This said, all joints were of the single lap configuration. In double pass welds, the two passes were made using the same tool and weld parameters, except that tool rotation was reversed for the second pass, Figure 49. This reversal causes the advancing sides of both welds to be adjacent to each other; the benefits of this will be evident shortly. For single pass welds, the travel speed was 5.4 in. / min and the rotational speed was 300 or 495 rpm. For double pass welds, the travel speed ranged from 5.4 to 13.1 in. / min, and the rotational speed from 300 to 983 rpm. The tool was tilted 2.5^{O}. The plunge depth (PD), defined in section 5.2, varied with shoulder diameter (SD) according to PD = 1/2 SD Sin 2.5^{O}. The joints were tested in tension-shear, and the specimens were provided with packing pieces to balance the effect of the offset sheet axes. Tension-shear testing was performed 120 hr after welding, to stabilize the microstructure, thereby minimizing property variations due to natural aging; it is thought, however,

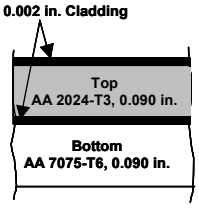

Figure 48: Clad AA 2024- AA 7075 lap joint.

[ii] *Since the subject investigation is European, it is presumed that 7075 is one of the local alloys that are similar to AA 7075.*

that AA 7075 can continue natural aging long after 120 hr. Tables in the publication list in detail all the welds that were tested together with relevant weld parameters, tool dimensions, the resulting failure loads, and the failure locations. The authors define a "theoretical tensile stress" that results in top and bottom sheets of an ideal lap

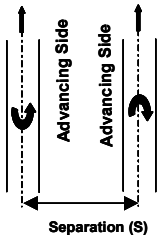

Figure 49: Rotation reversal in double pass lap welds.

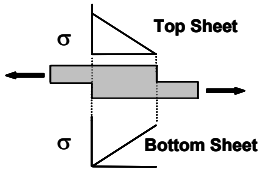

Figure 50: Theoretical tensile strength in a lap joint.

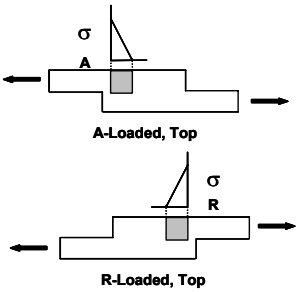

Figure 51: A-loaded and R-loaded single pass lap joints. The illustrations published by the authors did not depict the weld (see Figure 50).

lap joint, with no interface and no bending, loaded in tension-shear, Figure 50. [jj] In single pass welds, the authors, due to the asymmetric nature of FS welded joints, [kk] distinguish between A-loading and R-loading, Figure 51; A and R, respectively, designate the advancing and retreating sides. The reason appears to be as follows. In A-loading, for example, the maximum theoretical tensile stress in the top sheet would occur at the advancing side, whereas that in the bottom sheet would occur at the retreating side. Both stress contributions would be superimposed. However, due to the aforementioned joint asymmetry, the stress distribution in the various regions of the nugget, HAZ and TMAZ on the advancing side would be different from their counterparts on the retreating side. In other words, the stress at, say, the HAZ / TMAZ or nugget / TMAZ interface on the advancing side would not be the same as that at its counterpart on the retreating side. Similar reasoning would apply for R-loading. In double pass welds, the authors distinguish between R_1 and R_2 loading, Figure 52. It is felt that the top sheet was selected as reference, since lap joints do not typically penetrate far into the bottom sheet. The authors optically measured the upward and downward translation of sheet interfaces, and introduced an effective sheet thickness (EST) parameter to measure how much of the original sheet thickness was left, after welding, to carry the load. EST is the smallest distance between any unbonded interface and the top of the top sheet or bottom of the bottom sheet. The authors computed a joint efficiency by dividing the failure load of any given joint by the failure load of a sample of clad AA 2024-T3, the weaker material of the couple.

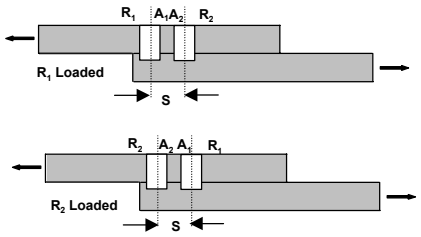

Figure 52: R_1 and R_2 loaded double pass lap joints. "S" designates the separation distance (see Figure 49). The illustrations published by the authors did not depict the weld (see Figure 50).

<u>Single Pass Welds</u>: Differences were noted between the properties of A-loaded and R- loaded specimens. In the R-loaded specimens, 80% of the failures occurred at the advancing side bottom sheet, whereas 20% occurred through the nugget. In the A-loaded specimens, 64% of the failures occurred at the advancing side top sheet, whereas 36% occurred through the nugget. No retreating side failures were observed in single pass welds. The high incidence of failure at the advancing side was attributed to the abrupt changes in the shape of the sheet interface at that location, which tend to give rise to stress concentration; by contrast, the interface at the retreating side was gently curved. The authors argue that a combination of the theoretical stress (Figure 50) and the bending stress present dictate the critical failure locations (see the Appendix). On the basis of EST determinations, the authors further argue that failure load increased with increasing EST, for those joints that did not fail through the nugget. The authors, however, did not provide an explanation for through-the-nugget failures [ll] and did not provide any schematics or macrographs depicting failure locations. The authors appear to conclude that failure

---

[jj] *A book was cited in the conference paper as the source of this information. The book is: Engineered Materials, vol. 3, Adhesives and Sealants (section 5), ASM International, 1990. The book, however, does not offer much detail and, instead, refers the reader to a 1938 publication in German. Interested readers may wish to consult said publication.*

[kk] *The nugget is typically skewed to the advancing side, and the widths of the HAZ and TMAZ on the advancing side are not equal to their counterparts on the retreating side.*

[ll] *Based on the theoretical tensile stress concept, invoked by the authors, it can be said that superposition of the top and bottom sheet contributions would result in maximum total stress at the central region of the weld. Accordingly, the tendency would be for failure to occur at the central regions, unless some other dominant factor intervenes. In single lap joints, the bending stresses present and the abruptness of the interface at the advancing side are examples of such dominant factors; note that the interface is an extension of the notch present on either side of the weld. The issue, however, is further complicated by the fact that the top and bottom sheet materials and strength properties are different.*

loads in the A-loaded specimens were higher than their counterparts in the R-loaded specimens. A review of the data, however, reveals considerable scatter for any conclusion to be drawn. In other results, the authors determined the harness profile across the joint at mid-thickness for both the top and bottom sheets. The results reflect trends similar to that depicted in Figure 15 (a).

<u>Double Pass Welds</u>: It was because of the advanced side failures described above that the authors devised the rotation reversal in double pass joints (Figure 49), so as to have two retreating sides exposed to the maximum stresses. Using a double pass joint also widens the weld region, effectively precluding through-the-nugget failures by shear. The authors investigated the effect of separation distance, in the 0.15-0.35 in. range. They report that the failure load increased with increasing the separation distance, even if an unbonded interface existed between the beads. The explanation is that a wider bead tends to inhibit bending and the associated adverse effects. For the R_1-loaded specimens, 100% of the failures occurred at the R_1 side, top sheet; there were no R_2 side, bottom sheet failures here. The authors propose that one of the reasons for this is the use of the weaker material (AA 2024) for the top sheet. For R_2 loaded specimens, 56% of the failures occurred failed at the R_2 side, top sheet and 44% occurred at the R_1 side, bottom sheet. In general, failure loads for R_2-loaded specimens were marginally higher than their R_1-loaded counterparts, and the failure load increased with increasing EST. Furthermore, the failure loads of the double pass welds were generally higher than their single pass counterparts. The authors, however, point out that the failure load of one of the single pass joints produced rivaled that of the best double pass joints. They indicate that this was achieved by influencing the geometry of the interfaces at the advancing and retreating sides, through changing the tool dimensions and the rotational and travel speeds. The authors further report that shorter pin lengths tend to generally cause interface pull down, causing an increase in the thickness of the weaker top sheet and a decrease in the thickness of the stronger bottom sheet. The authors also discuss the possible effects of the travel and rotational speeds and temperature on interface geometry. In other results, the authors determined the harness profile across the joint at mid-thickness for both the top and bottom sheets. The results reflect trends similar to that depicted in Figure 15 (a). There were indications, however, that the second pass may have softened the R_1 nugget. This may, in part, explain why the R_1-loaded specimens tended to be weaker than their R_2-loaded counterparts.

In the work just cited, it appears that future work should further characterize the dissimilar alloy region at the bottom of the weld. Interdiffusion, mixing and interaction between the dissimilar alloys can influence interfaces, properties and fracture locations. In other words, the implications of interdiffusion in dissimilar metal group welding in butt joints (section 6.6.1) are equally applicable here.

Matsumoto and Sasabe [109] investigated same metal lap joints made by FSW A 5182-O and AlMg0.5Si1-T4, [mm] 0.04 and 0.08 in. thick sheet stock. For either alloy, joints were made with the 0.04 or 0.08 in. stock as the top sheet that is in contact with the tool shoulder; i.e., there were no same thickness joints. Welding was performed using a tool having a left thread and a shoulder diameter of 0.7 in., a travel speed of 19.7 in. /min, and a rotation speed of 2500 rpm, with clockwise (CW) or counterclockwise (CCW) rotation. No other weld parameters or tooling information were disclosed. The joints were tested in tension-shear, with loading either top right or top left. While the authors did not clearly define these terms, it appears that the top right and top left loading configurations have to do with whether it is the advancing or retreating side that is closer to the top sheet loading point. In other words, the terms top left and top right are, respectively, different terms for the A and R-loading terms used by Cederqvist and Reynolds. [15] Reversing the rotation direction from CW to CCW, while maintaining the direction of travel, effectively switches the locations of the advancing and retreating sides with respect to the travel (welding) direction. The authors present schematics depicting failure locations in the tension-shear tests, together with the corresponding tensile-shear failure stress (failure load / width x thickness). Figure 53 is a rendering of said schematics, with the advancing and retreating sides identified according to the interpretation of the confusing in and out of paper symbols used by the authors. It should be noted that the schematics depict a stir zone (SZ) that has an inverted trapezoidal shape, extending to the bottom of the bottom sheet. The A 5182 macrographs published, however, show bowl type configurations (Figure 12), terminating a short distance above the bottom of the bottom sheet; no AlMg0.5Si1 macrographs were published. Furthermore, while the authors speak in terms of SZ, HAZ and TMAZ (referred to as HDAZ), the quality of the macrographs are such that the various zone interfaces could not be discerned. The authors seem to also consider the TMAZ as a part of the SZ. Having said all that, we now refer back to Figure 53. For the A 5182 joints, four (50%) of the failures occurred in the base metal of the thinner sheet, three (37.5%) in the SZ of the thinner sheet and one (12.5%) in the SZ of the thicker sheet. For the AlMg0.5Si1 joints, four (50%) of the failures occurred in the HAZ of the thinner sheet and four (50%) in the SZ of the thinner sheet. It is clear from those statistics that the thinner sheet tends to influence failure location. The authors hypothesize that CW rotation of the left thread pin rolls up the interface, leading to thinning of the top sheet, whereas CCW rotation rolls down that interface, leading to thinning of the bottom sheet, Figure 54. It appears that interface rolling would be important only when failure takes place within the SZ. No explanation is offered for the one fracture in the SZ of the thicker bottom sheet (A 5182). The authors, however, observe that

[mm] *A 5182 is a Japanese alloy similar to AA 5182. AlMg0.5Si1 is an international (ISO) alloy similar to AA 6063.*

joint strength is generally higher, when the thicker sheet is placed on top.

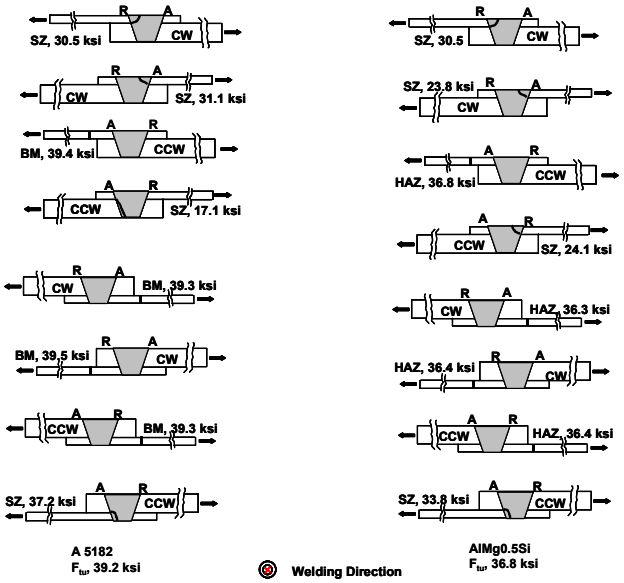

Figure 53: Eight loading and processing configurations were used in tension-shear testing. SZ (stir zone) and BM (base metal) indicate fracture location. The stress indicated in ksi was obtained by dividing the failure load by the cross sectional area (width x thickness). CW (clockwise) and CCW (counterclockwise) indicate pin rotation direction. R and A refer to the advancing and retreating sides, respectively. The symbol ⊙ is taken to indicate out of the paper.

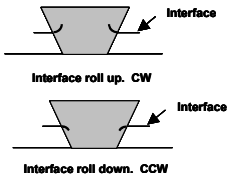

Figure 54; Interface roll up and roll down. CW and CCW, respectively, indicate clockwise and counterclockwise tool rotation.

Thomas *et al.* [39] reported on fatigue (S-N) performance of single lap joints of 0.24 in. thick 5083-H111 [nn] plate stock, FS welded at TWI using advanced skew techniques. These techniques rely on increasing the volume of the stirred metal, by introducing a skew tool motion that can be further augmented by incorporating such features as ovality and flats into pin design. The specimens from the FS welded joints were machined away from the start and stop points of the weld. The nominal stress range for the tests was computed using the applied load and the cross sectional area of one of the members (i.e., width x thickness). Packing pieces were used in the grip regions of the specimens, to accommodate lap offset and minimize bending stresses. The results of the welded specimens were compared to an "artificial lap" of similar geometry, from the same base metal, prepared by EDM (electro discharge machining) and also with joints made using a conventional tool with a threaded cylindrical pin. Two test orientations were used, ANE (advancing side near top sheet edge) and RNE (retreating side near top sheet edge); these, respectively, are the R and A-loading orientations described by Cederqvist *et al.* [15]

Welding with the conventional tool was performed at 4.7 in. / min travel speed and 548 rpm rotational speed, using a 0.31 in. long pin. Static tests revealed that the ANE orientation (R-loading) resulted in inadequate properties. Consequently, fatigue testing was performed using the RNE orientation (A-loading). The S-N curves published indicate that fatigue performance of the welded joints was inferior to that of the artificial lap joint.

Welding with the skew technique, was performed using rotational speeds in the 584-745 rpm range, a travel speed of 7.1 or 9.4 in. / min and pin lengths in the 0.28-0.35 in. range. Both the ANE and RNE orientations were tested. The results indicate that changing the rotational speed had little effect on fatigue performance of ANE joints. By contrast, fatigue performance of the RNE joints improved with

[nn] *5083 is a UK alloy similar to AA 5083.*

increasing the rotational speed. The ANE joints displayed better fatigue performance than the RNE joints, when longer pins and / or slower travel speeds were used. Using shorter pins and / or faster travel speeds reversed that order. In other words, whether ANE or RNE joints display superior fatigue performance depended on the combination of pin length and travel speed used. The authors indicate that the skew technique produces weld regions that are wider than those obtained by conventional tooling. This widening makes it unlikely for joints to fail by shear across the weld region. As a result, fatigue failures would almost certainly initiate at the notches present on either side of the weld region, where the bending stress, brought about by the lap offset, is tensile (see Appendix). The authors point out that widening of the weld region will not, in itself, increase fatigue strength, since notch morphology is of prime importance. The S-N curves published indicate that fatigue performance of joints produced by the skew technique, while inferior to that of the artificial lap joint, was superior to that of joints produced by conventional tooling. In other results, the authors report on the changes in interface movement, brought about by the skew technique and on the effect of rotation reversal on fatigue performance.

Welding of copper to aluminum is of interest to the electrical utility industry. Fusion welding of this dissimilar metal group couple, however, is difficult, due to the formation of brittle intermetallic compounds. FSW is an alternate process that is being considered in Japan. Elrefaey *et al.* [32] investigated the feasibility of producing FS welded lap joints between 0.08 in. thick A 1100-H24, [oo] hereinafter Al, sheet stock (top) and 0.04 in. thick tough pitch copper, hereinafter Cu, sheet (bottom). Welding was performed using rotational speeds in the 1002-2502 rpm range, travel speeds in the 7.8-11.8 in. / min range and an SKD61 steel [pp] tool, tilted 3^{O} with respect to the sheet normal. A schematic of the tool is shown in Figure 55, where the M 3 notation, not defined by the authors, is taken to designate a thread. Note that the tool used is a conventional one, not the one with the 2-shoulder design indicated by Brooker etal [14] for lap joints, Figure 3. This aside, the authors here define pin depth as the distance from the top surface of the upper sheet to the deepest point of pin penetration. Two pin depths were used, 0.079 and 0.083 in.; the first would put the pin just above the top surface of the bottom sheet, and the second would cause the pin to penetrate that top surface. The authors used a tension-peel test, Figure 56, to determine joint fracture loads. At a pin depth of 0.079 in., the joints obtained had very low strengths and most of them fractured during preparation of the peel test specimens. At pin depth of 0.083 in., the authors report joint fracture loads that varied widely; specifically, fracture loads ranged from 0 to 62.2 lbf. In spite of this scatter, the authors were able to discern that the fracture load tended to increase with increasing the rotational speed and with decreasing the travel speed. On the Al side, the authors report a stir zone (SZ) and a HAZ, and indicate that no TMAZ or onion ring pattern could be discerned. The SZ assumed a bowl shape (Figure 12), and displayed fine equiaxed grains that the authors attribute to dynamic recrystallization during welding, coupled with static recrystallization during subsequent cooling. The authors report that the SZ coarsened as the rpm was increased, and attribute that to the increased heat input. The hardness distribution across the joint profile, at mid thickness of the Al sheet, displayed a trend that is more or less similar to that depicted in Figure 15 (d). More welding flash was noted on the retreating side. Close to the Al / Cu interface, some Cu fragments were noted. On the Cu side, there was evidence of deformation close to the Al / Cu interface. Close to the Al / Cu interface on either side, there existed various constituents with different etching characteristics. Based on EDS and x-ray diffraction analyses and the Al-Cu phase diagram, the authors argue that these constituents represent regions containing various Cu-rich and Al-rich intermetallic compounds (AlCu, Al_2Cu and Al_4Cu_9); strictly speaking, however, these are intermediate phases. In all, it seems that the authors' findings are indicative of interdiffusion and some mixing and bonding, especially at the higher rotational and / or the lower travel speeds. SEM fracture surface analyses suggest that little, if any, bonding took place at the lowest rotational speed. At the higher rotational speeds, fracture appeared to follow the regions containing the "intermetallic compounds." The authors indicate that the results of their work suggest that, in order to obtain good quality joints with high strength, it will be necessary minimize or prevent the formation of the intermetallic compounds. They argue that this could be achieved by inserting an intermediate metal and / or by optimizing pin depth and pin design. It would be interesting to find out whether or not the authors have considered the use of the 2-shoulder tool (Figure 3), mentioned by Brooker *et al*. [14]

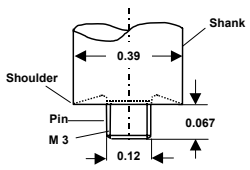

Figure 55: Tool used for lap joint.

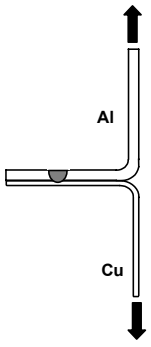

Figure 56: Tension-peel test.

In follow up work on dissimilar metal group welding, Elrefaey *et al.* [110] investigated the strength of lap joints produced by FSW of 0.08 in. thick A 1100-H24, hereinafter Al, sheet stock (top) to 0.05 in. thick low carbon (0.032

[oo] *A 1100 is a Japanese alloy similar to AA 1100.*
[pp] *SKD61 is a Japanese steel similar to H13 tool steel.*

wt.% C) steel, hereinafter steel, sheet stock (bottom). The base steel microstructure was ferritic, due to the very low carbon content. The authors used the tool, the welding parameters and the tension-peel test described above. Again, at a pin depth of 0.079 in., the joints obtained had very low strengths and most of them fractured during specimen preparation. At pin depth of 0.083 in., the authors report joint fracture loads that varied widely; specifically, fracture loads ranged from 0 to 229.4 lbf. In spite of this scatter, the authors were able to discern that fracture load tended to increase with increasing the rotational speed and with decreasing the travel speed. The Al macro / microstructure and hardness distribution across the joint were as reported earlier, except that here Fe, not Cu, fragments were present in the Al matrix. The authors here also report that the SZ coarsened as the rpm was increased, and attribute that to the increased heat input. On the steel side near the interface, there was a fine-grained zone, attributed to recrystallization of the steel that was deformed by the pin; the authors, however, did not identify this zone as the steel SZ. The fine-grained zone was surrounded by a coarse-grained HAZ. Within the fine-grained zone, there existed a layered structure; the Fe fragments in the Al matrix also displayed this layered structure. Based on EDS and x-ray diffraction analyses, the authors argue that the layered structure contains the intermetallic compounds Al_5Fe_2 and $Al_{13}Fe_4$. The layered structure and the fine-grained zone were not observed at the lowest rotational speed used in this work. The grains of the fine-grained zone became coarser as the rpm was increased and this was attributed to the increased heat input. As the travel speed increased, the grains of the fine-grained zone became finer and the zone itself became narrower; this was probably due to decreased heat input. Fracture generally followed the path of intermetallic compounds in the layered structure. The authors report on two specimens that displayed no layered structure. These specimens fractured mainly within the Al matrix and had the highest fracture loads; viz., 226.2 and 229.4 lbf. The authors indicate that said specimens were made from two separate joints, welded using different travel and rotational speeds. Interestingly, however, other specimens made from those same joints fractured at very low loads (0-35.2 lbf). In all, the authors' findings seem to indicate that interdiffusion took place and that more Al diffused in the steel than Fe in the Al. It should be noted here that the implications of interdiffusion in dissimilar metal group welding in butt joints (section 6.6.1) are equally applicable to this work and to the authors' earlier work. [32]

8.0 REVIEW OF SPOT JOINT PUBLICATIONS

FSW is being investigated as a replacement for traditional resistance spot welding and riveting in the automotive and similar industries. Spot welds can be of the butt or lap type. The work reviewed below, however, concerns lap spot joints. Mechanical testing of spot joints is generally performed utilizing the tension-shear configuration (see Appendix).

Schilling *et al.* [51] reported on lap joints produced by FS spot welding 6061-T4 [qq] sheet stock. Thickness of the top sheet varied from 0.039-0.12 in., whereas that of the bottom sheet was maintained at 0.12 in. Welding was performed using a specialized tool with a retractable pin and a two-shoulder design; [52] the retractable pin allows for closure of the end keyhole (see section 5.6), and the 2- shoulder design, depicted in Figure 3, was also mentioned by Brooker *et al*. [14] The pin length was adjusted to suit the thickness of the top sheet. The spot diameter varied 0.24 to 0.39 in. No weld parameters or other tooling information were disclosed. The authors show the profile of a joint between a 0.039 in. thick top sheet and a 0.12 in. thick bottom sheet. The joint was of the bowl type (Figure 12), with a nugget, predominantly in the top sheet, a TMAZ and a HAZ. Hardness measurements revealed that the top sheet generally suffered more softening than the bottom one, possibly due to its proximity to shoulder. Hardness distributions across the joint profile, at midthickness of the top and bottom sheets, displayed trends similar to that depicted in Figure 15 (a). The ratio between the lowest hardness reported (in the HAZ) and that of the base metal increased as the combined (top + bottom) sheet thickness decreased; this was probably due to the larger heat input required for thicker top sheets. In general, the hardness values obtained were higher than their counterparts obtained by resistance welding. Load-displacement curves were generated by shear testing; the details of the test, however, were not published. The results indicated the uniform behavior and reproducibility of joint properties. The maximum load increased with spot diameter and the results generally reflected the superiority of FSW over resistance welding. The authors point out that spot welds can fail in one of two modes; viz., shear and pullout. The failure mode is determined by sheet thickness, spot diameter and the local strength of the joint. Thicker sheets, smaller spot diameters and weak (or defective) joints favor shear failures.

Fujimoto *et al.*[111] developed a small gun, complete with a backing plate, to be manipulated by a robotic system, to execute FS spot welds on an industrial scale. They used this equipment to prepare FS spot welded lap joints of 0.04 in. thick 6xxx series aluminum alloy sheet stock. Welding was performed at 2500 rpm, using an axial force of 878.1 lbf and a tool having a shoulder diameter of 0.39 in. and a pin diameter of 0.14 in. No other weld parameters or tooling information were disclosed. In this work, the rotating pin was plunged in the top sheet and pushed down to penetrate the bottom sheet to some prescribed depth. Rotation and the specified axial force were maintained for an appropriate length of time (called the loading time), before the tool was withdrawn while still

[qq] *The designation 6061 appears in the French and UK alloy systems. AA 6061 is the US equivalent.*

rotating; i.e., no travel was involved. Naturally, a keyhole would be left when the pin was withdrawn; a bond, however, would have already been established. A ring of flash remained around the location where the tool shoulder was. The authors recognized a stir zone (SZ) and a HAZ. An approximate schematic of the joint profile is depicted in Figure 57. Hardness distribution across the joint profile around the hole, at midthickness of the top sheet, displayed a trend similar to that depicted in Figure 15 (c). Single-lap-tension-shear specimens were prepared and tested; the macrographs published indicate that significant bending took place. The results show that joint strength increased with loading time to a maximum, then decreased with further increases in loading time. The explanation given was as follows. Initially, strength is determined by the size of the SZ, where fracture takes place. Therefore, as the SZ grows in size with increasing the loading time, the strength increases. When the SZ reaches some critical size, the weakest section becomes the top sheet, due to the thinning brought about by penetration of the tool shoulder. Apparently, more thinning took place with further increases in loading time, resulting in a decrease in strength. The results also show that the strength increases as the keyhole depth increases; the keyhole depth is a measure of pin penetration in the bottom sheet. Increasing that penetration evidently results in increased strength.

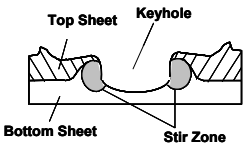

Figure 57: FS spot weld joint profile. HAZ not depicted.

9.0 Generating Joint Allowables

Due to the expanding use of FSW in the airframe industry, a discussion of design properties, AKA allowables, is in order. Mil-HDBK-5 (now MMPDS) explains techniques that can be used for generating allowables for fusion welded joints by coupon testing. Similar techniques may be used for FS welded joints, subject to agreement between the parties involved. One possible sequence of events is presented below, on a best effort basis.

(a) It seems that the first logical step is to perform a structural analysis to determine the types of stress fields that will be encountered in service. From that, a determination can be made as to the types of coupon data that need to be generated; i.e., tension, shear, peel, tension-shear and / or others, as the case might be.

(b) Once the required types of coupons are identified, the design activity should then recognize that the properties of metallurgical joints, especially FS welded joints, are material and process-dependant.

- **FS welded joint properties will depend on a multitude of welding variables that far exceed those encountered in conventional welding. These include, but are not limited to, the travel and rotational speeds, welding forces, rotation direction, tool configuration materials and tilt, plunge depth, penetration ligament / penetration depth, as applicable.**
- **Even when all process parameters have been fixed, FS welded joint properties can still depend on the exact chemistry of the alloy(s) being welded. This means that alloys from different producers can result in different joint properties. Stock thickness is not mentioned here, since it is a determining factor in selecting the welding parameters.**

The work of Okada, Oiwa, Hori, Hashimoto *et al*. [28, 79-81] clearly demonstrates how FSW is material and process dependent. Therefore, it is essential to optimize and fix all process variables and select one producer for each alloy to be welded, before attempting to generate coupon data.

(c) Once the material and process variables have been fixed, a decision should be made regarding the sample size (i.e., the number of coupons) required for each type of test. The MMPDS offers guidelines. While A and B values are most reliable, S values require a smaller sample size and, as such, may be attractive to design activities.

(d) When coupon testing has been completed and the information analyzed statistically, the design activity should recognize that the generated data are only applicable to one set of process variables and one producer for each alloy being welded. A new set of allowables should be generated, if any one of the processing variables or alloy producers is changed.

(e) It is wise for the design activity to establish some correlation between the coupon data and the actual structure or some representation thereof. This is especially so in view of the fact that joint properties tend to vary along the weld line and that keyholes (open or plugged) or other types of discontinuities may be present at the start, middle and / or end of the actual joint in the structure.

(f) Regardless of the type of allowables (A, B or S) to be used, it is wise to substantiate them by coupon testing on a lot basis, during actual production. Before testing, of course, a meaningful definition of a lot should be adopted and a rational sample size should be defined.

(g) If the structural analysis of (a) indicated that properties such as fatigue, impact, stress corrosion cracking and the like are of concern, then it is wise to conduct some coupon testing for these properties, to provide confidence in the structure. Such testing, however, is typically not subject to the A, B or S provisions, and a much smaller sample size would be required.

It is recognized here that FSW is a proprietary process in a highly competitive marketplace. This being so, users / processors will go to any length to protect their processing details. Accordingly, the expectation is that, for any

given alloy / temper, there will be one set of allowables for each FSW processor-alloy producer(s) combination. In fact, the likelihood is that there will be one set of allowables for each design fabricated by any one processor. The number of sets can rapidly multiply if stock thickness, form and country of origin are considered. National, let alone international, allowables do not appear to be realistic propositions at this time. On a similar note, Kamimuki and Imuta [112] consider that establishing a public (national) FSW process specification, complete with accept / reject criteria, to be a prerequisite for establishing design allowables. In the US, it is said that AWS D17.3 is slated to be just such national (public) FSW specification. It will be interesting to see how much information will finally be included there.

10.0 OBSERVATIONS & COMMENTS

10.1 The terms used to describe the various microstructural zones (nugget / DXZ, TMAZ / HDAZ, etc.) in FS welded joints are thought to be confusing, and they tend to vary depending on the particular author or group of authors involved. Furthermore, one or more of these zones may not be observed. This being so, the technical community may wish to consider the following proposal. The nugget, TMAZ and the region under the shoulder are all regions of rotation (i.e., deformation) and, as such, it would make sense to classify all of them as different regions of the stir zone (SZ). The SZ and HAZ would be defined as the weld zone.

10.2 In the never-ending effort to cut cost, the quest for the low bidder will remain a continuing fact of life. It is wise, however, not to change material sources or processors in the middle of production, since this can lead to different joint properties.

10.3 Design activities should recognize that joint properties would tend to vary along the weld line, and that there may also be discontinuities at the start, middle and / or end of the joint. These issues apply to both butt and lap joints and they should be taken into consideration in design analyses. Among other issues that need to be addressed are the repair of FS welded joints in service, and the effect of introducing FSW into any given design on the set intervals for structural inspection.

10.4 Most applications do not allow for post weld heat treatments and, as such, the as welded microstructures will enter service, subject only, when applicable, to natural aging. This is particularly of concern for 7xxx and certain other aluminum alloys, due to their tendency to naturally age for extended periods of time. In other words, these alloys would exhibit continuously changing microstructures, properties and dimensions and may even become susceptible to long term embrittlement (loss of ductility). There is another issue that concerns aluminum alloys and this pertains to the possible effect of strain, imparted by FSW, on aging (natural and artificial) kinetics and the attendant mechanical property evolution. It appears that some research is warranted here.

10.5 In tensile and fatigue testing of FS welded joints, authors often report failure loads / stresses (or S-N curves) without providing fracture schematics or sufficient information to permit visualization of the fracture paths. It is thought, however, that fracture paths and the failure loads / stresses (or S-N curves) are interdependent and that the latter cannot be rationalized without the former.

10.6 In butt joint work, authors frequently fail to indicate the welding direction with respect to the working directions (L, LT and ST) of the product. Knowing the weld direction is essential for comparing joint properties to those of the base metal; e.g., for computing joint efficiency.

10.7 Occasionally, authors do not indicate the location of the reported microhardness traverses with respect to the product. Reporting the location is essential in view of the asymmetry of the joints. This especially so when comparisons are being made, since a location shift can in and by itself lead to a change in the trend observed.

10.8 Identifying a unique deformation-thermal path based on microstructure only is very difficult. A determination of the temperature regimes and cooling rates involved (or the use of some validated model) would certainly be helpful in phase identification. Modeling or measuring of the strains and strain rates involved in FSW, if at all possible, would certainly be beneficial in this regard. It may be possible one day to use means similar to Prasad's processing maps to shed some light on the operating deformation mechanisms and the prevailing defects at different temperature-strain rate combinations (i.e., at different locations within the weld). The task of understanding microstructural evolution during FSW appears to be daunting, to say the least. This is due to the existence of temperature, strain and strain rate gradients, hence microstructural gradients, across the width, through the depth and along the length of a joint. In other words, rather than speaking of a typical microstructure within a zone, one should speak in terms of a typical microstructure at a given location (x, y, z) within that zone.

10.9 In FS welded joints, residual stress distribution and magnitudes depend on several factors, many of which are interrelated. These include the welding parameters (forces, speeds, tilt, etc.), tool design (configuration and materials), initial microstructure, the thermal effects associated with welding (heating, cooling and phase

transformations), the strains / strain rates resulting from metal deformation, the clamping specifics, and the preexisting residual stress fields (grit blasting, heat treatment, etc.). It seems that some modeling would be required to understand how these factors might interact to produce the final observed residual stress fields and how said factors might be modified to produce desirable effects.

10.10 In FS welding dissimilar members, the members effectively form a diffusion couple. There would be solid state interdiffusion across the butt line (but joints) or interface (lap joints). This interdiffusion would be by unequal exchange of various atoms, with the aim of eliminating concentration gradients. Interdiffusion, apart from causing the formation of new phases, can lead to shifting the original butt line or interface to a new location, and to the formation of voids. In diffusion terminology, said shift is referred to as the Kirkendall effect or Kirkendall shift (the original interface is referred to as the Matano interface), and said voids as the Kirkendall voids. The interface shift and the formation of new phases and voids can influence joint properties and, as such, they should be recognized in FSW of dissimilar couples.

REFERENCES

1. W. M. Thomas et al., 1991. US Patent No. 5,460,317.

2. ASM Handbook, 1993, vol. 6, " Welding, Brazing and Soldering," pp. 297-324.

3. Karl-Erik Knipstrom and B. Pekkari: Welding Journal, 1997, vol. 76 (9), pp. 55-57.

4. E. D. Nicholas: Advanced Materials & Processing, June 1999, pp. 69-71.

5. R. S. Mishra: Advanced Materials & Processing, Oct. 1998, pp. 43-46.

6. T. Shinoda, M. Kawai and H. Takegami: International Institute of Welding Pre-Assembly Meeting on Friction Stir Welding, Nagoya University, Nagoya, Japan, 9 July 2004.

7. C. Dalle Donne, E. Lima, J. Wegener, A. Pyzalla and T. Buslaps: Third International Symposium on Friction Stir Welding (Session 6), Kobe, Japan, 27-28 September 2001.

8. E. Litwinski: Third International Symposium on Friction Stir Welding (Session 4), Kobe, Japan, 27-28 September 2001.

9. J. Lumsden III, M. Mahoney, G. Pollock, D. Waldron, and A. Guinasso: First International Symposium on Friction Stir Welding (Session 5), Thousand Oaks, California, USA, 14-16 June 1999.

10. TWI web site. www.twi.co.uk

11. K. J. Colligan: Welding Journal, 1999, vol. 78(7), pp. 229s-237s.

12. C. J. Dawes and W. M. Thomas, First International Symposium on Friction Stir Welding (Session 7), Thousand Oaks, California, USA, 14-16 June 1999.

13. L. Ekman, A. Norlin and J. Backlund: Second International Symposium on Friction Stir Welding (session 1), Gothenburg, Sweden, 26-28 June 2000.

14. M. J. Brooker, A. J. M. van Deudekom, S. W. Kallee and P. D. Sketchley: Second International Symposium on Friction Stir Welding (session 9), Gothenburg, Sweden, 26-28 June 2000.

15. L. Cederqvist and A. P. Reynolds: Second International Symposium on Friction Stir Welding, Gothenburg (Session 1), Sweden, 26-28 June 2000. Also: Welding Journal, 2001, vol. 80 (12), pp 281s-287s.

16. R. Talwar, D. Bolser, R. Lederich and J. Baumann: Second International Symposium on Friction Stir Welding (session 9), Gothenburg, Sweden, 26-28 June 2000.

17. K. J. Colligan, P. J. Konkol, J. J. Fisher, and J. R. Pickens: Welding Journal, 2003, vol. 82 (3), pp. 34-40.

18. S. Hirano, K. Okamoto, K. Aota, H. Okamura, Y. Aono and T. Odakura: Third International Symposium on Friction Stir Welding (Session 1), Kobe, Japan, 27-28 September 2001.

19. S. Kallee and A. Mistry: First International Symposium on Friction Stir Welding (Session 2), Thousand Oaks, California, USA, 14-16 June 1999.

20. R. J. Ding and P.A. Oelgoetz, First International Symposium on Friction Stir Welding (Session 1), Thousand Oaks, California, USA, 14-16 June 1999.

21. A. Oosterkamp, L. D. Oosterkamp and A. Nordeide: Third International Symposium on Friction Stir Welding (Session 7), Kobe, Japan, 27-28 September 2001. Also: Welding Journal, 2001, vol. 83 (8), pp 225s-231s.

22. H. G. Salem, A. P. Reynolds and J. S. Lyons: Journal of Materials Engineering & Performance, (ASM), 2004, vol. 13 (1), pp. 24-31.

23. G. Oertelt, S. S. Babu, S. A. David and E. A. Kenik: Welding Journal, 2001, vol. 80 (3), pp 71s-79s.

24. T. J. Lienert and R. J. Grylls: First International Symposium on Friction Stir Welding (Session 11), Thousand Oaks, California, USA, 14-16 June 1999.

25. J. B. Lumsden III, M. W. Mahoney, C. G. Rhodes and G. A. Pollock: Corrosion, 2003, vol. 59 (3), pp 212-219.

26. P. Zettler, S. Lomolino, T. Donath, F. Beckmann, T. Lippman and D. Lohwasser: International Institute of Welding Pre-Assembly Meeting on Friction Stir Welding, Nagoya University, Nagoya, Japan, 9 July 2004.

27. G. J. Bendzsak, T. H. North and C. B. Smith: Second International Symposium on Friction Stir Welding (session 7), Gothenburg, Sweden, 26-28 June 2000.

28. T. Okada, S. Iwaki, N. Eguchi, S. Tanaka, N. Oiwa, and K. Namba: International Institute of Welding Pre-Assembly Meeting on Friction Stir Welding, Nagoya University, Nagoya, Japan, 9 July 2004.

29. J. H. Ouyang and R. Kovacevic: Journal of Materials Engineering & Performance, (ASM), 2002, vol. 11 (1), pp 51-63.

30. J. A. Schneider and A. C. Nunes, Jr.: Metallurgical & Materials Transactions B, 2004, vol. 35B (8), pp. 777-783.

31. H. Larsson, L. Karlsson, S. Stoltz and E-L Bergqvist: Second International Symposium on Friction Stir Welding (session 4), Gothenburg, Sweden, 26-28 June 2000.

32. A. Elrefaey, M. Takahashi and K. Ikeuchi: International Institute of Welding Pre-Assembly Meeting on Friction Stir Welding, Nagoya University, Nagoya, Japan, 9 July 2004.

33. T. Shibayanagi and M. Maeda: International Institute of Welding Pre-Assembly Meeting on Friction Stir Welding, Nagoya University, Nagoya, Japan, 9 July 2004.

34. G. Biallas, C. Dalle Donne, G. Staniek and W. A. Kaysser: First International Symposium on Friction Stir Welding (Session 3), Thousand Oaks, California, USA, 14-16 June 1999.

35. C. Dalle Donne, G. Biallas and G. Raimbeaux: Second International Symposium on Friction Stir Welding (session 8), Gothenburg, Sweden, 26-28 June 2000.

36. M. W. Mahoney, C. G. Rhodes, J. G. Flintoff, R. A. Spurling, and W. H. Bingel: Metallurgical Transactions, 1998, vol. 29 A (7), pp. 1955-1964.

37. Diffraction Notes, Lambda Research, No. 29, Summer 2002.

38. J. B. Lumsden, M. W. Mahoney, G. Pollock and C. G. Rhodes: Corrosion, 1999, vol. 55, p 1127.

39. W. Thomas, D. Nicholas, D. Staines P. J. Tubby and M F Gittos: International Institute of Welding Pre-Assembly Meeting on Friction Stir Welding, Nagoya University, Nagoya, Japan, 9 July 2004.

40. K. Colligan, I. Ucok, K. McTernan, P. J. Konkol and J. R. Pickens: Third International Symposium on Friction Stir Welding (Session 5), Kobe, Japan, 27-28 September 2001.

41. F. Marie: Third International Symposium on Friction Stir Welding (Session 4), Kobe, Japan, 27-28 September 2001.

42. C. D. Sorensen, T. W. Nelson and S. M. Packer: Third International Symposium on Friction Stir Welding (Session 5), Kobe, Japan, 27-28 September 2001.

43. M. Maeda, H. Liu, H. Fujii and T. Shibayanagi: International Institute of Welding Pre-Assembly Meeting on Friction Stir Welding, Nagoya University, Nagoya, Japan, 9 July 2004.

44. T. Hashimoto, S. Jyogn, K. Nakata, Y. G. Kim and M. Ushio: First International Symposium on Friction Stir Welding (Session 9), Thousand Oaks, California, USA, 14-16 June 1999.

45. Y. J. Chao and X. Qi: First International Symposium on Friction Stir Welding (Session 4), Thousand Oaks, California, USA, 14-16 June 1999.

46. T. J. Lienert, W. L. Stellwag, JR., B. B. Grimmett and R. W. Warke: Welding Journal, 2003, vol. 82 (1), pp 1s-9s.

47. M. Karlsen, S. Tangen, O. Frigaard and O. Grong: Third International Symposium on Friction Stir Welding (Session 7), Kobe, Japan, 27-28 September 2001.

48. Automotive Engineering Int., Oct. 1998. Pp96-99.

49. G. Engelhard, T. Hillers and D. Pellkofer: Third International Symposium on Friction Stir Welding (Session 1), Kobe, Japan, 27-28 September 2001.

50. R.J. Ding: Second International Symposium on Friction Stir Welding (session 6), Gothenburg, Sweden, 26-28 June 2000.

51. C. Schilling, A. Von Strombeck, J. F. dos Santos and N. Von Hessen: Second International Symposium on Friction Stir Welding (session 10), Gothenburg, Sweden, 26-28 June 2000.

52. A. Von Strombeck, C. Schilling and J. F. dos Santos: Second International Symposium on Friction Stir Welding (session 6), Gothenburg, Sweden, 26-28 June 2000.

53. H. Sato, S. Hiratsuka and H. Hara: International Institute of Welding Pre-Assembly Meeting on Friction Stir Welding, Nagoya University, Nagoya, Japan, 9 July 2004.

54. G. Kohn: Israeli Patent Application 142101 from March 19, 2001.

55. G. Kohn, Y. Greenberg, I. Makover and A. Muntiz: Welding Journal, 2002, vol. 81 (2), pp46-48.

56. G. E. Shepherd: Second International Symposium on Friction Stir Welding (session 9), Gothenburg, Sweden, 26-28 June 2000.

57. R. Johnson and P. I. Threadgill: Third International Symposium on Friction Stir Welding (Session 3), Kobe, Japan, 27-28 September 2001.

58. K. Colligan, J. J. Fisher, J. E. Gover and J. R. Pickens: Advanced Materials & Processes, September 2002, pp. 39-41.

59. S. Tanaka, M. Kumagai and H. Yoshida: International Institute of Welding Pre-Assembly Meeting on Friction Stir Welding, Nagoya University, Nagoya, Japan, 9 July 2004.

60. M. Strangwood, J. E. Berry, D. P. Cleugh, A. J. Leonard and P. L. Threadgil: First International Symposium on Friction Stir Welding (Session 11), Thousand Oaks, California, USA, 14-16 June 1999.

61. G. Bussu, P. E. Irving: First International Symposium on Friction Stir Welding (Session 3), Thousand Oaks, California, USA, 14-16 June 1999.

62. F. Hannour, A. J. Davenport and M. Strangewood: Second International Symposium on Friction Stir Welding (session 10), Gothenburg, Sweden, 26-28 June 2000.

63. Y. J. Chao, Y. Wang and W. Miller: Welding Journal, 2001, vol. 80 (8), pp. 196s-200s.

64. M. Kumagai, S. Tanaka, H. Hatta, H. Yoshida and H. Sato: Third International Symposium on Friction Stir Welding (Session 6), Kobe, Japan, 27-28 September 2001.

65. G. Cao and S. Kou: Welding Journal, 2005, vol. 84 (1), pp 1s-8s.

66. G. Campbell and T. Stotler: Welding Journal, 1999, vol. 78 (12), pp. 4-47.

67. M. A. Sutton, A. P. Reynolds, D. Q. Wand and C. R. Hubbard: Journal of Engineering Materials and Technology, April 2002, vol. 124, pp. 215-221.

68. L. E. Murr, Y. L. Li, R. D. Flores, and J. C. McClure: Mater. Res. Innovation, 1998, 2, pp. 150-163.

69. J. C. McClure, Z. Feng, L. E. Murr, and X. Guo: Fifth International Conference on Trends in Welding Research, Pine Mountain, GA, USA, 1-5 June 1998.

70. Y. S. Sato, H. Kokawa, M. Enomoto, S. Jogan and T. Hashimoto: Third International Symposium on Friction Stir Welding (Session 6), Kobe, Japan, 27-28 September 2001.

71. H. Hori, S. Makita, T. Minamida, S. Watanabe, E. Anzai and H. Hino: Third International Symposium on Friction Stir Welding (Session 5), Kobe, Japan, 27-28 September 2001.

72. X. Yun, T. Ito, Y. Motohashi and A. Goloborodko: International Institute of Welding Pre-Assembly Meeting on Friction Stir Welding, Nagoya University, Nagoya, Japan, 9 July 2004.

73. Lars-Erik Svensson and L. Karlsson: First International Symposium on Friction Stir Welding (Session 5), Thousand Oaks, California, USA, 14-16 June 1999.

74. M. Ericsson, R. Sandstrom and J. Hagstrom: Second International Symposium on Friction Stir Welding (session 8), Gothenburg, Sweden, 26-28 June 2000.

75. D. Bolser, R. Talwar and R. Lederich: International Institute of Welding Pre-Assembly Meeting on Friction Stir Welding, Nagoya University, Nagoya, Japan, 9 July 2004.

76. A. Von Strombeck, J. F. dos Santos, F. Troster, P. Laureano and M. KoÇak: First International Symposium on Friction Stir Welding (Session 9), Thousand Oaks, California, USA, 14-16 June 1999.

77. A. J. Leonard: Second International Symposium on Friction Stir Welding (session 7), Gothenburg, Sweden, 26-28 June 2000.

78. L. Magnusson and L. Kallman: Second International Symposium on Friction Stir Welding (session 2), Gothenburg, Sweden, 26-28 June 2000.

79. N. Oiwa, S. Iwaki, T. Okada, N. Eguchi, S. Tanaka and K. Namba: International Institute of Welding Pre-Assembly Meeting on Friction Stir Welding, Nagoya University, Nagoya, Japan, 9 July 2004.

80. H. Hori, H. Tanikawa, T. Miyamichi and K. Namba: International Institute of Welding Pre-Assembly Meeting on Friction Stir Welding, Nagoya University, Nagoya, Japan, 9 July 2004.

81. T. Hashimoto, J. Takeda and K. Namba: International Institute of Welding Pre-Assembly Meeting on Friction Stir Welding, Nagoya University, Nagoya, Japan, 9 July 2004.

82. A. Lamarre and M. Moles: Second International Symposium on Friction Stir Welding (session 7), Gothenburg, Sweden, 26-28 June 2000.

83. K. Nakata, S. Inoki, Y. Nagano, T. Hashimoto, S. Johgan and M. Ushio: Third International Symposium on Friction Stir Welding (Session 2), Kobe, Japan, 27-28 September 2001.

84. K. Katoh and H. Tokisue: International Institute of Welding Pre-Assembly Meeting on Friction Stir Welding, Nagoya University, Nagoya, Japan, 9 July 2004.

85. N. Saito, I. Shigematsu, K. Suzuki, T. Sakurai and M. Aritoshi: International Institute of Welding Pre-Assembly Meeting on Friction Stir Welding, Nagoya University, Nagoya, Japan, 9 July 2004.

86. W. M. Thomas: First International Symposium on Friction Stir Welding (Session 10), Thousand Oaks, California, USA, 14-16 June 1999.

87. T. J. Lienert and J. E. Gould: First International Symposium on Friction Stir Welding (Session 10), Thousand Oaks, California, USA, 14-16 June 1999.

88. P. J. Konkol, J. A. Mathers, R. Johnson and J. R. Pickens: Third International Symposium on Friction Stir Welding (Session 2), Kobe, Japan, 27-28 September 2001.

89. M. Posada, J. P. Nguyen, D. R. Forrest, J. J. DeLoach and R. DeNale: AMPTIAC (Advanced Materials and Processes Technology Information Analysis Center) Quarterly, 2003, vol. 7 (3), pp. 13-19.

90. J. E. Beach, D. D. Bruchman and J. P. Sikora: AMPTIAC (Advanced Materials and Processes Technology Information Analysis Center) Quarterly, 2003, vol. 7 (3), pp. 5-11.

91. E. J. Czyryca, D. P. Kihl and R. DeNale: AMPTIAC (Advanced Materials and Processes Technology Information Analysis Center) Quarterly, 2003, vol. 7 (3), pp. 63-70.

92. H. Kokawa, S. H. C. Park, Y. S. Sato, K. Okamoto, S. Hirano and M. Inagaki: International Institute of Welding Pre-Assembly Meeting on Friction Stir Welding, Nagoya University, Nagoya, Japan, 9 July 2004.

93. S. H. C. Park, Y. S. Sato, H. Kokawa, K. Okamoto, S. Hirano and M. Inagaki: International Institute of Welding Pre-Assembly Meeting on Friction Stir Welding, Nagoya University, Nagoya, Japan, 9 July 2004.

94. S. Klingensmith, J. N. DuPont and A. R. Marder: Welding Journal, 2005, vol. 84 (5), pp 77s-85s.

95. M. C. Juhas, G. B. Viswanathan and H. L. Fraser: Second International Symposium on Friction Stir Welding (session 5), Gothenburg, Sweden, 26-28 June 2000.

96. M. Juhas, N. Kargal, J. Williams and H. Fraser: Third International Symposium on Friction Stir Welding (Session 2), Kobe, Japan, 27-28 September 2001.

97. Y. V. R. K. Prasad, T. Seshacharyulu, S. C. Medeiros, W. G. Frazier, J. T. Morgan and J. C. Malas: Advanced Materials & Processing, June 2000, pp. 85-89.

98. V. V. Balasubrahmanyam and Y. V. R. K. Prasad: Journal of Materials Engineering & Performance, 2001, vol. 10(6), pp. 731-739.

99. Y. V. R. K. Prasad: Journal of Materials Engineering & Performance, 2003, vol. 12(6), pp. 638-645.

100. N. Ravichandran: Journal of Materials Engineering & Performance, 2003, vol. 12(6), pp. 653-655.

101. P. V. Sivaprasad and S. Venugopal: Journal of Materials Engineering & Performance, 2003, vol. 12(6), pp. 656-660.

102. S. Venugopal and P. V. Sivaprasad: Journal of Materials Engineering & Performance, 2003, vol. 12(6), pp. 674-686.

103. S. Tamirisakandala, B. V. Vedam and R. B. Bhat: Journal of Materials Engineering & Performance, 2003, vol. 12(6), pp. 661-673.

104. C. G Andersson and R. E. Andrews: First International Symposium on Friction Stir Welding (Session 10), Thousand Oaks, California, USA, 14-16 June 1999.

105. M. Michiuchi, S. H. C. Park, Y. S. Sato and H. Kokawa: International Institute of Welding Pre-Assembly Meeting on Friction Stir Welding, Nagoya University, Nagoya, Japan, 9 July 2004.

106. T. Ishii, M. Tsubaki, M. Fukumoto and T. Shinoda: International Institute of Welding Pre-Assembly Meeting on Friction Stir Welding, Nagoya University, Nagoya, Japan, 9 July 2004.

107. Y. Shimoda, M. Tsubaki, T. Yasui, M. Fukumoto and T. Shinoda: International Institute of Welding Pre-Assembly Meeting on Friction Stir Welding, Nagoya University, Nagoya, Japan, 9 July 2004.

108. K. Kimapong and T. Watanabe: Welding Journal, 2004, vol. 83 (10), pp. 277s-282s.

109. K. Matsumoto and S. Sasabe: Third International Symposium on Friction Stir Welding (Session 5), Kobe, Japan, 27-28 September 2001.

110. A. Elrefaey, M. Gouda, M. Takahashi and K. Ikeuchi: Journal of Materials Engineering & Performance, (ASM), 2005, vol. 14 (1), pp. 10-17.

111. M. Fujimoto, M. Inuzuka, S. Konga and Y. Seta: International Institute of Welding Pre-Assembly Meeting on Friction Stir Welding, Nagoya University, Nagoya, Japan, 9 July 2004.

112. K. Kamimuki and M. Imuta: International Institute of Welding Pre-Assembly Meeting on Friction Stir Welding, Nagoya University, Nagoya, Japan, 9 July 2004.

APPENDIX

Mechanical Testing of Welded Joints

This appendix presents a brief account of the mechanical test methods used for friction stir (FS) welded joints. Here, the sections, references and figures will be identified by the letter "A" followed by a number, so as not to be confused with those in the main text. For the purposes of this appendix, the joint profile obtained in friction stir welding (FSW) will be said to consist of a stir zone (SZ), comprised of the nugget, the TMAZ and the region under the shoulder, and a HAZ (heat affected zone), in addition to the base metal. The SZ and HAZ will constitute the weld zone, where the microstructures and properties would be different from those of the base metal.

A1.0 Butt Joints [A1-A4]

In general, butt joint profiles in FSW are similar to those obtained in conventional (fusion) welding; in fusion welds, the fusion zone (FZ) would be analogous to the SZ. The specimen configurations and the tests used for both types of welds are similar. In the FSW work reviewed in this document, all the tests listed below were utilized.

A1.1 Tensile Testing

Tensile testing of butt joints may be transverse or longitudinal, using flat or round specimens. In transverse testing, the specimens, referred to as transverse-weld specimens, are loaded transverse to the weld direction. In longitudinal testing, the specimens, referred to as longitudinal-weld specimens, are loaded along the weld direction.

Transverse-Weld Specimens: Transverse-weld specimens, Figure A1 (a), can be flat or round. The flat specimens, however, are more frequently used in FSW work. In transverse specimens, the SZ, HAZ and base metal regions, with their respective microstructures, are all represented along the gage length. During tensile testing, each region is loaded to the same stress. Two cases arise. When the strength of the SZ exceeds that of the base metal (overmatching), nearly all the plastic deformation occurs outside that SZ, usually in the HAZ. As such, the test will not provide any information about the SZ or any defects therein. When the SZ is weaker than the base metal (undermatching), the plastic strain and failure would occur mainly in the SZ. As such, the test may not reveal undesirable HAZ or base metal features that might be present. In either case, the elongation is based on the entire gage length (i.e., based on all the regions and microstructures) and, accordingly, the % elongation data can be misleading.

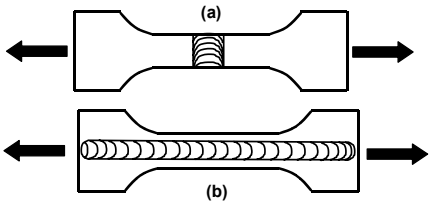

Figure A1: Transverse (a) and longitudinal (b) specimens. The specimens may be flat or round. Flat specimens are typical in FSW. Block arrows indicate loading direction.

Longitudinal-Weld Specimens: Flat longitudinal-weld specimens, Figure A1 (b), are used to generate tensile data parallel to the weld. The width of the specimen includes the SZ, HAZ and possibly also the base metal. During testing, the SZ, HAZ and base metal regions are all strained equally and simultaneously. There are no standards, however, to control the relative lengths of HAZ and base metal to be included in specimen width. This can lead to data variability. Furthermore, any region with poor ductility will often force crack initiation within that region, usually at low stress levels. Regions with good ductility may sustain loads to strength levels higher than their own. In other words, longitudinal test results can be misleading, and it is best if the data is used in conjunction with transverse test data. Occasionally, it is necessary to generate region-specific data. In such cases, longitudinal round or flat specimens may be excised from certain regions, such as the SZ or a particular region thereof (all-weld specimens) or HAZ, Figure A2. Typically, specimen dimensions need to be adjusted to fit within the envelope of the selected region. Occasionally, microspecimens (exceptionally small specimens) must be used to generate the required data. Data generated from small and large size specimens can be different and, as such, care must be taken in comparing data from different size specimens.

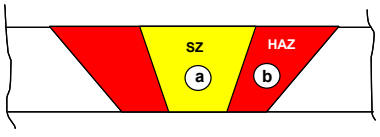

Figure A2: Longitudinal specimens. Specimens shown here are round; flat specimens are also used. (a) Within the SZ (all weld metal specimens). (b) Within the HAZ.

A1.2 Fatigue & Fracture Mechanics Testing

Butt joints can be fatigue tested to generate S-N type data, using transverse or longitudinal specimens (Figure A1 and section A1.1). Specimens may also be excised from certain regions (Figure A2), to generate region-specific data. S-N fatigue specimens may be round (axial and rotating beam tests) or flat (axial and bending tests). Butt joints can also be tested to generate fracture mechanics information, such as fatigue crack growth data (da / dN), using the compact tension specimen, Figure A3. The notch may be aligned with any direction of interest, Figure A4, to generate region-specific data.

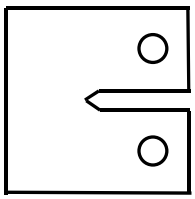

Figure A3: The compact tension specimen.

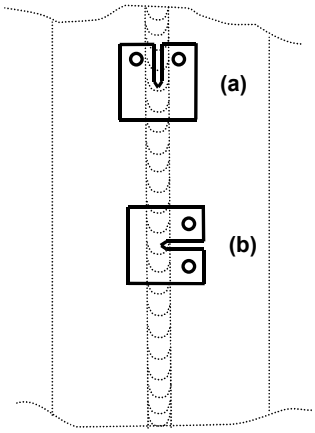

Figure A4: Notch along (a) and normal to (b) joint centerline.

A1.3 Shear Testing

Ultimate shear strength data can be generated by single-shear testing, using thin flat specimens. The specimen contains side notches oriented in such a way that, when the specimen is loaded in tension, fracture would be guided along a "shear path," Figure A5. This type of test is ideal for generating shear strength data for specific regions or interfaces in butt joints, simply by placing the shear path at the desired location, along the direction of interest, Figure A6. No yield or elongation data are obtained in this test.

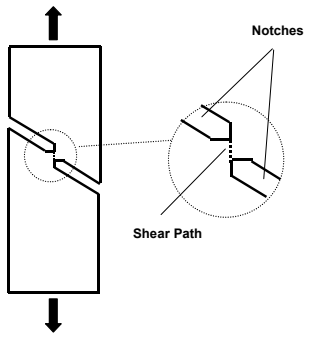

Figure A5: Single-shear test specimen. Block arrows indicate loading direction.

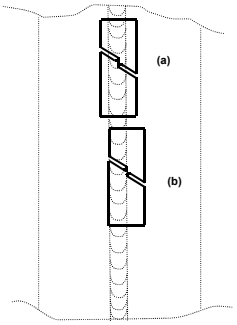

Figure A6: Shear path oriented along the center of the joint (a) and along one of the joint edges (b).

A1.4 Bend Testing

In the FSW work reviewed here, bend testing was used to provide qualitative, as opposed to quantitative, information about longitudinal and transverse joint ductility. The tests can be designed so that the outer fiber tension is at the face, root or side of the weld. The results are expressed in terms of the minimum bend radius that can be used, or the maximum outer fiber elongation that can be sustained, without cracking. Bending may be performed over a mandrel, or by using means such as a plunger-die combination or simple beam loading.

A1.5 Impact Testing

Impact data is typically generated using Charpy (V-notch) specimens. Here, the notch may be aligned with any desired direction, to obtain region-specific information.

A2.0 Lap & Spot Joints

In this section, it is necessary to trace FS weld joint testing back to its origin in conventional weld joint testing. The need for this is brought about by the very use of the terms lap and spot joints in the FSW literature reviewed.

A2.1 Conventional Fillet & Spot Joints [A1, A3, A4]

In conventional (fusion) welding, a fillet joint is obtained by depositing a fused weld filler, approximately triangular in shape, to join two surfaces or members approximately at right angles to each other in a lap, T or corner joint configuration, Figure A7. A spot joint is obtained without filler between two overlapped members, usually in the lap configuration; spot welds can also be used with T and corner joint configurations. The joint may exist only at the interface between the two members, Figure A8, as would be the case in resistance spot welds. Alternately, the joint may penetrate to various depths into the lapped (bottom) member, Figure A9, as would be the case in arc or laser spot welds.

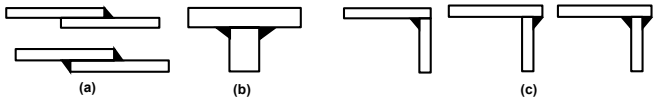

Figure A7: The lap (a), T (b) and corner (c) fillet joint configurations.

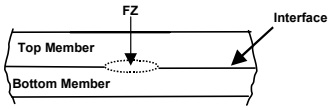

Figure A8: Spot lap joint. Joint is at interface.

The tension-shear test is used extensively to generate data for fillet and spot welds. For fillet welds, two basic types of specimen are available. The first is the longitudinal-tension-shear specimen, Figure A10. The second is

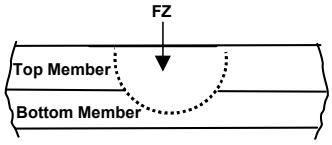

Figure A9: Spot lap joint. Joint penetrates into bottom member.

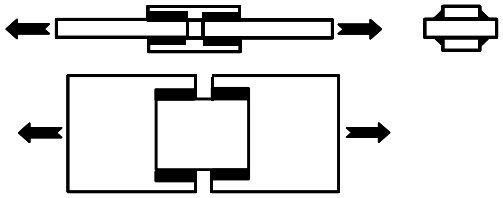

Figure A10: The longitudinal-fillet-weld-tension-shear specimen. Block arrows indicate loading direction.

the transverse-tension-shear specimen, which may be of the single-lap or double-lap configuration, Figure A11. The double-lap test specimen is preferred, since it prevents the bending effects associated with single-lap specimens, and it also minimizes data sensitivity to preparation parameters, such as the gap between the overlapped members. Ultimate shear strength data may be expressed either in psi / ksi, based on fillet throat (where fracture is expected to take place), or in lbs per lineal inch of the fillet weld. No yield or elongation data are obtained here. The transverse-single lap-tension-shear type of specimen, Figure A11 (a), is often used generate axial fatigue S-N data. Variants of the longitudinal-weld-tension-shear specimen of Figure A7 may also be used for the same purpose; however, no illustrations are given here.

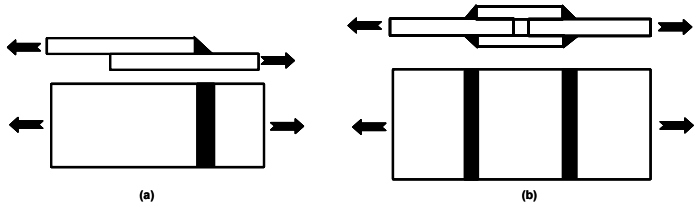

**Figure A11: The transverse-fillet-weld-tension-shear specimens. Block arrows indicate loading direction.
(a) Single-lap configuration.
(b) Double-lap configuration.**

A conventional spot weld is generally tested in tension-shear or in peel. The tension-shear test utilizes the single-lap specimen, Figure A12, and it can be used to generate strength or fatigue data. The peel test is used mainly as a shop control test, and it utilizes manual means to grip and apply the pealing force, Figure A13. The peel test appears to be mentioned only in conjunction with spot joints that exist at the interface between the overlapped details.

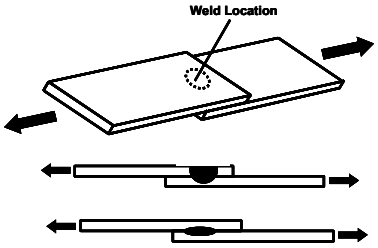

Figure A12: Tension-shear testing of spot joints. Block arrows indicate loading direction.

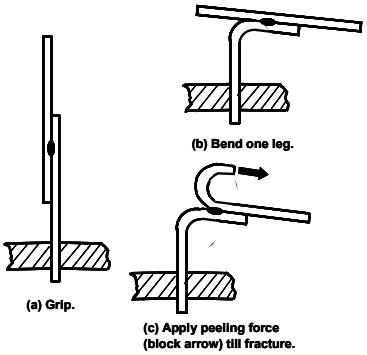

Figure A13: Peel test as shop control means.

A2.2 FS Welded Joints

There is considerable interest within the FSW community in joining two overlapping sheet or plate members in the lap configuration. In the work reviewed in this document, joining was accomplished by means of continuous or localized welds. Respectively, the resulting joints are referred to as lap and spot joints. Strictly speaking, both are lap joints. In what follows, however, they will be identified as lap and spot joints. It is worth noting that, in conventional welding, the corresponding joints would be referred to as fillet and spot joints, for the continuous and localized welds, respectively. FS welded lap and spot joints may be tested by tension-shear or by peel. In the lap joint work reviewed here, the double-lap-tension-shear test was not used. Most authors used the single-lap-tension-shear test, Figure A11 (a), to generate strength and S-N fatigue data for their lap joints. However, some authors [A5, A6] used a special tension-peel test, Figure A14, to generate strength data; this test is not listed among the standard tests used for conventional welds. In the spot joint work reviewed here, only tension-shear testing was used, and it was only used to generate strength data.

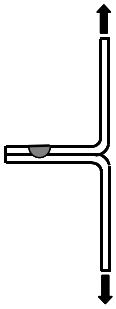

Figure A14: A non-standard tension-peel test. Block arrows indicate direction of loading.

In single-lap-tension-shear testing, bending stresses develop as a result of the offset between the axes of the lapped members. Thomas *et al*. [A7] graphically depicted the subject bending, Figure A15, pointing out that the maximum bending tensile stresses occur around the weld joint, at the bottom of the top member and at the top of the bottom member. These bending stresses would add to test severity, regardless of whether the test is being used to generate static (strength) or dynamic (fatigue) data. As pointed out by Cederqvist and Reynolds, [A8] it is necessary to provide the single-lap test specimens with packing pieces in the grip regions, Figure A16, in order to balance the offset axes of the lapped details, and minimize bending effects. Thomas *et al*. [A7] also used packing pieces in their single-lap-tension-shear testing. The other authors cited in this document did not explicitly indicate that packing pieces were used with their single-lap specimens.

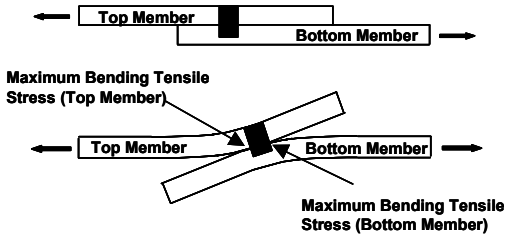

Figure A15: Bending in single-lap-tension-shear testing.

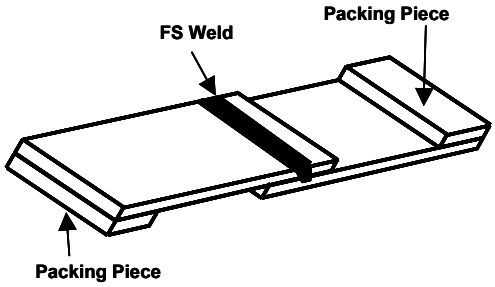

Figure A16: Packing pieces in single-lap-tension-shear specimens.

A3.0 Issues in Testing

Booker *et al*. [A9] point out a fundamental problem in tension-shear testing of single-lap joints. They indicate that loading would lead to a stress state that is a combination of shear and peel stresses. Accordingly, the strength data generated cannot be directly compared to base metal ultimate tensile strength, obtained in a tension test, or seen as pure shear strength, if failure occurs through the weld; it is thought that this problem is also applicable to

tension-peel testing. Although not expressly stated by the authors, their views appear to be equally applicable to FS welded and conventionally produced joints when tested in tension-shear in the single-lap configuration, without using packing pieces. Packing pieces or not, there is another fundamental problem with lap joints, and it stems from the multiplicity of fracture paths available.

FS welded lap joints display profiles that are more or less of the type shown in Figure A9, except that a SZ would replace the FZ. In tension-shear testing, the notches, on either side of the SZ, are potential crack initiation sites. The HAZ in the bottom member may become sufficiently weak as to offer a crack propagation path. Alternately, crack propagation may occur across a narrow SZ or along the SZ / base metal interface (bottom member) in shallow joints or in joints with oxidized interfaces. If local thinning of the top member takes place under the tool shoulder, the center of the joint may become a weak path for crack propagation. In thin sheet stock, the base metal away from the joint could become the preferred site for crack initiation and propagation. What is being said here is that there is no particularly week point (e.g., a fillet throat) where failure would be typically expected to take place. Rather, failure can occur at any of several potential locations (Figure A17), each with its own failure load or fatigue properties. As to where failure occurs will depend on the welding parameters, tool design, amount of thinning in the top sheet, geometry of the notches, and the base metal material, thickness and temper / condition. The above multiplicity of potential fracture paths is thought to be true for single-lap joints, regardless of whether or not packing pieces are used, and for double-lap joints.

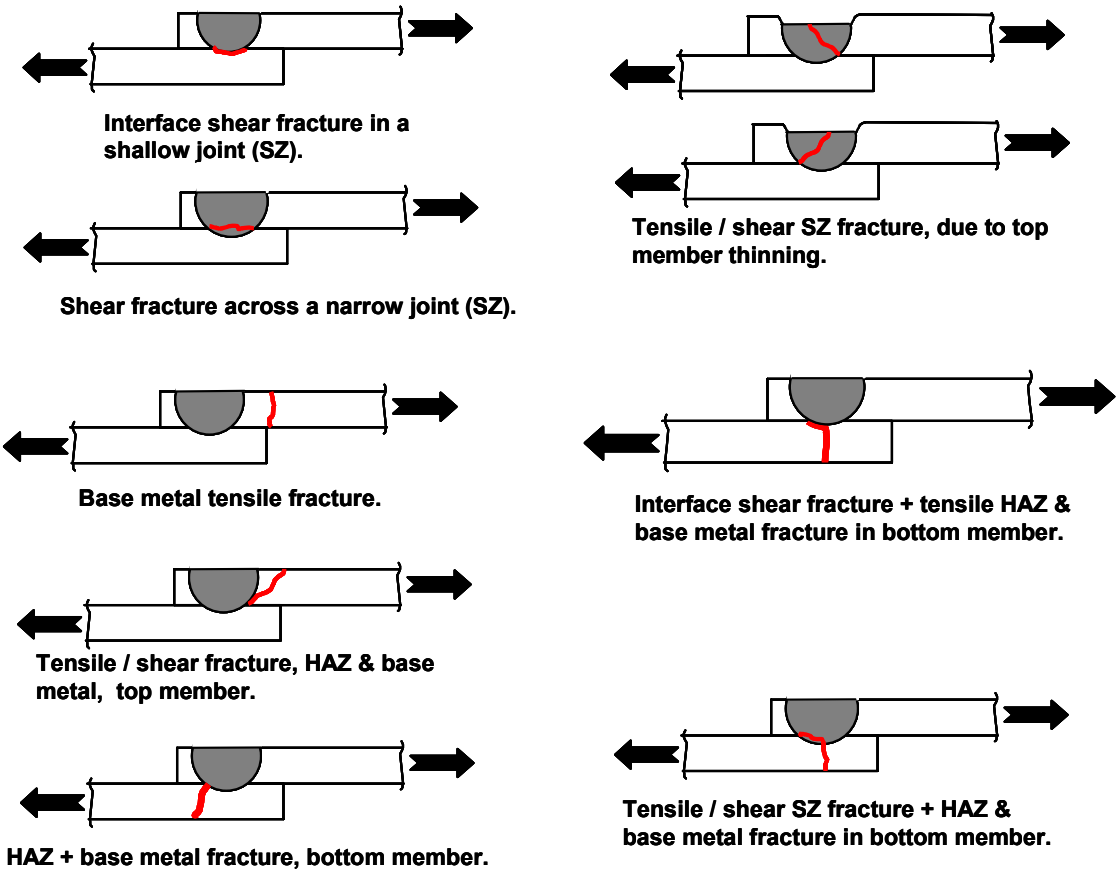

Figure A17: Some fracture paths in single-lap joints.

Thus, in static tension-shear testing, there may be no "datum" on which to base a computation of ultimate shear strength. In fact, as can be seen in Figure A17, some failures may involve no shear at all. As a result, some authors report strength as the failure load per lineal inch of the weld, while others report strength values based on some arbitrary cross section, such as that of one of the overlapped members. The presence of weld defects in lap joints can introduce additional initiation sites and / or crack propagation paths. In tension-shear fatigue testing,

the multiplicity of fracture paths could introduce undesirable data scatter. It is wise, therefore, to always interpret lap joint data in terms of the observed fracture paths. A similar situation exists in FS welded spot joints; multiplicity may even be augmented in those cases where keyholes are present. While the discussions presented here focus on FS welded lap and spot joints, similar implications are thought to potentially exist in FS welded butt joints as well as in joints produced by conventional welding.

Appendix References:

A1. J. J. Vagi, R. P. Meister, and M. D. Randall, DMIC Report 244, Defense Metals Information Center, Battelle Memorial Institute, August 1968.

A2. ASM Handbook, 1985, vol. 8, " Mechanical Testing," pp. 62-68.

A3. Welding Kaiser Aluminum, 1967, Kaiser Aluminum & Chemical Sales, Inc., pp (22-24)-(22-31).

A4. AWS C1.1-66, Spot Welding.

A5. A. Elrefaey, M. Takahashi and K. Ikeuchi: International Institute of Welding Pre-Assembly Meeting on Friction Stir Welding, Nagoya University, Nagoya, Japan, 9 July 2004.

A6. A. Elrefaey, M. Gouda, M. Takahashi and K. Ikeuchi: Journal of Materials Engineering & Performance, (ASM), 2005, vol. 14 (1), pp. 10-17.

A7. W. Thomas, D. Nicholas, D. Staines P. J. Tubby and M F Gittos: International Institute of Welding Pre-Assembly Meeting on Friction Stir Welding, Nagoya University, Nagoya, Japan, 9 July 2004.

A8. L. Cederqvist and A. P. Reynolds: Second International Symposium on Friction Stir Welding, Gothenburg (Session 1), Sweden, 26-28 June 2000. Also: Welding Journal, 2001, vol. 80 (12), pp 281s-287s.

A9. M. J. Brooker, A. J. M. van Deudekom, S.W. Kallee and P. D. Sketchley: Second International Symposium on Friction Stir Welding (session 9), Gothenburg, Sweden, 26-28 June 2000.